DIPARTIMENTO SCIENZE DELLA VITA

DOTTORATO DI RICERCA IN SCIENZE DELLA VITA

CICLO XXXIV

COORDINATORE Prof. Massimo Valoti

Cell based assays used to quantify neutralizing antibodies against SARS-CoV-2 in human samples

SETTORE SCIENTIFICO-DISCIPLINARE: MED/42

DOTTORANDO: Elisa Casa

DocuSigned by:
Elisa Casa
26F98E73BCAC4ED...
2/23/2022

TUTOR aziendale: Dr.ssa Silvia Grappi
Vismederi s.r.l, Siena, Italy

CO-RELATORE: Prof. Emanuele Montomoli
Dipartimento di Medicina Molecolare e dello Sviluppo

A.A. 2021-2022

TABLE OF CONTENTS

1. ABSTRACT

Since the SARS-CoV-2 outbreak at the end of December 2019 in China, it has become extremely important to have well-established and validated diagnostic and research-use-only assays for this new emerging virus. The microneutralization assay is a fundamental serological test in virology, immunology, vaccine assessment and epidemiological studies, and represents one of the most used methods to evaluate the immune response induced by SARS-CoV-2 infection or vaccination.

In this Phd project different microneutralization methods are presented which can be used to measure anti-SARS-CoV-2 neutralizing antibodies (nAbs) in human serum samples. The aim of the first project of this thesis (Project I) was to compare a microneutralization assay (MN) with a read out based on the cytophatic effect (CPE) and a MN based on a colorimetric read out for the detection of nAbs against SARS-CoV-2 Wild type strain. In the first method the cell monolayers were microscopically inspected for inhibition of CPE at each serum dilution (subjective method), while in the MN based on a colorimetric read out the healthy cell monolayer was stained with neutral red solution, a vital dye. The plates were then read by a spectrophotometer at 540 nm (objective method). A panel of 83 human serum samples were previously tested in enzyme-linked immunosorbent assay (ELISA) as a pre-screening. All the samples found to be positive, borderline, and negative in this ELISA were then tested to determine the nAbs titers through the MN CPE and Colorimetric MN. The comparison between log2-trasformed MN titers obtained through these two methods showed comparable values, and the strong agreement in evaluating neutralizing antibodies against SARS-CoV-2 Wild type strain was also confirmed by Correlation (r^2=0,9955), Bland-Altman, and intra-class correlation (ICC) analysis (ICC value of 0.993, which is indicative of an excellent agreement). This suggests the suitability of performing the MN assay using an 'objective' colorimetric-based read out method.

To better investigate if the classical MN CPE yielded similar results to those obtained with other MN methods, we compared this "classical" MN to a new MN platform: the Virospot MN assay (Project II). This method combines classic virus culture techniques with automated sensitive detection of immunostained virus infected cells. In the Virospot MN, a virus-specific immunostaining was used for plate reading and then the images of all wells were acquired by a CTL ImmunoSpot analyzer. The 80% (MN80) or 90% (MN90) neutralization titers are calculated according to the method described by Zielinska et al. 2005. This titer calculation is based on the serum dilutions above and below the reduction point, 80% or 90% neutralization. The MN CPE and Virospot methods were compared using a panel of 47 human serum samples against SARS-CoV-2 Wild type and Alpha variant. The results of this project showed that the these two different MN assays produce similar titer results against the Wild Type virus, with good correlation values (correlation MN80 r^2=0,9091; correlation MN90 r^2=0,8900). A lower agreement between the MN CPE and Virospot MN assay was observed

when SARS-CoV-2 Alpha variant was used (correlation MN80 r^2=0,7226; correlation MN90 r^2=0,6673).

Overall, these results showed a good agreement between the MN CPE assay and the two different MN methods, Colorimetric MN and Virospot MN assay, in detecting neutralizing antibodies against SARS-CoV-2 in human serum samples.

Despite the need for further standardization and/or the differences noticed during the assessment of nAbs against SARS-COV-2 variants, the Colorimetric-based and Virospot MN demonstrate to have advantages over the classical MN CPE, both being completely automated methods, and hence offering a higher throughput, while inspection of each dilution well by means of the optical microscope slows down the process. However, to ensure that these correlation studies can provide meaningful results, further analysis with a bigger number of samples and with other SARS-CoV-2 variants would be an added value. Moreover, to make the data more comparable it would be necessary convert all the results to international standard unit (IU/mL) allowing the accurate calibration of assays to an arbitrary unit, thereby reducing inter-laboratory variation, and creating a common language for reporting data.

The SARS-CoV-2 Virospot MN assay offers attractive advantages over the MN assay with a read out based on the cytophatic effect, including the relative insensitivity to variation in amount of infectious virus used in the test, independence from virus replication kinetics and suitability for high throughput analyses.

Since many new SARS-CoV-2 variants occurred during the last two years, to make the Virospot more sensitive and robust in detecting neutralizing antibodies against these new variants, the third project (Project III) focused on the optimization study of this MN assay. Several new conditions were adapted to optimize the method and make it more sensitive for the analysis of samples against the Wild Type, Alpha, Beta, and Gamma SARS-CoV-2 variants. Carboxymethyl cellulose (CMC) overlay was introduced to make the spot count more accurate avoiding the viral spread after the first infection. Moreover, different sample matrices (serum and plasma), culture media with and without the CO2 supplementation, and different incubation time points and temperatures were assessed to evaluate and improve the assay performance and robustness.

This optimization study has a planned follow-up, which can possibly include samples not only from infected/convalescent individuals but also from vaccinated donors (with two or more doses) or from people with hybrid immunity (such as breakthrough infections). Additionally, further analyses with additional SARS-CoV-2 variants to strengthen these finding will also be part of the next study. This project is worth to be conducted as the Virospot MN assay is likely to have importance for the pre-clinical evaluation and eventual licensing of the SARS-CoV-2 vaccines.

2. INTRODUCTION

2.1 New emerging viruses: viral evolution and genetic host shift

Since the first descriptions of AIDS in the early 1980s, much has been written about the causes and consequences of emerging viral diseases. Although research efforts, viral infections continue to appear in human and wildlife populations. Defining emerging viruses as those that have just appeared or have recently increased in prevalence and/or geographical range reveals some important general patterns. First, almost all emerging viruses have RNA rather than DNA genomes, although RNA viruses are normally more common than DNA viruses. Secondly, almost all emerging viruses have an animal reservoir, such that the viral emergence process can usually be classified as transmission between species. For instance, type 1 HIV (HIV-1), the leading cause of AIDS, has its origins in the related simina immunodeficiency virus (SIV) present in chimpanzees, while severe acute respiratory syndrome (SARS-CoV) coronavirus has close relatives in Himalayan palm owls, although it is not yet established whether these are the population of origin for the human form of the virus. In many cases, the specific cause of the emergence - i.e virus crossing from animals to humans - can be assigned to ecological factors, often related to changes in land use and deforestationChanges in the proximity of donor and receiving populations (so that humans have a greater chance of exposure to animal pathogens), or changes in the size and density of donor and receiving populations (which increases both exposure and the likelihood that sustained transmission networks will be established once a virus has entered a new species) are important causes of new viral diseases emergence in humans.[1]

The elemental nature of the evolutionary interaction between host and pathogen is fundamental to understand the mechanics of viral emergence. Basically, different viruses or strains within a specific viral family may differ in their ability to recognize the cell receptors of a new host species or in their ability to successfully transmit between individuals in the new host species.[1] It is this fact that gives RNA viruses an evolutional advantage, the mutation rates of RNA viruses are many orders of magnitude greater than those of their DNA counterparts. They have a relatively high mutation rate in the order of 10^{-6}–10^{-4} substitutions per nucleotide site per cell infection, and they have evolved by developing various proofreading mechanisms. Indeed, viral replication can be an imprecise and discontinuous process. The rapid insertion of bases during RNA elongation may be subject to misincorporation of mismatched nucleotides, leading to RNA-dependent RNA-polymerase (RdRp) dysfunction.[45] Similarly, while many DNA viruses lead to persistent infections in their hosts, many RNA viruses generate acute infections. This is critical to the viral emergence process because a short duration of infection means that the most likely way for RNA viruses

to infect new host species is through cross-species transmission, rather than long-term co-species, which is usually associated with persistence. It may seem strange that with their considerable mutation power RNA viruses are unable to exploit any adaptive solution. Ironically, the adaptive constraints faced by RNA viruses can be a function of their high mutation rates, as this can limit their genome size, which in turn hinders their ability to increase complexity. The causal link between mutation rate and genome size can be made by invoking the concept of "error threshold". This theory was first introduced by Eigen as a crucial element in the evolution of early RNA replicators, although it can actually be extended to any living system.[1]The rapid evolution of RNA viruses complicates the management of chronic infections and the control of emerging infectious agents. The ongoing global AIDS pandemic and the resurgence of influenza highlight the difficulties associated with these genetically labile pathogens. RNA viruses have also been responsible for recent sporadic epidemics of emerging and reemerging viral diseases including dengue, West Nile fever, and Ebola.[13] Emerging infectious diseases affecting humans, wildlife, and agriculture are often the result of a pathogen jumping from its original host into a novel host species. Host shifts have resulted in multiple human pandemics, such as HIV from chimps and the H1N1 ‘‘Spanish flu’’ from birds, which have both killed tens of millions of people.NA viruses are the most likely group of pathogens to jump between hosts, possibly because of their ability to rapidly adapt to new hosts. The susceptibility of potential hosts varies enormously, and an important predictor of susceptibility is how closely related a novel host is to a pathogen’s natural host. Reconstructions of host shifts in nature have confirmed that pathogens are more likely to shift between closely related species. Accordingly, the high mutation rate of RNA viruses could explain why they shift host more frequently than other pathogens.[2]

2.1.1 Antigenic drift and shift

The potential for genetic variability of RNA viruses has long been considered to be fundamental to their evolution, adaptation and escape from host responses. However, the effects of changes in replication fidelity, susceptibility to accumulation of deleterious mutations and lethal mutagenesis are not well studied for many viruses. Genetic determinants including size of genome and presence of repair mechanisms such as proofreading, replicase fidelity and recombination, as well as other as yet undetermined factors may have evolved quite differently in distinct virus families. The high mutation rates of RNA viruses also render them particularly susceptible to repeated genetic bottleneck events during replication, transmission between hosts or spread within a host, resulting in progressive deviation from the consensus sequence associated with decreased viral fitness and sometimes extinction.[46]

A major step that allowed genome expansion in coronaviruses (COVs) was the acquisition of a series of RNA-processing enzymes that improved the low fidelity of RNA replication. The expansion of the CoV genome has allowed the acquisition and maintenance of genes that encode different accessory proteins that can promote the adaptation of the virus to specific

hosts and often contribute to the suppression of immune responses, as well as virulence. Accessory proteins differ in number and sequence even among CoVs belonging to the same lineage, raising interesting questions about their origin and evolution. The acquisition or loss of novel protein-coding genes has the potential to drastically modify viral phenotypes. Thus, tracing these gain/loss events may help identifying important turning points in viral evolution. Clearly, CoV genomes do not only evolve by gene gains and losses, but also via subtler changes that modify protein sequences, and recombination has an important role in reassorting variants.

From an evolutionary standpoint, nonstructural proteins have attracted less attention than the structural components. This is likely due to the fact that proteins exposed on the virus surface represent the preferential targets of the host immune response. Thus, analyzing and describing their variability and evolutionary dynamics has a clear relevance for the development of preventive strategies (e.g., vaccines) and of treatment options (e.g., administration of neutralizing antibodies). Moreover, structural proteins, and the S protein in particular, determine the first and essential steps in infection and most likely represent the major determinants of host and tissue tropism.[11]

Nucleotide substitution has been proposed to be one of the most important mechanisms of viral evolution in nature (**Figure 1**). The rapid spread of SARS-CoV-2 raises intriguing questions such as whether its evolution is driven by mutations. Mutations in the spike surface glycoprotein might induce its conformational changes, which probably led to the changing antigenicity.[12] The evolutionary dynamics of RNA viruses are complex and their high mutation rates, large population sizes and the rapid replication kinetics present a challenge to traditional population genetics. Quasispecies theory is a mathematical theory that was initially formulated to explain the evolution of life in the ‘‘precellular RNA world.’’[13] This theory established a link between Darwinian evolution and information theory and represented a deterministic approach to evolution. It was soon recognized that such an approach had limitations due to the nondeterministic nature of mutagenesis and to statistical fluctuations.[47] It is based on classical population genetics, but seeks to explore the consequences of error-prone replication and almost infinite population size for genome evolution. More recently, quasispecies theory has been used to describe the evolutionary dynamics of RNA viruses, and many of its predictions have been experimentally validated in model systems. Some of these observations challenge more traditional views of evolution and have profound implications for the control and treatment of viral diseases. Most viruses encode enzymes responsible for replicating their DNA or RNA genomes. The intrinsic error rate of replication determines the mutation rate for that virus and the range of genetic variation on which natural selection can act. Given the large population sizes observed in both experimental and natural infections, it is estimated that every possible point mutation and many double mutations are generated with each viral replication cycle and may be present within the population at any time.

Because RNA viruses exist as swarms of similar variants that are continuously regenerated by mutation of related sequences, our ability to predict the outcome of an infection or a therapeutic intervention from studies of isolated clones is limited. Even a defined molecular clone will quickly turn into a collection of related sequences when introduced into cells. This collection is the quasispecies and is organized around a master sequence. The genetic organization of populations is often depicted using the concept of sequence space, a geometric representation of all possible sequences where physical distance reflects genetic similarity. According to population genetics, the frequency of a given variant within a population is closely approximated by its ability to survive and reproduce—its fitness. The environment factors and its selective pressures determine the contours of the corresponding landscape, and adaptation to an environment involves a mutational walk from one point in the fitness landscape to another.[13]

Between environmental factors, alterations resulting from human intervention (deforestation, agricultural activities, global climatic changes, etc.) may alter dispersal patterns and provide new adaptive possibilities to viral quasispecies.[48]

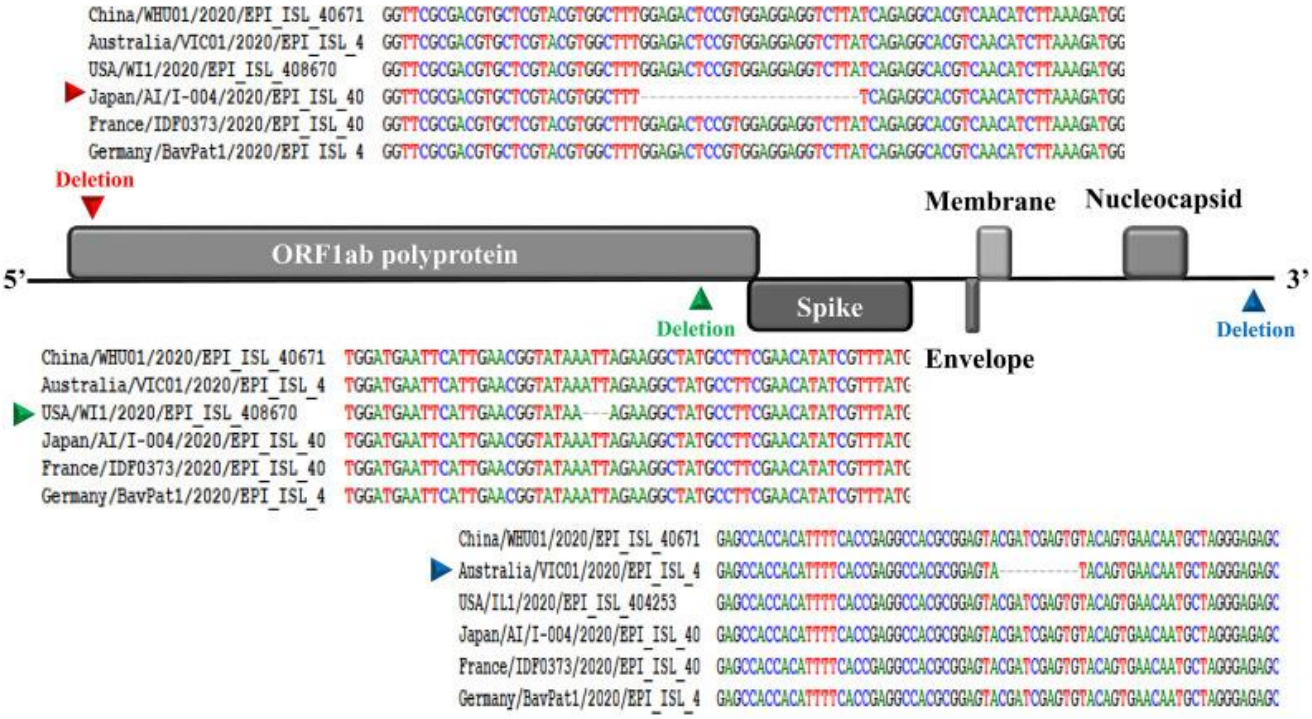

Figure 1. Genomic organization of SARS-CoV-2 and pairwise nucleotide sequence alignment showing deletions in the ORF1ab polyprotein and in the 3' end of the genome. Genetic analysis discovered three deletions in the genomes of SARS-CoV-2 from Japan (Aichi), USA (Wisconsin), and Australia (Victoria) . Two deletions (three nucleotides and twenty-four nucleotides) were in the ORF1ab polyprotein, and one deletion (ten nucleotides) was in the 3' end of the genome (from Elsevier Public Health Emergency Collection).

Given their high mutation rates, it is not surprising that many discussions of RNA virus evolution focus on the relationship between genetic diversity and adaptability. While it is clear that RNA viruses have the capacity to quickly explore large regions of sequence space, genome size and selective constraints place significant limitations on the amount of diversity that is actually expressed. Most RNA virus genomes are relatively small and contain either

overlapping reading frames or sequences that serve both coding and structural functions. Similarly, coding mutations that mediate escape from host immune surveillance may compromise protein function.[13] Given the high prevalence and wide distribution of coronaviruses, the large genetic diversity and frequent recombination of their genomes, and increasing human–animal interface activities, novel coronaviruses are likely to emerge periodically in humans owing to frequent cross-species infections and occasional spillover events.[37]

2.2 SARS-CoV viruses and their epidemiology

Soon after the first transmission emergence of SARS-CoV, from animals to humans in China in 2003, a genetically evolved beta-coronavirus genus similar to human viruses was discovered in Chinese horseshoe bats. To date, pneumonia is epidemiologically caused by diverse viruses. For example, adenovirus, influenza virus, Middle East respiratory syndrome virus (MERS-CoV), parainfluenza virus, respiratory syncytial virus (RSV), SARS-CoV and enteric enveloped CoV can cause pneumonia in human hosts.

Three coronaviruses have crossed the species barrier to cause deadly pneumonia in humans since the beginning of the 21st century: SARS-CoV, Middle East respiratory syndrome coronavirus (MERS-CoV), and severe acute respiratory syndrome coronavirus 2 (SARS-CoV-2).[6] At the end of December 2019 in Wuhan, Hubei Province, China, a novel CoV strain, called SARS-CoV-2 by the International Committee on Taxonomy of Viruses (ICTV), caused 27 cases of pneumonia of unidentified etiology. Due to the rapid and uncontrollable spread of the virus in almost every country in the world, the World Health Organization (WHO) officially declared the pandemic status in March 2020 and reported the official terminology of the 2019-Novel Coronavirus (2019-nCoV) on 13 January 2020. On February 11th, WHO edited the name of the disease caused by 2019-nCoV to Coronavirus Disease-2019 (COVID-19).[10] Whilst numerous comparisons can be drawn between SARS-CoV-2 and its predecessors (SARS-CoV and MERS-CoV, responsible for the SARS and MERS epidemics, respectively), SARS-CoV-2 has unquestionably proved to be the most deadly. [17] Unlike previous episodes of coronavirus spread, where it took months to identify the cause of infection and perform genome sequencing, advancement in science and technology made it possible to identify the causative organism swiftly. Within a few weeks of the outbreak, different laboratories across the world had sequenced the whole viral genome and had also provided structural and functional insights into the essential proteins required by the virus for its survival. These immediate scientific inputs helped with developing diagnostic kits and defining treatment strategies for effective prognosis and prevention.[15]

Coronaviruses belongs to the subfamily *Coronavirinae* in the family of *Coronaviridae* and the subfamily contains four genera: Alphacoronavirus (α-CoV), Betacoronavirus (β-CoV), Gammacoronavirus (γ-CoV), and Deltacoronavirus (δ-CoV). The 2019 nCoV or Sars-Cov-2

belong to the β-CoV genus and are zoonotic and cause mammalian infection, causing respiratory disease in the human lung. The α-CoV and β-CoV genus target mammal hosts while the δ-CoV and γ-CoV genus target avians and certain mammals. The β-CoV genus has A, B, C and D lineages. Among these, lineage B includes SARS-CoV and SARS-CoV-2. Lineage C includes MERS-CoV. The B lineage SARS-CoV and C lineage MERS-CoV, which are classified as β-CoVs, exhibit lethal rates of 10% and 35% in humans, respectively.[3] Coronaviruses are single-stranded RNA viruses easy to mutate, which increases the diversity of the species and give them the ability to rapidly adapt to new hosts. Nevertheless, the evolution and development of CoVs were not only the consequence of the coronavirus phylogeny and biology, but also the results of the interaction between CoVs and their hosts. Bats are the only mammals naturally capable of true and sustained flight. As bats have been identified to be the natural reservoirs of various emerging viruses (including SARS-CoV-2) the concept of zoonotic origin of important viral pathogens becomes widely accepted.[4]

2.3 Pathogenesis

SARS-CoV-2 is transmitted predominantly via fomites and respiratory droplets during close unprotected contact between the infected and uninfected. Symptomatic and asymptomatic patients are the main source of infection. The virus can also spread through indirect contact transmission - virus-containing droplets can contaminate hands, people then contact the mucous membranes of the mouth, nose, and eyes, causing infection.

The transmission of SARS-CoV-2 is not limited to the respiratory tract. Some studies have demonstrated the aerosol transmission of SARS-CoV-2.[6] Primary viral replication is presumed to occur in mucosal epithelium of upper respiratory tract (nasal cavity and pharynx), with further multiplication in lower respiratory tract and gastrointestinal mucosa, giving rise to a mild viremia.[18] The major spread route of SARS-CoV-2 is person-to-person, it could happen in family, hospital, community, and other gathering of people. Most cases of the person-to-person transmission of the early stage in China happened in family clusters. This kind of spreading has the possibility to occur during the incubation period. The most common manifestations of COVID-19 are fever and dry cough. The majority of the patients showed bilateral pneumonia. Old males with comorbidities are more likely to be affected by SARS-CoV-2. The blood counts of patients showed leucopenia and lymphopenia.

COVID-19 is divided into three levels according to the severity of the disease: mild, severe, and critical. The majority of patients only have mild symptoms and recover. Asymptomatic infection cases were also reported, but most of the asymptomatic patients went on to develop disease since the data of identification manifestations of COVID-19 and three different levels of COVID-19 divided according to the severity.[6] Currently, COVID-19 patients are the main source of infection, and severe patients are considered to be more contagious than mild ones. Asymptomatically infected persons or patients in incubation who show no signs or symptoms of respiratory infection proven to shed infectious virus, may also be

potential sources of infection.[14] Additionally, samples taken from patients recovered from COVID-19 continuously show a positive real time polymerase chain reaction (RT-PCR) test, which has never been seen in the history of human infectious diseases. In other words, asymptomatically infected persons and patients in incubation or recovered from COVID-19 may pose serious challenges for disease prevention and control.[5] However, the clinical manifestation surely depends on multiple factors, such as genetic background (HLA, gene polymorphisms–such as for Angiotensin-converting enzyme EC 3.4.15.1 , or ACE) and the individual variability in environmental/personal risk factors (age, smoking, diet, physical activity, vaccination scheme, contact history with other coronaviruses). Another general issue causally linked to the higher winter incidence of the respiratory disease relevant to innate immunity is vitamin supplementation and availability. The vitamin D could be the key factor with its multiple immunoregulatory functions in the combination with sun exposure.

COVID-19 mortality and severity is not only gender, but also age-biased. It has been shown that SARS-CoV-infected old macaques had a stronger host response to virus infection than young adult macaques. They expressed higher levels of proinflammatory cytokines, whereas expression of IFNs type I was reduced. In contrast to the elevation of macrophages, a significant decrease of NK cells in severe cases of COVID-19 was detected. A significant increase of NKG2A expression in COVID19 patients was also observed. Upregulation of NKG2A was associated with the exhaustion of cytotoxic T cells and NK cells at the early stage of SARS-CoV-2 infection, and therefore, was associated to severe disease progression. So far, the results suggest that in severe cases of COVID-19 myeloid cell lineages, especially macrophages, play prominent role in the disease progression through their overactivation, whereas NK cell activity is reduced.[19]

2.4 The structure of SARS-COV-2

As a member of coronavirus family, the genome size of CoVs is approximately 29.9 kb. It is a single-stranded positive-sense RNA (+ssRNA) which is larger than any other RNA viruses.[5]

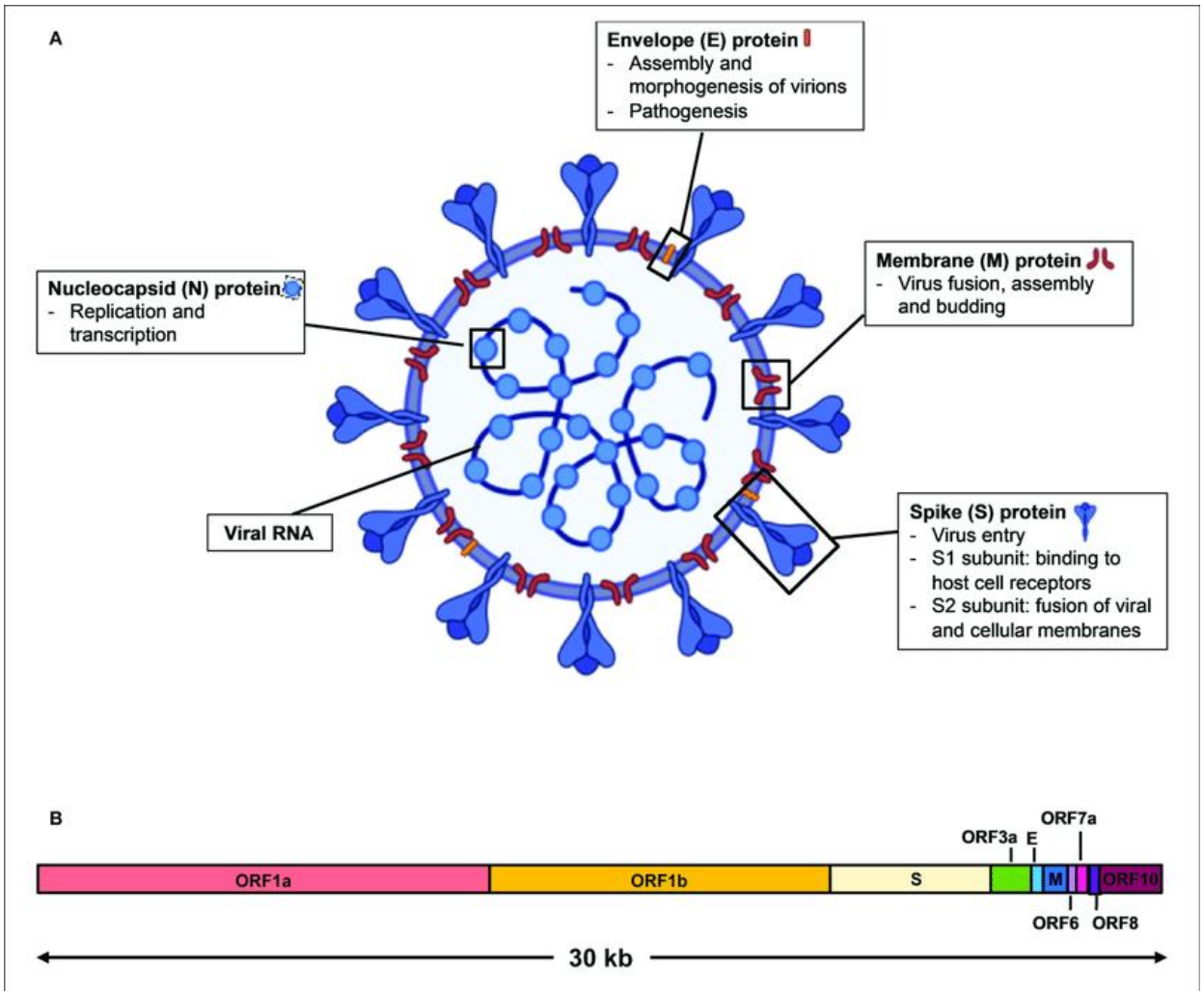

Figure 2. Schematic diagram of SARS-CoV-2 virus structure and genome organization. (A) The viral surface proteins, spike (S), envelope (E), and membrane (M) are embedded in a lipid bilayer. The single stranded positive-sense viral RNA is associated with the nucleocapsid (N) protein. Diagram was created with BioRender. (B) The genome organization of SARS-CoV-2 viral RNA, which is adapted from GenBank accession number: MN908947, is characterized by sequence alignment against two representative members of the betacoronavirus genus. The entire genome sequence is ~30 kilobases (kb) long.

Like other coronavirus, this virus has at least six extra open reading frames (ORFs) in its genome. The first ORFs (ORF1a/b) are about two-thirds of the whole genome length and encode 16 nonstructural proteins(nsp1-16). These ORFs produces two polypeptides, including p1a and pp1ab. One-third of the genome near the 3' -terminus encodes four main structural proteins, including the nucleocapsid, spike, envelope, and membrane proteins (**Figure 2**).[24] The nucleocapsid protein (N) formed the capsid outside the genome and the genome is further packed by an envelope which is associated with three structural proteins: membrane

protein (M), envelope protein (E) and the spike protein (S).[5] The N protein of coronavirus is multipurpose. Among several functions, it plays a role in complex formation with the viral genome, facilitates M protein interaction needed during virion assembly, and enhances the transcription efficiency of the virus. It contains three highly conserved and distinct domains, namely, an N Terminal-domain (NTD), an RNA-binding domain or a linker region (LKR), and a C Terminal domain (CTD). The NTD binds with the 3' end of the viral genome, perhaps via electrostatic interactions, and is highly diverged both in length and sequence. It also modulates the antiviral response of the host by working as an antagonist for interferon (IFN) and RNA interference. The M protein is the most abundant viral protein present in the virion particle, giving a definite shape to the viral envelope. It binds to the nucleocapsid and acts as a central organizer of coronavirus assembly. The coronavirus E protein is the most enigmatic and smallest of the major structural proteins. It plays a multifunctional role in the pathogenesis, assembly, and release of the virus. It is a small integral membrane polypeptide that acts as a viroporin (ion channel). The inactivation or absence of this protein is related to the altered virulence of coronaviruses due to changes in morphology and tropism.[16] Nsp1 mediates RNA processing and replication. Nsp2 modulates the survival signaling pathway of host cell. Nsp3 is believed to separate the translated protein. Nsp4 contains transmembrane domain 2 (TM2) and modifies ER membranes. Nsp5 participates in the process of polyprotein during replication. Nsp6 is a presumptive transmembrane domain. The presence of nsp7 and nsp8 significantly increased the combination of nsp12 and template-primer RNA. Nsp9 functions as an ssRNA-binding protein. Nsp10 is critical for the cap methylation of viral mRNAs. Nsp12 contains the RNA dependent RNA polymerase (RdRp), which is a critical composition of coronavirus replication/transcription. Nsp13 binds with ATP and the zinc-binding domain in nsp13 participates in the process of replication and transcription. Nsp14 is a proofreading exoribonuclease domain. Nsp15 has Mn(2+)-dependent endoribonuclease activity. Nsp16 is a 2'-O ribose methyltransferase. One study shows that there are some NSP-mediated effects on splicing, translation, and protein trafficking to inhibit host defenses. Upon SARS-CoV-2 infection, NSP16 binds mRNA recognition domains of the U1 and U2 snRNAs to suppress mRNA splicing. NSP1 binds to 18S ribosomal RNA in the mRNA entry channel of the ribosome to interfere with the translation of mRNA. NSP8 and NSP9 binds to the 7SL RNA which locates at the Signal Recognition Particle to disrupt protein trafficking to the cell membrane. The coronaviruses entry into host cells is mediated by the transmembrane spike glycoproteins (S proteins) that form homotrimers protruding extensively from the viral surface.[5]

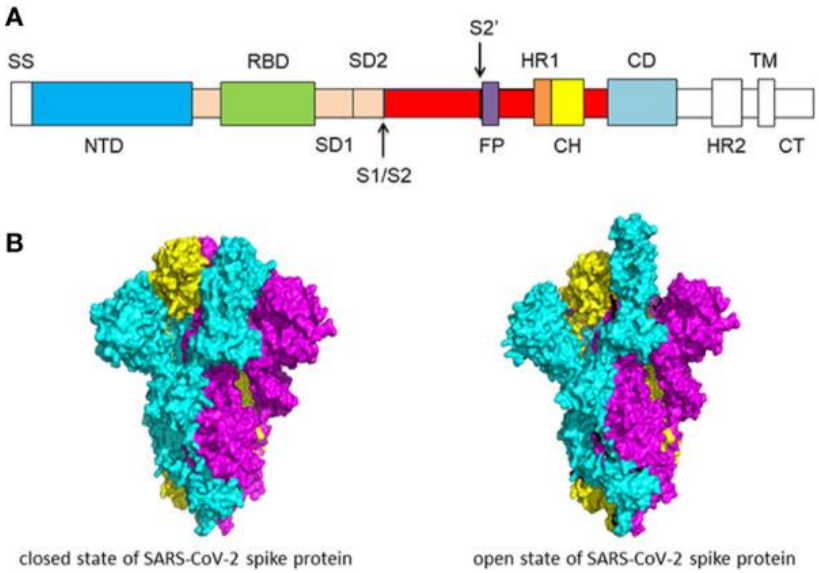

Figure 3. A) Schematic of SARS-CoV-2 spike protein primary structure. Different domains are shown by different colors. SS, single sequence; NTD, N-terminal domain; RBD, receptor-binding domain; SD1, subdomain 1; SD2, subdomain 2; S1/S2, S1/S2 protease cleavage site; S2', S2' protease cleavage site; FP, fusion peptide; HR1, heptad repeat 1; CH, central helix; CD, connector domain; HR2, heptad repeat 2; TM, transmembrane domain; CT, cytoplasmic tail. The protease cleavage site is indicated by arrows. (B) Cryo-EM structure of the SARS-CoV-2 spike protein. The closed state (PDB: 6VXX) of the SARS-CoV-2 S glycoprotein (left) the open state (PDB: 6VYB) of the SARS-CoV-2 S glycoprotein (right).

2.5 Life Cycle

Virus entry in mammalian cells proceeds in three steps: attachment and entry into the cell, transcription of viral replicase, genomic transcription and replication, translation of structural proteins, and virion assembly and release. First, the viral spike protein binds to a host through a recognized receptor or entry point. The S protein represents a classic class-I fusion protein, characterized by the presence of a trimer of α-helical coiled-coils in the protein's active site. It is structurally similar to that of SARS-CoV and is the major viral determinant for host tropism by dictating cell entry through binding cellular receptors and initiating fusion, and hence infection.[9]

Coronaviruses can bind to a range of host receptors, with binding conserved only at the genus level. SARS-CoV-2 has a high affinity for human ACE2, which is expressed in the vascular epithelium, other epithelial cells, and cardiovascular and renal tissues, as well as many others. The binding process is guided by the molecular structure of the spike protein, which is structured in three segments: an intracellular domain, ectodomain, and a transmembrane anchor.[8] The intracellular domain shows a short intracellular tail. The ectodomain region has S1 subunit responsible for binding to the host cell receptor and S2 subunit for the fusion of the viral and cellular membranes. The S1 domain of spike protein acts as a major surface antigen. It contains NTDand CTD. The S1-CTD acts as a receptor-binding domain (RBD). The RBD interacts with the 18 residues of ACE-2. RBDs are shielded by glycosylation which is

commonly observed in viral glycoproteins including S proteins from SARS-CoV.[7] The distal S1 subunit comprises the receptor-binding domain(s) and contributes to stabilization of the prefusion state of the membrane-anchored S2 subunit that contains the fusion machinery. For all CoVs, S is further cleaved by host proteases at the so-called S2 0 site located immediately upstream of the fusion peptide.[6] A cellular protein called transmembrane protease serine 2 (TMPRSS-2) carries out this cleavage.[9] This cleavage has been proposed to activate the protein for membrane fusion via extensive irreversible conformational changes. As a result, coronavirus entry into susceptible cells is a complex process that requires the concerted action of receptor-binding and proteolytic processing of the S protein to promote virus-cell fusion.[6] Cleavage at a second site within S2 by these same proteases activates S for fusion by inducing conformational changes (**Figure 3**). The viral membrane can then fuse with the endosomal membrane to release the viral genome into the host cytoplasm. Once the virus enters a host cell, the replicase gene is translated and assembled into the viral replicase complex. This complex then synthesizes the double-stranded RNA (dsRNA) genome from the genomic ssRNA(+). The dsRNA genome is transcribed and replicated to create viral mRNAs and new ssRNA(+) genomes (**Figure 4**). From there, the virus can spread into other cells. In this way, the genome of SARS-CoV-2 provides insight into the pathogenic behavior of the virus.[7]

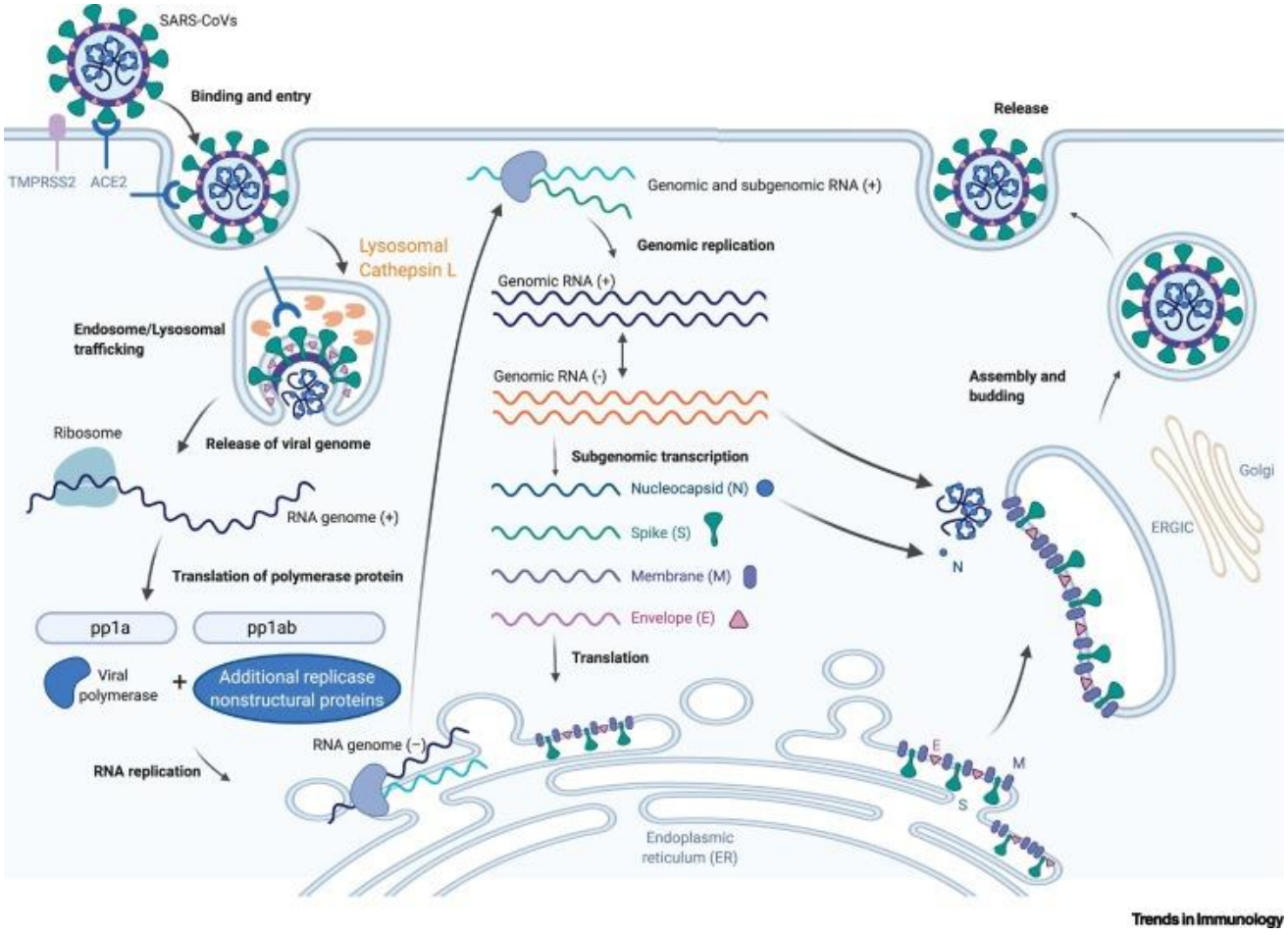

Figure 4. The Severe Acute Respiratory Syndrome Coronavirus 2 (SARS-CoV-2) Lifecycle. The SARS-related coronavirus lifecycle starts by the binding between the Spike protein to its receptor, angiotensin-converting enzyme 2 (ACE2). The cell entry then depends on: (i) cleavage of the S1/S2 site by the surface transmembrane protease serine 2 (TMPRSS2); and/or (ii) endolysosomal cathepsin L, which mediate virus–cell membrane fusion at the cell surface and endosomal compartments, respectively. Through either entry mechanism, the RNA genome is released into the cytosol and there it is translated into the replicase proteins (open reading frame 1a/b: ORF1a/b). The polyproteins (pp1a and pp1b) are cleaved by a virus-encoded protease into individual replicase complex nonstructural proteins (nsps) (including the RNA-dependent RNA polymerase: RdRp). Replication begins in virus-induced double-membrane vesicles (DMVs) derived from the endoplasmic reticulum (ER), which ultimately integrate to form elaborate webs of convoluted membranes. Here, the incoming positive-strand genome then serves as a template for full-length negative-strand RNA and subgenomic (sg)RNA. sgRNA translation results in both structural proteins and accessory proteins (simplified here as N, S, M, and E) that are inserted into the ER–Golgi intermediate compartment (ERGIC) for virion assembly. Positive-sense RNA genomes are incorporated into newly synthesized virions, which are secreted from the plasma membrane.

The genomic RNA (sgRNA) serves as a transcript and allows the cap-dependent translation of ORF1a producing polyprotein pp1a. Next, a slippery sequence and an RNA pseudoknot towards the end of ORF1a leads to 25–30% of the ribosomes to undergo frameshifting, hence continuing translation on ORF1b and producing a longer polyprotein pp1ab. The autoproteolytic cleavage of pp1a and pp1ab generates 15–16 nonstructural proteins (nsps) which possess specific functions. The RNA dependent RNA polymerase (RdRP) activity is encoded by nsp12, whereas the nsp3 and nsp5 respectively encodes papain-like protease (PLPro) and the main protease (Mpro). Then, nsp3, 4, and 6 induce the rearrangement of the cellular membrane to form double-membrane vesicles (DMVs), where the coronavirus replication transcription complex (RTC) is assembled and anchored. Programmed ribosomal

frameshifting (PRF) is possibly regulated by viral and host factors apart from the RNA secondary structures. A host RNA binding protein called annexin A2 (ANXA2) was shown to bind the pseudoknot structure within the infectious bronchitis virus (IBV) genome. In terms of DMVs formation and RTC assembly, several host factors of the early secretory pathway seem to be involved. Golgi-specific brefeldin A–resistance guanine nucleotide exchange factor1 (GBF1) and its effector ADP ribosylation factor 1 (ARF1) are both essential for normal DMV formation and efficient RNA replication of mouse hepatitis virus (MHV), a prototypic beta coronavirus which primarily infects mice. The RNA genome of SARS-CoV-2 works as a template for replicase to synthesize full-length antisense genome; this serves as a template for the synthesis of new genomic RNA.[9] As the coronavirus S glycoprotein is surface-exposed and mediates entry into host cells, it is the main target of neutralizing antibodies (Abs) upon infection and the focus of therapeutic and vaccine design. S trimers are extensively decorated with N-linked glycans that are important for proper folding and for modulating accessibility to host proteases and neutralizing Abs.[5-6]

2.6 Immune response against Sars-CoV-2 infection

2.6.1 COVID-19 and innate immunity

In spite of the fact that the precise mechanisms of interaction between the innate immune system and SARS-CoV-2 have not been described yet, it is suggestive that the innate immune responses and relevant cell types play a vital role in the clinical symptoms and severity of COVID-19 disease.[19] Innate immune sensing serves as the first line of antiviral defense and is essential for immunity to viruses. The virus-host interactions involving SARS-CoV-2 are likely to recapitulate many of those involving other CoVs, given the shared sequence homology among CoVs and the conserved mechanisms of innate immune signaling.[21] It was shown that SARS-CoV triggers various innate recognition and response pathways. The general anti-viral innate mechanisms to SARS-CoV-2, including the fact that “self” vs. “non-self” discrimination is mainly mediated via recognition of the viral nucleic acids as pathogen-associated molecular pattern (PAMPs) by specific pathogen recognition receptors (PRRs) in the cytosol[19] that include C-type lectin receptors, nucleotide-binding oligomerization domain-like receptors(NLRs), RIG-I-like receptors (RLRs) and Toll-like receptors (TLRs).[24] The feauture of this concept is in a case of RNA viruses sensing of the double-stranded RNA (dsRNA) as an obligatory intermediate of the viral reproduction cycle. Recognition of the dsRNA is mediated by several receptor systems, particularly important for recognition of the coronavirus RNA is RIG-I like helicase MDA5 synergizing with other host dsRNA PRRs (PKR and OAS). Coronaviruses encode multiple proteins that interfere with PRR-mediated viral sensing and subsequent effector viral-controlling mechanisms, most importantly blocking IFN responses

or viral RNA recognition via PAMP receptors. Viral own enzymatic machinery could be involved in this process as coronavirus endoribonuclease (EndoU) targets viral polyuridine sequences to evade activating host sensors.

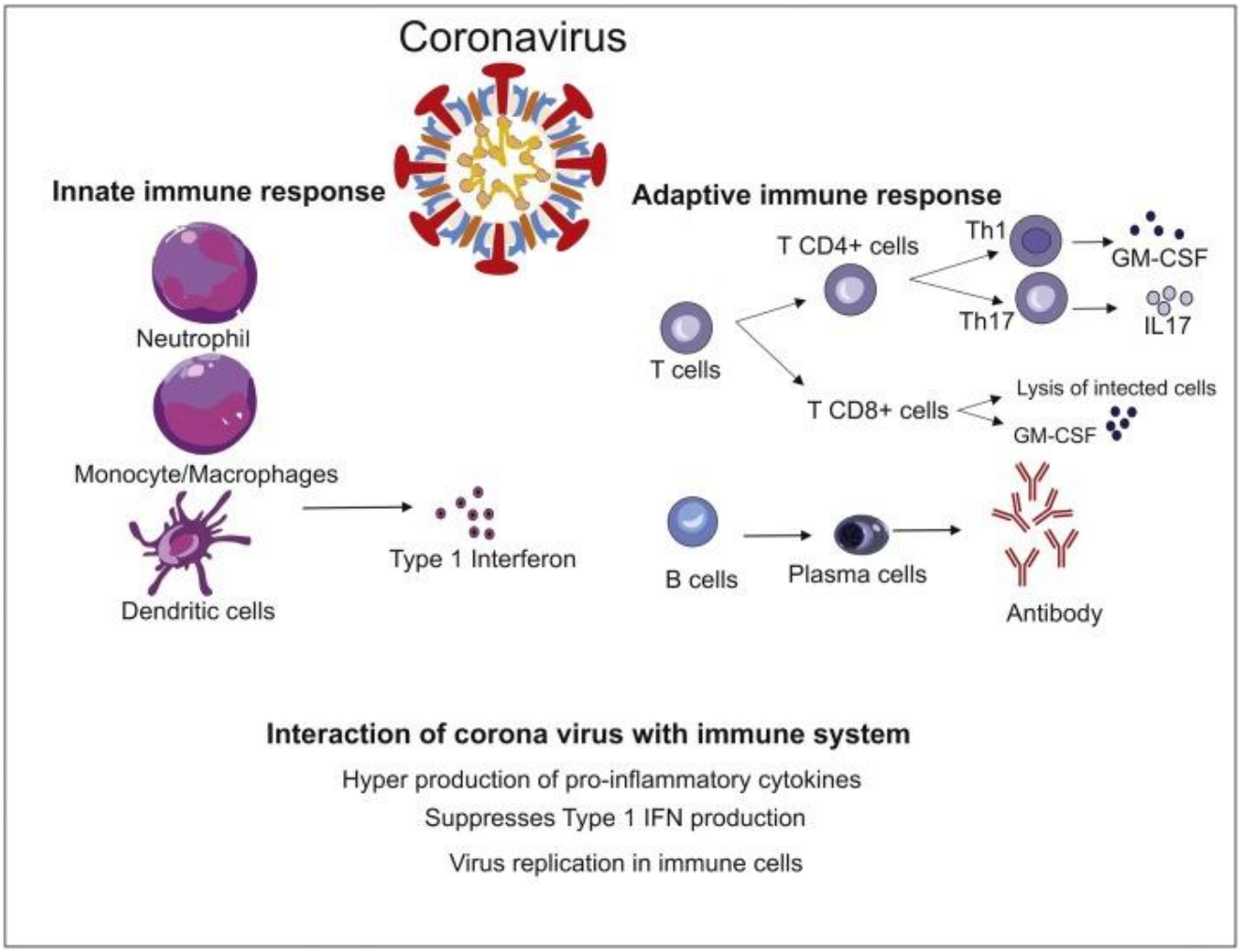

Figure 5. The innate and adaptive immune responses against coronavirus (CoV) infection. The induction of neutrophils, monocytes/macrophages and dendritic cells leads to the production of various pro-inflammatory cytokines , called "cytokine storm". This process results in to lung immunopathology. Specific CD + Tcells, Th1 and Th17,can be activated and exacerbate lung injury. Cytotoxic T-lymphocyte (CTL) contributes to virus clearance by lysis of infected cells. B cells produce virus specific antibodies and neutralize viruses.

Mucosal surfaces, presenting the first line of defense, are protected against the virus via mucosaassociated lymphoid tissues (MALT). Due to the fact that SARSCoV-2 has been described to enter the human body through the respiratory tract, oral mucosa and conjunctival epithelium, mucosal IgA supposedly protects these physical barriers. A trend has been observed with an increase in the IgA response in severe cases of COVID-19. ACE2 is the main receptor for SARS-Cov-2 and allows the virus entry into the cell. Virus infected epithelial cells produce interferons, which are associated with interferon responsive genes and those allow a robust innate immune response to occur. Dendritic cells, macrophages, and

neutrophils as the first line of defense start the immune reaction and affect its type and intensity. These macrophages showed a significant production of IL-6, suggesting they may contribute to the excessive inflammation in COVID19 disease.[19]

2.6.2 COVID-19 and adaptive immunity

The adaptive immune system has the capacity to cause immunopathogenesis.[22] There is a great uncertainty about whether adaptive immune responses to SARS-CoV-2 are protective or pathogenic, or whether both scenarios can occur depending on timing, composition, or magnitude of the adaptive immune response.[23] The innate and adaptive immune systems (**Figure 5**) are often described as contrasting, separate arms of the host response; however, they usually act together, with the innate response representing the first line of host defense, and with the adaptive response becoming prominent after several days, as antigen-specific T and B cells have undergone clonal expansion. Components of the innate system contribute to activation of the antigen-specific cells. Additionally, the antigen-specific cells amplify their responses by recruiting innate effector mechanisms to bring about the complete control of invading microbes. Thus, while the innate and adaptive immune responses are fundamentally different in their mechanisms of action, synergy between them is essential for an intact, fully effective immune response.[49] The adaptive immunity can be subdivided into humoral and cellular response, the first mediated by specific antibodies against the virus and the second mediated by T cells (CD4+ and CD8+).

2.6.2.1 Cellular Immunity

A major role of the T cell arm of the immune response is to identify and destroy infected cells. T cells can also recognize peptide fragments of antigens that have been taken up by APC through the process of phagocytosis or pinocytosis. The way the immune system has evolved to permit T cells to recognize infected host cells is to require that the T cell recognize both a self-component and a microbial structure. The elegant solution to the problem of recognizing both a self-structure and a microbial determinant is the family of MHC molecules. MHC molecules (also called the human leukocyte-associated [HLA] antigens) are cell surface glycoproteins that bind peptide fragments of proteins that either have been synthesized within the cell (class I MHC molecules) or that have been ingested by the cell and proteolytically processed (class II MHC molecules).[49] Once activated in the lymphatic system by APCs antigen presentation, CD4+ T cells induce the expansion of CD8+ T cells and B cells and contribute to viral clearance through the IFN pathways. Based on the expression profiles of cytokines produced, activation of CD4+ *naïve* T cells may result in differentiation into T helper 1 (Th1) CD4+ or T helper 2 (Th2) cells.[50] It is presumed that COVID-19 induces a similar Th1 type immune response as other viral infections. The count of CD8+ T cells was reported to be decreased during COVID-19 infection, and, in severe cases, memory CD4+ T cell and T regulatory cell count was significantly reduced. These findings were accompanied by a decreased number of CD4+ and CD8+ T cells in lymph nodes. Since the most common clinical symptom of COVID-19 remains fever, the involvement of proinflammatory cytokines is

evident. Increased serum levels of IL-6 were observed in more than 50% of the patients. Studies further revealed that as the disease severity progresses, the serum levels of pro-inflammatory cytokines increase as well. This rise of pro-inflammatory cytokines is also associated with the depletion and functional exhaustion of T cells. SARS-CoV-2, similarly to other coronaviruses, restrains antigen presentation by downregulating MHC class I and II molecules, which inhibits the T cell-mediated immune responses.[19]

2.6.2.2 Humoral Immunity

Humoral immune responses also play a substantial role in COVID-19 infections. This kind of immunity is considered to be involved largely in host immune reaction during microbial infection. The multi-isotype antibodies in serum include IgA, IgD, IgG, IgM, and IgE, of which IgG is the most abundant, while IgD and IgE are extremely scarce. Thus, assessment of antibody responses has been focused on the titers of IgA, IgG, and IgM. Antibodies to SARS-CoV-2 can target many of its encoded proteins, including structural and nonstructural antigens. One is the abundant nucleoprotein (NP), which is found inside the virus or inside infected cells. However, because of the biological function of NP and because it is shielded from antibodies by viral or cellular membranes, it is unlikely that NP antibodies can directly neutralize SARS-CoV-2. The second structural protein often used as a target for characterizing the immune response to SARS-CoV-2 is the spike protein.[25] Before the emergence of SARS-COV-2, the only estimation could be done from the immunology memory studies performed on SARS-CoV, where SARS-specific antibodies were maintained for an average of 2 years. The titer of the virus-specific antibodies was correlated with the disease severity, and it has been shown that a high titer of SARS-CoV-2 antibodies serves as an independent risk factor for critical manifestation of COVID-19. It has been shown that COVID-19 patients generate SARS-CoV-2-specific neutralizing antibodies (NAbs), which are produced by B cells after infection with the virus and can block the virus from entering the host cells.[19] Neutralising antibodies(Nab), isolated from COVID-19 patients, were shown to reduce viral titers in animal models, indicating the important role of NAb during control of SARS-CoV-2 infection.[51] It will be critical to understand the robustness of the antibody response in the mild cases, including its longevity and functionality, so as to inform serosurveys and to determine levels and duration of antibody titers that may be protective against reinfection.

Immunological memory is the basis for durable protective immunity after infections or vaccinations. Duration of immunological memory after SARS-CoV-2 infection and COVID-19 is unclear. Immunological memory can consist of memory B cells, antibodies, memory CD4+ T cells, and/or memory CD8+ T cells. Knowledge of the kinetics and interrelationships among those four types of memory in humans is limited. Understanding immune memory to SARS-CoV-2 has implications for understanding protective immunity against COVID-19 and assessing the likely future course of the COVID-19 pandemic. Substantial immune memory is generated after COVID-19, involving all four major types of immune memory. About 95% of subjects retained immune memory at ~6 months after infection. Circulating antibody titers were not predictive of T cell memory. Thus, simple serological tests for SARS-CoV-2 antibodies

do not reflect the richness and durability of immune memory to SARS-CoV.[26] However, to date, there were few studies in characterizing the immune responses, specially adaptive immune responses to SARSCoV-2 infection.[20]

2.7 Strategies for vaccine intervention

In little more than a year, the COVID-19 pandemic has reached every continent, causing 98 million confirmed cases and over 2 million deaths. Equally rapid has been the progress in vaccine development, with clinical trials commencing just months after the initial release of the severe acute respiratory syndrome coronavirus 2 (SARS-CoV-2) genome on Jan 10, 2020.[27] It is important to note that natural infection induces both mucosal antibody responses (secretory immunoglobulin A (IgA) and systemic antibody responses (IgG). The upper respiratory tract is thought to be mainly protected by secretory IgA, whereas the lower respiratory tract is thought to be mainly protected by IgG. It is therefore possible that most vaccines currently in development induce disease-preventing or disease-attenuating immunity, but not necessarily sterilizing immunity.

Traditional vaccine development is a lengthy process (**Figure 6**), and a development time of 15 years is common.[28] The evaluation of safety, immunogenicity and clinical efficacy of vaccines is divided in 3 distinct phases. When there is an effective treatment for a human disease, challenge trials in which volunteers agree to pathogen exposure after vaccination is a valuable means to test vaccines where no animal models are available (eg, HPV and malaria). Phase I studies are focused on safety profile of the vaccine candidate. If the results are promising and funding is available, a vaccine candidate is then moved into Phase II that are focused on establishing an immunogenicity proof of concept and dose ranging (sometimes efficacy data), and larger phase III studies are designed to evaluate whether the dosing and vaccination schedule can deliver the desired impact on the clinical problem with an acceptable safety (efficacy and safety).[52]

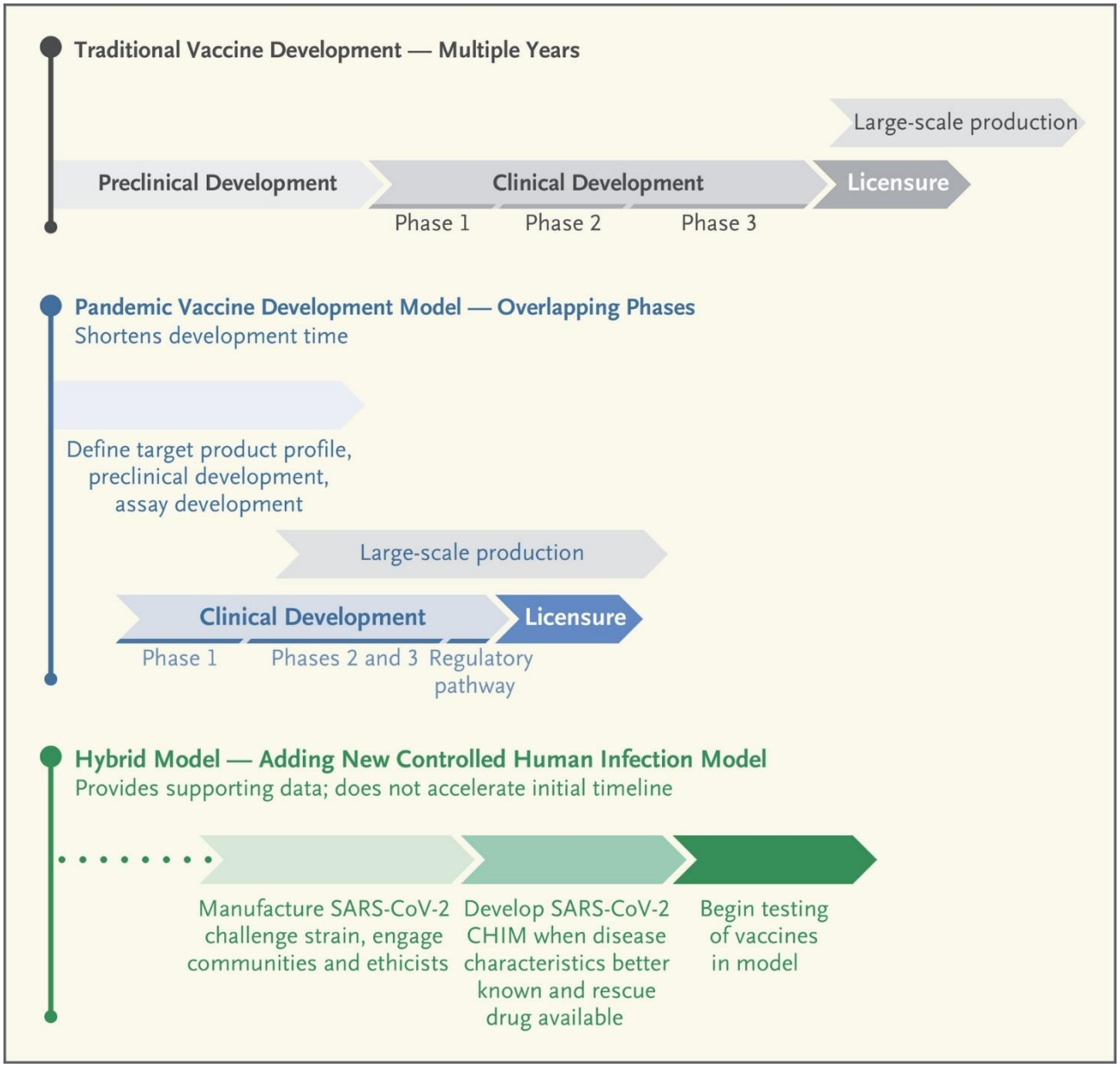

Figure 6. Steps and timelines are shown for traditional and pandemic models of vaccine development. The hybrid approach reflects the addition of a controlled human infection model, illustrating the later start date and steps necessary before vaccine testing could begin.

If the outcome of phase III trials meets the pre-defined end points, a biologics license application is filed with regulatory agencies.. Currently, both classic vaccine platforms and next-generation vaccine platforms can be distinguished. Classic include those that are based on vaccines already licensed and used in humans. These vaccines are either virus-based or protein-based.[28] The next generation vaccines do not require the actual viral particle and can be developed solely on the sequence of the antigenic viral proteins. The material present in the vaccine containing information about the protein coding sequence leads to its biosynthesis and thus to an immune response. Next-generation vaccines include viral vector, nucleic acid-based and antigen-presenting cells vaccines.[29]

Vaccine technology has significantly evolved in the last decade, including the development of several RNA and DNA vaccine candidates, licensed vectored vaccines (e.g., Ervebo, a vesicular stomatitis virus [VSV]-vectored ebolavirus vaccine, licensed in the European Union), recombinant protein vaccines (e.g., Flublok, an influenza virus vaccine made in insect cells, licensed in the United States), and cell-culture-based vaccines (e.g., Flucelvax, an influenza virus vaccine made in mammalian cells). SARS-CoV-2 was identified in record time, and its genomic sequence was swiftly made widely available by Chinese researchers. In addition, data from the preclinical development of vaccine candidates for SARS-CoV and MERS-CoV enabled the initial step of exploratory vaccine design to be essentially omitted, saving a considerable amount of time.[28] It is known from studies on SARS-CoV-1 and the related MERS-CoV vaccines that the S protein on the surface of the virus is an ideal target for a vaccine. In SARS-CoV-1 and SARS-CoV-2, this protein interacts with the receptor ACE2, and antibodies targeting the spike can interfere with this binding, thereby neutralizing the virus. The structure of the S protein of SARS-CoV-2 was solved in record time at high resolution, contributing to our understanding of this vaccine target.[30] Most of the COVID-19 vaccine development projects ongoing all over the world are using S protein as target antigen. The full length spike glycoprotein or RBD of virion are able prevent host and virus interaction by inducing neutralizing antibodies and hence is considered as most important vaccine target antigen.[31] The World Health Organization (WHO) has set forth essential criteria for conducting SARS-CoV-2 challenge studies. Minimizing risk to participants, staff, and the community and ensuring robust scientific and clinical standards are critical considerations.[32] The first clinical trial of a vaccine candidate for SARS-CoV-2 began in March 2020. Trials were designed such that clinical phases are overlapping and trial starts are staggered, with initial phase I/II trials followed by rapid progression to phase III trials after interim analysis of the phase I/II data. The FDA has released a guidance document for the development and licensure of SARS-CoV-2 vaccines, which—as well as providing additional details—states that an efficacy of at least 50% will be required. It is very important to point out that moving forward at financial risk is the main factor that has enabled the accelerated development of SARS-CoV-2 vaccine candidates, and no corners have been or should be cut in terms of safety evaluation.[28]

2.7.1 Sars-Cov-2 vaccine types

2.7.1.1 SARS-CoV-2 vaccine production platforms: Replicating and non replicating vectors

Based on their capability to replicate in the host cell, these can be replicating and non replicating recombinant viral vectors. These are evaluated as delivery of viral genome encoding the gene of interest. The longevity of the immune response generated by vaccine depends on the type of viral vector used. The most commonly used viral vector is the Adenoviral (Ad) vector. The major advantage of this platform is the capability to induce both humoral and cellular immunity. Despite the complex production of viral vector based vaccines, these are known to induce strong immunological response. However, sometimes

these are not capable of inducing immunogenicity due to the presence of preexistent immunity.[31]

Several Ad vector features are particularly attractive for vaccine use. Ad5 has been the most extensively developed non-replicating Ad vector. A recent finding of long-term persistence of replication defective Ad-recombinant-induced CD8+ T cells in mice indicated that the recombinant Ad genomes were transcriptionally active at low levels for long periods of time. In this regard, the non-replicating recombinants exhibited some features of replication-competent Ad, as the mice maintained active effector CD8 T cells as well as central memory T cells. The extent to which this characteristic impacts vaccine efficacy is a subject for further investigation. Whether replicating Ad-recombinants exhibit greater persistence because of their initial robust replication *in vivo* will also require further study. Replication-competent Ad vectors share the common features of replication-defective vaccines. The main scientific advantage of replicating Ad-recombinants is their mimicking of a natural Ad infection, resulting in induction of cytokines and co-stimulatory molecules that provide a potent adjuvant effect. Overall, the replicating vector can provide a complete immune response, including elements of innate immunity, an important component of a rapid response to an invading organism, as well as humoral, cellular, and mucosal immune responses.[35] A recombinant replicating vaccine, Ervebo is licensed in the European Union as ebolavirus vaccine. The adenoviral vector Ad5 being used for COVID-19 vaccine development is a cost effective approach and has already been used for Ebola virus.

One of the limitations of Ad5 vectors is their association with high prevalence in the human population and therefore an additional trial using chimpanzee derived adenoviruses (ChAd) is being conducted to combat preexisting immunity. Currently, there are 9 COVID-19 vaccine candidates developed using non replicating vector platform in clinical evaluation and 19 candidates in preclinical evaluation stage. Four COVID-19 vaccine candidates developed using replicating vector platform is in clinical evaluation stage and 18 candidates are in preclinical evaluation stage.[31]

2.7.1.2 DNA platform

Were introduced two decades ago and these are non-infectious and non-replicating. These are easy to produce within a short duration and are stable and cost-effective at the same time. These confer long term immunogenicity to the host, however these remain hopeless when used in humans due to their poor immunogenic property. Also these are easily degraded by host enzymes and there is always the risk of its integration into host DNA.[31]

2.7.1.3 RNA platform

In this different type of vaccines, the mRNA is directly injected into the host's cell, which undergo translation in the cytoplasm (**Figure 7**). Currently, there are two kinds of mRNA-based vaccines established: non-amplifying mRNA based vaccines and self-amplifying mRNA based vaccines. The self-amplifying mRNA based vaccines (SAM) capable of being rapidly

developed are potentially feasible for epidemics or disease outbreaks.[31] The technology has so many advantages over conventional vaccine approaches. Once immunized with the vaccine, the mRNA can be translated for a long period of time, "on site" in the body, thus saving time/costs that would have been associated with expressing and purifying the proteins (in the correct conformation) in the lab. In addition to this, the spike protein, once expressed in the body, is post-translationally modified, thus circumventing post-translational modification-related issues associated with proteins expressed in the lab[34].

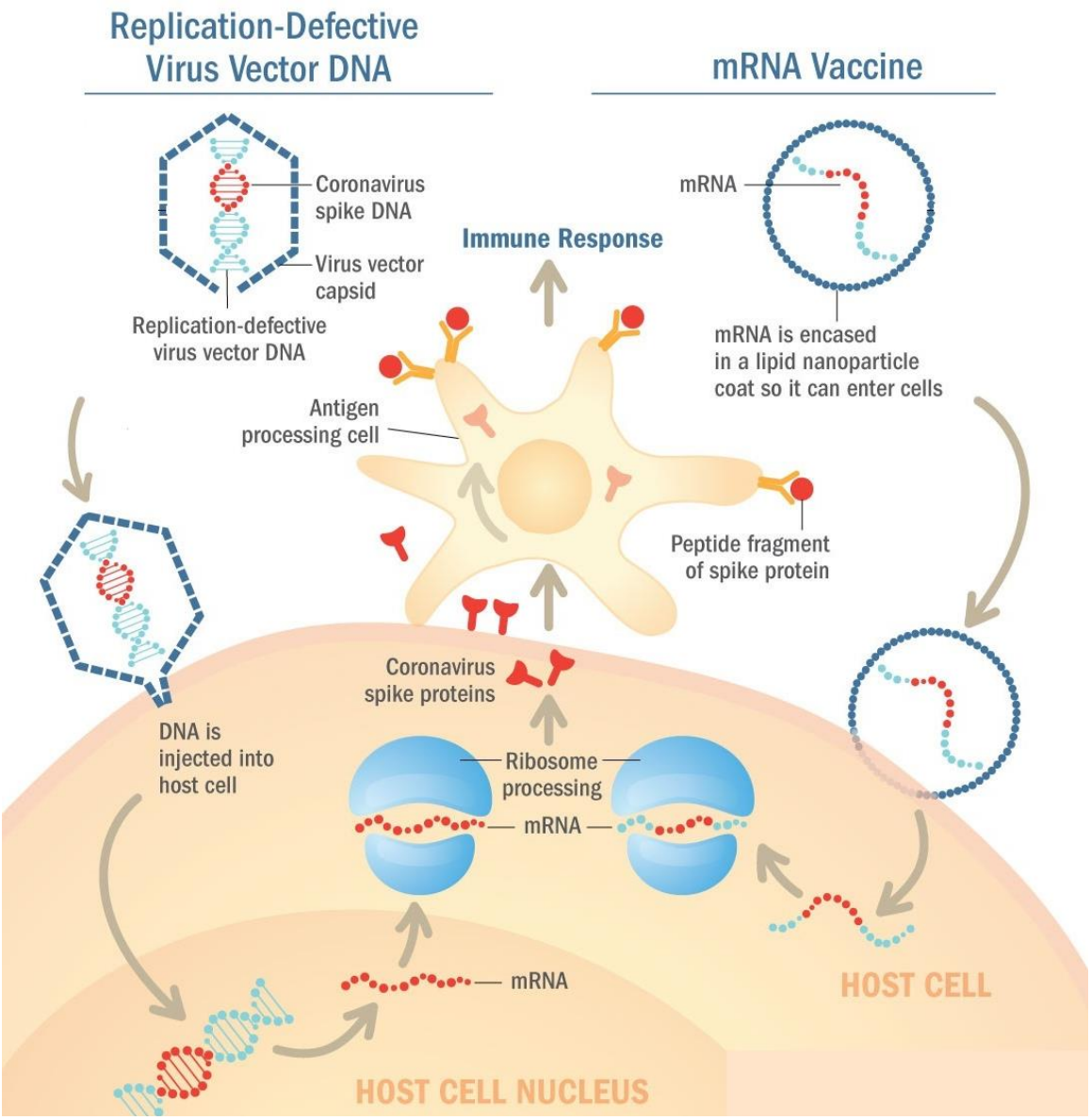

Figure 7. Replication-defective virus vector DNA and mRNA vaccines (from https://www.mdedge.com). In the DNA and mRNA vaccines the nucleic acid codifying for an immunogenic protein of the pathogen is captured by antigen-presenting cells that use it to express and present the antigen.

2.7.1.4 Recombinant protein based vaccine

Highly purified recombinant proteins from different etiologic agents are most common candidates under investigation for vaccines. Different genes from virus particles encoding the antigenic determinant have been processed (cloned, expressed in various expression system and purified) as recombinant proteins and established as vaccines [31].

2.7.1.5 Live attenuated vaccines

The most common traditional method which involves manually weakened live pathogen which is no longer able to induce infection but able to induce immune response and hence mimic features of natural infection. These kind of vaccines are easy to produce for some viruses but challenging for complex pathogens. Currently, there are only 3 candidates as COVID-vaccines and they are in preclinical evaluation stage [31].

2.7.1.6 Inactivated vaccines

These are produced by completely inactivating or killing the pathogen, on injecting it to the host, they primarily induce protective antibodies against epitopes present on thesurface of virus. These vaccines tend to produce a weaker immune response than live attenuated vaccines, [31-33] thus they require several doses because the microbes are unable to multiply in the host and so one dose does not give a strong signal to the adaptive immune system; approaches to overcome this include the use of several doses and giving the vaccine with an adjuvant.[33]

2.8 Serological Methods for Evaluation of Sars-CoV-2 Vaccines Immunogenicity

Validated and accurate laboratory testing for SARS-CoV-2 is a crucial part of the timely management of COVID-19 disease, supporting the clinical decision-making process for infection control at the healthcare level and detecting asymptomatic cases. The relatively qiuick discovery of the composition of the full genome of SARS-CoV-2 early during the epidemics made it easier to develop specific starters and normalized laboratory protocols for COVID-19.[36]

An important application of serological tests is to understand the antibody responses mounted upon SARS-CoV-2 infection and vaccination. Assays that inform on antibody titer and/or show antibody functionality (e.g., virus neutralization) will be extremely useful to answer important scientific questions about immune protection from reinfection. Several academic laboratories have developed robust, specific serological assays. The key challenge will be to apply and deploy these tests in a strategic manner to safely bring communities out of the current pandemic response back to the realm of “normal” life.[53] Vaccine-induced

immune responses are often multifaceted, but single components such as antibody responses may correlate with the level of protection. In fact, most of the currently accepted correlates of protection are based on antibody measurements. Two studies, by Khoury et al. and Earle et al. , now connect neutralizing antibody responses to SARS-CoV-2 with vaccine efficacy and bring researchers and clinicians closer to having a correlate of protection for vaccines against COVID-19.[54] Understanding the relationship between measured immunity and clinical protection from SARS-CoV-2 infection is urgently needed to plan the next steps in the COVID-19 vaccine program. Placebo-controlled vaccine studies are unlikely to be possible in the development of next-generation vaccines, and therefore correlates of immunity will become increasingly important in planning booster doses of vaccine, prioritizing next-generation vaccine development, and powering efficacy studies. The work of Khoury et al. [55] uses available data on immune responses and protection to model both the protective titer and the long-term behavior of SARS-CoV-2 immunity. It suggests that neutralization titer will be an important predictor of vaccine efficacy in the future as new vaccines emerge. The model also predicts that immune protection from infection may drop with time as neutralization levels decline, and that booster immunization may be required within a year. However, protection from severe infection may be considerably more durable given that lower levels of response may be required or alternative responses (such as cellular immune responses) may play a more prominent role. To date, RT-PCR is the most widely employed method of diagnosing COVID-19. However, rapid, large-scale testing has been prevented by the high volume of demand and the shortage of the materials needed for mucosal sampling. Standardized serological assays able to measure antibody responses may help to overcome these issues and may support a significant number of relevant applications. Indeed, serological assays are the basis on which to establish the rate of infection (severe, mild and asymptomatic) in a given area, to calculate the percentage of the population susceptible to the virus and to determine the fatality rate of the disease. It has been demonstrated in a non-human primate model that, once the antibody response has been established, re-infection and, consequently, viral shedding, is unlikely. Furthermore, serological assays can help to identify subjects with strong antibody responses, who could serve as donors for the generation of monoclonal antibody therapeutics. The S-protein has been found to be highly immunogenic, and the RBD is possibly considered the main target in the effort to elicit potent neutralizing antibodies. [38]

The Enzyme Linked-immunosorbent assay (ELISA) is one of the most used method for total antibodies detection. This method is able to detect all the immunoglobulins (class and subclass) present in a given sample able to bind the specific antigen of interest coated in a dedicated plate. It is fast, cheap and safe because it does not require the handling of live pathogens. The ELISA suffer from the fact that it is not able to give a precise indication about the functionality of the antibodies detected.[56] Given this limitation, the neutralization assay is an attractive alternative for the assessment of baseline sero-status and the evaluation of the humoral responses following natural infection and/or vaccination.[57]

To date, the complexity of the systemic immunoglobulin G (IgG) together with IgG subclasses and IgM and IgA, in terms of responses against SARS-CoV-2, have not been elucidated yet. Moreover, data comparing the differences between these responses and the neutralizing responses detected by functional assays such as Micro-Neutralization test (MN), are still not well defined. Undoubtedly, it is well recognized that the IgG levels have a crucial role for protection from viral disease. In humans, the four IgG subclasses (IgG1, IgG2, IgG3, IgG4) differ in function and IgG1 and IgG3 play a key role in many fundamental immunological functions, including virus neutralization, opsonization and complement fixation.[38]

2.8.1 Enzyme Linked Immunoassobent Assay (ELISA)

Compared to the other serological assays, the ELISA can be implemented to measure different immunoglobulin (Ig) classes (IgM, IgA, and IgG) and subclasses (IgG1, IgG2, IgG3, etc) of specific antibodies in serum samples and nasal washes by using subclass/isotype-specific conjugated secondary antibodies. ELISA measures the actual amounts of Ig, and the use of standards allows good intra- and interlaboratory agreement. This assay is particularly suitable for testing large panels of samples for several reasons. Primarily because ELISA is less-time consuming, more cost-effective, and easier to perform compared to previously mentioned serological assays. Furthermore, it can be fully automated. Additionally, the ELISA reagents can be standardized with a positive impact on results reproducibility. Another advantage of the ELISA is that a wide range of antigen preparations (whole-inactivated virus, subunit vaccines or purified antigens) can be used as coating antigens[39] and a further advantadge is the possibility of avoiding the requirement for a high containment laboratory (Biosafety level 3, BSL3). However, most of these assays present some limitations, such as low specificity and sensitivity, and use of alternative purified proteins that can be produced in different hosts (human-derived cells vs insect cells). In addition, the mismatch between results obtained from the same samples, using different ELISA reagents and coatings (eg, source of antigen), may lead to confusion. To date, the Micro-Neutralization assay (MN), currently considered the gold-standard is the most specific and sensitive serological assay capable of evaluating and detecting, functional neutralizing antibodies.[10]

2.8.2 Micro-neutralisation assay (MN)

MN assays were developed in 1990.[58-59] This is a functional assay, and it is able to detect neutralizing antibodies capable of prevent the virus infection of different mammalian cell lines. The neutralization activity is then measured as the ability of the sera to reduce the cytopathic effect (CPE) due to inhibition of viral entry and subsequent replication.[55] Compared to the ELISA-based methods, the results derived by the MN represent a more precise and relevant estimation of antibody-mediated protection in-vitro.[60] On the other hand, MN is more complex to manage due to some requirements: the need of live viruses and biosecurity level 4, 3 or 2+ laboratories (in case of class IV, III or II pathogens), the costs associated with the assay and the difficulties in protocol standardization across laboratories (e.g. cell lines,

infective dose, days of incubation and readout).[56] Neutralizing antibodies are a key component of adaptive immunity against many viruses that can be elicited by natural infection or vaccination.[40] Neutralising antibodies can be detected using the MN assay and plaque reduction neutralisation test. These assess the ability of patient-derived serum samples containing SARS-CoV2-specific antibody to inhibit infection of cells cultured in vitro.[41] Two of the more common methods for measuring the immunogenicity of the COVID-19 vaccine candidates are the the MN endpoint dilution assays based on the cytophatic effect (CPE), which in turn requires a cell line that can be infected and killed by the virus of interest and the ViroSpot microneutralization assay. Coronaviruses have been demonstrated to be capable of infecting Vero E6 cell line that are commonly used for virus production and for MN assays.[42]

2.8.2.1 Microneutralisation assay CPE-based (MN CPE)

The conventional MN assay is based on inhibition of the virus-induced cytopathic effect (CPE) on susceptible cells. In the MN CPE-based (MN-CPE) assay, serially diluted serum samples are pre-incubated with a standard amount of virus. Afterwards, the serum/virus mixture is added to 96-well plates pre-seeded with a standard concentration of cells. The plates are then incubated at 37°C, 5%CO_2 and the readout can be performed 3 days later under an optical microscope. Non-neutralized viruses will infect the cells, making it possible to determine which is the highest serum dilution that induces at least 50% inhibition of CPE.[60]

2.8.2.2 ViroSpot MN assay

The Virospot MN assay is a novel assay that combines classic virus culture in multi-well microtiter plates and virus specific immunostaining[44] (**Table 1**). The readout for this assay is based on staining of the virus nucleoprotein (NP), which provides quantitative assessment of inhibitory concentration and does not rely on cumbersome and subjective visual inspection of cytopathic effect.[43]

This assay has been recently developed for automated imaging, detection and counting of infected cells using the SX UV analyzer. A precise counting procedure and quality control are required to allow a reliable measurement of inhibitory concentration 50% (IC50) values of the antibody/inhibitor concentration, as well as the Plaque Forming Units (PFU) or the Tissue Culture Infectious Dose 50% (TCID50) measurement of the virus. The ViroSpot MN assay offers several favorable properties: a standardized dose of input test virus with limited influence of the virus replication kinetics and cell-to-cell transmission, limiting its sensitivity to variation in input virus dose, in contrast to other MN formats, and infected cells are detected in an automated fashion, based on a precipitating substrate, suitable for high throughput use.[44] In the MN Virospot assay serially diluted serum samples are pre-incubated with a standard amount of virus. After 1 hour, the mixture is added to a 90% confluent monolayer of Vero E6 cells. The plates are then incubated for 24 hours at 37°C in a humidified atmosphere with 5% CO2. The day after virus-infected cells are immunostained with a monoclonal antibody which targets the SARS-CoV NP protein, followed by a secondary goat anti-mouse IgG peroxidase conjugate and TrueBlue substrate. This forms a blue precipitate

on NP positive cells. Images of all wells are acquired by a CTL ImmunoSpot analyzer, equipped with software to quantify the NP-positive cells (= virus signal). The 50%,80% 90% neutralization titers are calculated according to the method described by Zielinska et al.[61] This titer calculation is based on the serum dilutions above and below the reduction point, here 50% 80% or 90% neutralization:

$X = (a-b)(e-c)/(c-d) + a$

Where:
a = log10 of dilution above the 50%, 80%,90% reduction point
b = log10 of dilution below the 50%, 80%,90% reduction point
c = average % Spots above the 50%, 80%, 90% reduction point (corresponds with a)
d = average % Spots below the 50%, 80%, 90% reduction point (corresponds with b)
e = value of 50%,80%, 90% reduction of average virus control count
X is the exponent of the Log10 titer.

	Process	MN CPE	VIROSPOT MN
Test virus preparation	*Dilution Factor*	To obtain 100 TCID50/well	To obtain 30-350 spots/well
	Target concentration	Depends on kinetics of virus replication and cell to cell trasmission.	30-350 spots/well
Neutralisation method	*Mix virus and serum*	60 min	60 min
	Indicator cells (VEROE6) to monitor	Add mix serum virus to semi-confluent cell monolayer	Add mix serum virus to confluent cell monolayer
	Replace Inoculum with overlay fresh medium	No	Yes, replace inoculum with medium after 60 min
	Incubation	3 days	18-20 hrs
	Fixation of cell monol	No	Formalin
	Read-out	Optical microscope: Observation of the cytocpatyc effect in each well	NP-Immunostaining (True Blue)
	Signal	No	Well area covered
	Neutralisation titer	The highest serum dilution that induces at least 50% inhibition of CPE	Serum dilutions above and below the reduction point, 50% 80% or 90% neutralization described by Zielinska et al.

Table 1. Microneutralisation (MN) assay: Comparison of similarities and differences of MN CPE and Virospot MN.

2.8.2.3 Pseudotypes-based microneutralization assay

Working with the SARS-CoV-2 virus, designated as a Category 3 biosafety level pathogen, implies the need for high biosafety levels laboratories (BSL3). By contrast, pseudotyped viruses (PVs) bearing the SARS-CoV-2 spike protein permit extensive and widespread serum/plasma screening in a BSL2 laboratory. This system, which has already been successfully adopted in the fight against emerging and re-emerging viruses, constitutes a useful, safe and versatile tool for studies on viral tropism, vaccine immunogenicity, efficacy of antiviral compounds, including therapeutic mAbs, and serosurveillance studies [86-87].
Pseudotypes or pseudotype particles are chimeric “viruses” made by a surrogate virus core surrounded by a lipid envelope with the surface glycoproteins of another virus. By removing the genetic element of the virus being studied, and replacing it with a suitable reporter, viruses, can be studied in this safer, single-step infection and therefore provides a poor model for real infectious processes.The use of cores from lentiviral human immunodeficiency virus

(HIV) and gammaretroviruses such as murine leukemia virus (MLV) predominate in the influenza pseudotype literature. Recent development of systems involving rhabdoviruses, in particular the vesicular stomatitis virus (VSV), has also been used to produce SARS-CoV-2 pseudotype with promising results [90]. Replication-competent recombinant VSVs (rVSVs) are a far more authentic and powerful tool for investigating infection both in vitro and in vivo [88-89]. The simple structure and rapid high titer growth of VSV in mammalian and many other cell types has made it a favored tool for molecular and cell biologists in the past years, and this was further strengthened with the establishment of the reverse genetic system for VSV. The VSV system has already been used to generate pseudotype virus for studying the role of the Ebola virus transmembrane glycoprotein in cell entry. The use of pseudotype particles is limited to a single-step infection and therefore provides a poor model for real infectious processes. Replication-competent recombinant VSVs are a far more authentic and powerful tool for investigating infection both in vitro and in vivo. Such recombinant viruses may help to overcome some of the limitations required to work with viruses that require BSL3 and BSL4 containment [89]. However, the question of which core to use to produce pseudotypes often depends on preference and availability [88].

2.9 SARS-CoV-2 Variants Of Concern

Since the pandemic began in China in December 2019, thousands of SARS-CoV-2 variants have emerged.[62] Despite the extraordinary speed of vaccine development against COVID-19 and continued mass vaccination efforts across the world, the emergence of these new variants strains could render vaccine-induced or naturally immune humans vulnerable to re-infection and such possible effects are still under investigation.[64] A subset of these variants have been denoted as Variant Of Concern (VOC) by the WHO[69] (**Figure 8**). The VOCs are associated with enhanced transmissibility or virulence, reduction in neutralization by antibodies obtained through natural infection or vaccination, the ability to evade detection, or a decrease in therapeutics or vaccination effectiveness.[62-68] There are currently four COVs that the Center for Disease Control and Prevention (CDC) is monitoring: Alpha, Beta, Gamma and Delta variant.[66]

2.9.1 Alpha variant

The first major variant of concern was observed in December 14, 2020, in United Kingdom. It has been estimated that the variant, reported as SARS-CoV-2 VOC, lineage B.1.1.7, also referred to as VOC 202012/01 or 20I/501Y.V1, has emerged in September 2020 and has quickly become the dominant circulating SARS-CoV-2 variant in England [63] and became known as the “alpha” variant according to the WHO[65]. It causes point mutations of asparagine to tyrosine in the receptor-binding domain (RBD) of the spike protein. This N501Y mutation

became a growing concern due to the virus being able to adhere to the ACE2 receptor more strongly.[63]

2.9.2 Beta variant

The second major VOC was the 501Y.V2 variant in South Africa, labeled as the Beta variant according to the WHO[65]. This strain is characterized by mutations in the S protein, including residues in the RBD—K417N, E484K, and N501Y.[62]

2.9.3 Gamma variant

One of Brazil's discovered variant of SARS-CoV-2 is the P.1 variant, a descendant of B.1.1.28. This a highly different variable, which includes the E484K, K417T and N501Y mutations. According to the WHO has been labeled has the Gamma variant. The N501Y, K417N, and E484K mutations, which are also found in the Alpha and Beta variants, have been associated with enhanced binding affinity to human ACE2 and an increase in the transmissibility [64].

2.9.4 Delta variant

The most notable gene mutations that are suspected to allow the Delta variant, B.1.617.2 to be the most transmissible variant are the mutations found in the spike proteins. The Delta variant of SARS-CoV-2 bears 23 mutations compared to the first one (Alpha variant). Twelve of those mutations are in the spike protein. The more the spike proteins mutate, the harder it is for the immune system to identify them and for the antibodies to attach for the subsequent eradication of the virus. This new spike protein evading the immune system allows for a better attachment to human cells, thus infecting them more effectively[66]. The rapid spread of the highly transmissible Delta variant has continued to drive sharp resurgences in the three months since the last risk assessment in many countries across all six WHO regions. In almost all countries in which Delta has been reported, it has replaced all other variants including other VOCs, quickly becoming the dominant circulating variant.[67]

Currently designated Variants of Concern:

WHO label	Pango lineages	GISAID clade	Nextstrain clade	Additional amino acid changes monitored*	Earliest documented samples	Date of designation
Alpha	B.1.1.7	GRY	20I (V1)	+S:484K +S:452R	United Kingdom, Sep-2020	18-Dec-2020
Beta	B.1.351 B.1.351.2 B.1.351.3	GH/501Y.V2	20H (V2)	+S:L18F	South Africa, May-2020	18-Dec-2020
Gamma	P.1 P.1.1 P.1.2	GR/501Y.V3	20J (V3)	+S:681H	Brazil, Nov-2020	11-Jan-2021
Delta	B.1.617.2 AY.1 AY.2	G/478K.V1	21A	+S:417N	India, Oct-2020	VOI: 4-Apr-2021 VOC: 11-May-2021

Figure 8. SARS-CoV-2 Variants of Concern as of 29 July 2021 (SARS-CoV-2 variants of concern as of 22 December 2021 (europa.eu).

2.10 MN VIROSPOT optimization

The SARS-CoV-2 virus is continuously evolving with many variants emerging across the world that allowed the virus to escape human immunity easier. As there was little or no natural immunity in the human population or specific anti-COVID-19 drugs, vaccines were developed at an unprecedented speed to stop the pandemic.[70]

At the time that the MN VIROSPOT was started and validated was available for the SARS-CoV-2 Wild type strain for measuring SARS-CoV-2 neutralizing antibodies in serum samples taken from naturally immunised human samples. However, during the last period, interpretation of the MN VIROSPOT results has become complicated because of mutations occurred in the virus. For instance, quantitation of plaque numbers in a plaque reduction assay is difficult when there is a significant variation in plaque size induced by individual viruses.[71]

Some different conditions were tested in order to optimize this assay and to obtain a more sensitive results for all the SARS-CoV-2 variants occurred so far.

The optimization has been focused on:

1) The benefit of the application of the carboxymethyl cellulose (CMC) at 1%,2% and 3% (final concentration). Indeed, after the virus inoculation the CMC is used as an immobilizing overlay medium to prevent viral infection from indiscriminately spreading through the mechanical flow of the liquid in order to have a well-defined spots count.
2) The effect of an alternative culture medium (MEM) without the use of CO2 on MN titer results and spot counts.
3) The effect on MN titer and spot count by using different time points for the pre-incubation of the serum/virus mixture and for the second incubation of the serum/virus mixture on the VERO E6 cells.
4) The effect on MN titer spot count by using different temperatures during the first incubation period (serum/virus mixture)
5) That both serum samples and EDTA plasma samples can be uses in this assay. The samples originate from the same donor and same timepoint after infection with SARS-CoV-2 virus.

The optimization of this assay has been performed using four different SARS-CoV-2 variants: Wild Type, Alpha, Beta and Gamma.

3. AIM OF THE STUDY

The aim of the present study was to compare different microneutralization methods which can be used to quantify anti-SARS-CoV-2 neutralizing antibodies (nAbs) in human samples. The first project was focused on the comparison of a microneutralization assay (MN) with a read out based on the cytophatic effect (CPE) and a MN based on a colorimetric read out (Colorimetric MN CPE) for the detection of nAbs against SARS-CoV-2 Wild type strain.

In the first method the cell monolayer was microscopically inspected for inhibition of CPE at each serum dilution (subjective read out) while, in the Colorimetric MN CPE, the healthy cell monolayer was stained with neutral red solution, a vital dye. The plates were then read by a spectrophotometer at 540 nm (objective read out). A panel of 83 human serum samples has been previously tested in enzyme-linked immunosorbent assay (ELISA) as a pre-screening. All the samples found to be positive, borderline, and negative in this ELISA were then tested to determine the nAbs titers through the MN CPE and the Colorimetric MN CPE.

To better investigate if the classical MN CPE correlate with other new MN methods, the second aim of this study focused on the comparison of the MN CPE and a new MN platform: the Virospot MN assay. In this method, a virus specific immunostaining was used as readout and then the images of all wells were acquired by a CTL ImmunoSpot analyzer. It combines classic virus culture techniques with automated sensitive detection of immunostained virus infected cells.

These two MN methods were compared using a panel of 47 human serum samples against SARS-CoV-2 Wild type strain.

To conclude this research project the third aim focused on the optimization and assesment of the Virospot MN assay robustness for the detection and quantification of neutralizing antibodies against four different SARS-CoV-2 variants in human samples.

Serum and plasma samples (originating from the same donor) were compared against the four different SARS-CoV-2 variants Wild type, Alpha, Beta, Gamma. Furthermore, to optimize the assay performance, the use of the carboxymethyl cellulose (CMC) at different concentrations (1%,2%, 3%) was implemented and evaluated at different time points (8,24,32 hours) and the effect of an alternative culture media without the supplementation of external CO2 was evaluated on MN titer results. Different timepoints (30 minutes, 60min, 120 min) for the pre-incubation of the serum/virus mixture and for the second incubation of the serum/virus mixture on the VERO E6 cells, as well as different temperatures (37°C/room temperature) during the pre-incubation period were investigated for evaluating the effect on MN titers and spot counts.

4. MATERIALS AND METHODS

4.1 MATERIALS

4.1.1 Samples

To compare MN CPE, MN Colorimetric CPE and ELISA assay (Project I) a total of 83 human serum samples were collected as part of a seroepidemiological study performed in the laboratory of Molecular Epidemiology of the University of Siena, Italy. Serum samples were anonymously collected in compliance with Italian ethics law. The human monoclonal antibody IgG1-CR3022 (absolute antibody) was tested along with the serum samples in the MN assay and ELISA. Hyperimmune sheep antisera against Influenza A/H1N1/ California/7/2009 (10/218), B/Brisbane/60/2008 (13/312), and A/Anhui/ 1/2013 (15/248) strains were purchased from the National Institute for Biological Standard and Controls (NIBSC, UK) and used as negative controls. Hyperimmune rabbit serum samples against Adenovirus Type 4 (V204-502-565) were provide by the National Institute of Allergy and Infectious Diseases (NIH, Bethesda). Human serum minus IgA/IgM/IgG (S5393-1VL) (Sigma, St. Louis, MO) was used as a negative control.

To compare MN CPE and Virospot MN assays (Project II), a panel of 30 human commercial serum samples (BIOIVT, Cambridge Biosciences) and another panel of 15 pre-pandemic samples (2015) collected by the laboratory of Molecular Epidemiology of the University of Siena, were used. Samples were previously heat-treated at 56°C for 30 minutes, and then tested against SARS-CoV-2 Wild type and SARS-CoV-2 Alpha (B.1.1.7) variant. Information about gender and age was not provided. The convalescent human serum samples S.46-S.47 (BIOIVT) and the human serum pool S.48 (Boca Biolistics) were used as positive controls.

Eleven matched serum and EDTA plasma samples (from identical donations) taken from convalescent patients were purchased from In.vent Diagnostica GmbH (Hennigsdorf , Germany) and used for the third project (Project III) in which the Virospot MN assay was optimized. Information about gender and age are reported in the Appendix 1. As done with the previous panels, these samples were heat inactivated at 56°C for 30 minutes and tested against four SARS-CoV-2 variants: Wild type BavPat1/2020, Alpha (B.1.1.7), Beta (B.1.351) and Gamma variant (P.1). The following positive control sample was used: COVID-19 convalescent pooled serum, VC-Lot# VC-2120140051, individual serum obtained from Boca Biolistics.

4.1.2 Cells

VERO cells, an African Green monkey kidney cell line, were purchased from the European Collection of Authenticated Cell Cultures (ECACC - Code 84121903). VERO cells were cultured in Eagle's minimum essential medium (EMEM) (Lonza, Milano, Italy) supplemented with 2 mM L-Glutamine (Lonza, Milano, Italy), 100 IU/mL penicillin-streptomycin mixture (Lonza, Milano, Italy) and Fetal Bovine Serum (FBS) (Euroclone, Pero, Italy) to a final concentration of 5%, at 37°C, in a 5% CO2 humidified incubator. VERO E6 cells, an epithelial cell line from the kidney of a normal monkey (Cercopithecus aethiops), were acquired from the American Type Culture Collection (ATCC - CRL 1586). Huh-7 cells, an epithelial cell line from Human hepatocellular carcinoma, were kindly provided by the University of Siena (ECACC- Code 01042712). Both VERO E6 and Huh-7 cells were cultured in Dulbecco's Modified Eagle's Medium (DMEM)-high glucose (Euroclone, Pero, Italy) supplemented with 2 mM L-Glutamine (Lonza, Milano, Italy), 100 IU/mL penicillin-streptomycin mixture (Lonza, Milano, Italy) and 10% of FBS, at 37°C, in a 5% CO2 humidified incubator. Adherent sub-confluent cell monolayers of VERO, VERO E6, and Huh-7 were prepared in growth medium, E-MEM or D-MEM high glucose containing 2% FBS in T175 flasks or 96-well plates for propagation or titration and neutralization tests of SARS-CoV-2, respectively. Cell lines above described were used in setup experiments aimed at determining the best culture conditions for MN CPE and MN colorimetric assay. VERO E6 cells cultured as above were chosen as the cell line to be used in the MN CPE and MN colorimetric assays.

Vero C1008 (Vero76, clone E6, Vero E6), purchased from the American Type Culture Collection (ATCC CRL-1586), were used for performing the MN VIROSPOT. VeroE6 for MN Virospot were cultured in:

- Dulbecco's Modified Eagle's Medium (DMEM)-high glucose (Euroclone) supplemented with 200 mM L-Glutamine (Lonza), 1000 IU/mL penicillin-streptomycin mixture (Lonza) and 10% of Fetal Bovine Serum (FBSHI, Capricorn Scientific), at 37°C, in a 5% CO2 humidified incubator. One day before inoculation, the cells were seeded in a 96-well plate at such a density that a confluent monolayer (≥ 90%) is achieved at the day of the assay (1.5 x 10^4 cells/well).

- Minimum Essential Medium (MEM, Gibco) supplemented with 200 mM L-Glutamine (Lonza), Non-Essential Amino Acids (NEAA;100 X, Gibco), HEPES (1M, Gibco), 10% of FBS-HI, Antibiotic-Antimycotic (100X, Gibco) at 37°C, in humidified incubators without CO2. One day before inoculation, the cells were seeded in a 96-well plate at such a density that a confluent monolayer (≥ 90%) is achieved at the day of the assay (1.5 x 10^4 cells/well).

4.1.3 Viruses

To perform the MN CPE assays, SARS-CoV-2 2019-nCoV strain 2019-nCov/Italy-INMI1-wild type virus (purchased from the European Virus Archive goes Global (EVAg, Spallanzani Institute, Rome) and SARS-CoV-2 Alpha variant (Human nCoV19 isolate/England/MIG457/2020 (lineage B.1.1.7) Ref-SKU: 004V-04032) were used. To perform the MN Colorimetric assay, the SARS-CoV-2 2019-nCoV strain 2019-nCov/Italy-INMI1 above described was used.

The two variants were titrated in serial 1 log dilutions (from 1 log to 11 log) to obtain a 50% tissue culture infective dose (TCID50) on 96-well culture plates of VERO E6 cells. The plates were observed daily for a total of 4 days for the presence of CPE by means of an inverted optical microscope. The end-point titres were calculated according to the Reed & Muench method[72] based on eight replicates for titration.

To perform the MN Virospot experiments, the following viruses were used:
SARS-CoV-2 Wild Type Strain, isolate BetaCoV/Munich/BavPat1/2020, purchased from the European Virus Archive goes Global (EVAg); SARS-CoV-2 Alpha variant, Isolate USA/CA_CDC_5574/2020 (B.1.1.7), Beta variant (B.1.351) Isolate hCoV-19/South Africa/KRISP-EC-K005321/2020 and Gamma variant (P.1) Isolate hCoV-19/Japan/TY7-503/2021 were purchased from BEI Resources.

The SARS-CoV-2 WT used in MN Virospot assay was propagated in VERO E6 cells cultured in DMEM Infection Medium (IM); complete medium with 3% FBS (Capricorn Scientific), 1% Penicillin (10000 IU/mL, Lonza) and 1%L-Glutamine (200 mM, Lonza). Alpha, Beta and Gamma variants for the MN Virospot optimization were propagated in VEROE6 TMPRSS2 cultured in DMEM IM with 3% FBS (Capricorn Scientific), 1% Penicillin (10000 IU/mL, Lonza) and 1%L-Glutamine (200 mM, Lonza).

4.2 METHODS

4.2.1 Methods I

4.2.1.1 Enzyme-linked immunosorbent assay

Specific anti-SARS-CoV-2 IgG antibodies were detected through a commercial ELISA kit (Euroimmun, Lübeck, Germany). ELISA plates are coated with recombinant structural protein (S1 domain) of SARS-CoV-2. According to the manufacturer, cross-reactions may occur with anti- SARS-CoV(-1) IgG antibodies, due to the close relationship between SARS-CoV-1 and SARS-CoV-2, while cross-reactions with other human pathogenic CoVs (MERS-CoV, HCoV-229E, HCoV-NL63, HCoV-HKU1, and HCoV-OC43) are excluded. The assay provides semi-quantitative results by calculating the ratio of the OD of the serum sample over the OD of the calibrator. According to the manufacturer's instructions, positive samples have a ratio ≥1.1, borderline samples a ratio between 0.8 and 1.1, and negative samples a ratio <0.8. The ELISA

assay was performed as pre-screening analysis on samples from project one in order to determine the binding capacity of serum samples before performing the MN CPE and MN Colorimetric assays.

4.2.1.2 Viral growth in cell culture

The SARS-CoV-2 Wild-type virus 2019-nCoV strain 2019-nCov/Italy-INMI1 was seeded and propagated in VERO, VERO E6, and Huh-7 cells by using EMEM (for VERO and Huh-7) and DMEM high glucose (for VERO E6) both supplemented with 2% FBS and 100 IU/mL penicillin-streptomycin. Cells were seeded in T175 flasks at a density of 1×10^6 cells/mL. After 18 to 20 hours, the sub-confluent cell monolayer was washed twice with sterile Dulbeccos's phosphate buffered saline (DPBS). After removal of the DPBS, the cells were infected with 3.5 mL of EMEM/DMEM 2% FBS containing the virus at a multiplicity of infection of 0.001 and 0.01. After 1 hour of incubation at 37°C in a humidified atmosphere with 5% CO2, 50 mL of EMEM (for VERO and Huh7) or DMEM (for VERO E6) containing 2% FBS was added to the cells. The flasks were daily observed, and the virus was harvested when 80%-90% of the cells manifested CPE. The culture medium was centrifuged at +4°C 1600 rpm for 8 minutes, to remove the cell debris, then it was aliquoted and stored at −80°C.

4.2.1.3 Micro-neutralization assays

Serum samples were heat-inactivated for 30 minutes at 56°C; two-fold serial dilutions, starting from 1:10, were then mixed with an equal volume of viral solution containing 100 TCID50 of SARS-CoV-2. The serum-virus mixture was incubated for 1 hour at 37°C in a humidified atmosphere with 5% CO2. After incubation, 100 µL of the mixture at each dilution was added in duplicate to a cell plate containing a semi-confluent VERO E6 monolayer. The plates were incubated for 3 days (SARS-CoV-2 WT strain 2019-nCov/Italy-INMI1) or 4 days (SARS-CoV-2 Alpha variant, Human nCoV19 isolate/England/MIG457/2020) at 37°C in a humidified atmosphere with 5% CO2. The readout incubation time for each strain was established based on previous setup experiments (not shown) according to the back titration results and the development of a consistent CPE.

4.2.1.3.1 CPE-read out

After 3 (for SARS-CoV-2 WT strain 2019-nCov/Italy-INMI1) or 4 (for SARS-CoV-2 Alpha variant, Human nCoV19 isolate/England/MIG457/2020) days of incubation, the plates were inspected by an inverted optical microscope. The highest serum dilution that protected more than the 50% of cells from CPE was taken as the neutralization titre.

4.2.1.3.2 Colorimetric read-out

After 3 days of incubation (SARS-CoV-2 WT strain 2019-nCov/Italy-INMI1), the supernatant of each plate was carefully discarded and 100 µl of a sterile DPBS solution containing 0.02% neutral red (Sigma, St. Louis, MO) was added to each well of the MN plates. After 1 hour of incubation at room temperature, the neutral red solution was discarded, and the cell monolayer was washed twice with sterile DPBS containing 0.05% Tween 20. After the second incubation, the DPBS was carefully removed from each well; then, 100 µL of a lysis solution

made up of 50 parts of absolute ethanol (Sigma, St. Louis, MO), 49 parts of MilliQ and 1 part of glacial acetic acid (Sigma) was added to each well. Plates were incubated for 15 minutes at room temperature and then read by a spectrophotometer at 540 nm. The highest serum dilution, showing optical density (OD) value greater than the cut-off value, was considered as the neutralization titre. The cut-off value is calculated as the average of the OD values of the cell control wells divided by two. In each of the two methods, the geometric mean titer (GMT) between the 2 data obtained for each sample was calculated. Sera negative at a dilution of 1:10 were assigned a titer of 5.

4.2.2 Methods II

4.2.2.1 MN Virospot

In this project the SARS-CoV-2 MN Virospot assay was used to compare the MN results with those obtained through the MN CPE. In the Virospot MN assay, a standard number of SARS-CoV-2 infectious units (aimed between 30 – 350 spots/well) was incubated with serial dilutions of serum samples previously heat-inactivated for 30 minutes at 56°C. After a 60 min pre-incubation period at 37°C of the virus/serum mixtures, 100µL of the mixture was added to 80-90% confluent VEROE6 cell monolayer. One hour later the virus/serum mixture was replaced with fresh IM and incubated for 16-24 hours. After this incubation, cells were formalin-fixed followed by an incubation with a monoclonal antibody which targets the viral nucleocapsid protein (SARS-CoV/SARS-CoV-2 Nucleocapsid monoclonal antibody, Sino Biological, Cat# 40143-MM05). Then, a secondary anti-human IgG peroxidase conjugate (Goat anti-Mouse IgG-HRP, Thermo Scientific, Cat# A16072) was added and incubated for a hour and eventually a TrueBlue substrate that formed a blue precipitate on nucleocapsid-positive cells.

Images of all wells were acquired by a CTL ImmunoSpot analyzer, equipped with a software used to quantitate the nucleocapsid-positive cells (=virus signal). This method utilizes spot counts that represent infectious units above and below the reduction point 50%, 80%, 90% to calculate the MN titer as reported in Zielinska method. [61]

4.2.3 Methods III

4.2.3.1 Virospot MN optimization

The SARS-CoV-2 Virospot MN assay previously described has been fully validated for measuring SARS-CoV-2 neutralizing antibodies in serum samples using SARS-CoV-2 WT, which was isolated early 2020. In this optimization project several new conditions were introduced to the SARS-CoV-2 Virospot MN assay to make it suitable for testing samples against new emerging virus variants. The carboxymethyl cellulose (CMC) has been implemented as overlay, important to avoid secondary infections and contain progeny virus at the site of the primary infection, thereby causing the immunostained virus-positive spots of different virus variants to become of similar size and shape and ensuring accurate quantification of the virus inoculum. Other changes, related to incubation conditions have been implemented to make the assay more sensitive and robust.

4.2.3.2 Design of the MN Virospot assay optimization

To optimize the SARS-CoV-2 Virospot MN assay, different conditions were tested (Run I, II, III IV and V, **Table 2**). A total of 11 matched serum and plasma samples taken from the same donor were used against four different SARS-CoV-2 variants (Wild type, Alpha, Beta and Gamma) in two runs (I and II, **Table 2**). Once evaluated the MN titer of each sample and based on WT MN titers, three runs (III, IV, V run, as shown in **Table 2**) were carried out using 6 out of 21 samples of which:

- One serum and one plasma sample with a high MN titer (High-Positive samples, H-P)
- One serum and one plasma sample with a mid-low MN titer (Mid-Positive samples, M-P)
- One serum and one plasma sample with a low MN titer (Low-Positive samples, L-P)

The 50%,80%,90% neutralization titers have been evaluated as previously described using Zielinska formula.[61]

The use of DMEM Infection Medium (IM) with CO2 was compared to MEM IM without CO2 (Run II). Both media were supplemented with 200 mM L-Glutamine (Lonza), Non-Essential Amino Acids (NEAA;100 X, Gibco), HEPES (1M, Gibco), 3% of FBS-Heat Inactivated (HI) and Antibiotic-Antimycotic (100X, Gibco).
Different time points (30 min, 60 min, 120 min) were evaluated for the pre-incubation of the serum/virus mixture and for the second incubation of the serum/virus mixture on the VERO E6 cells (Run III and IV).

The effect on MN titer spot count by using different temperatures (37°C/room temperature) during the first incubation period (serum/virus mixture) was also assessed (Run III).

Finally, Carboxymethyl cellulose (CMC, Sigma Aldrich, Cat# D4888) was implemented and used at different percentages (1%, 2%, 3%). Moreover, different incubation timepoints (8, 24, and 32 hours) were evaluated for the last incubation step (after the adding of CMC) (Run V). To better investigate the effect of this overlay on the spot count and spot size no samples were used and a viral titration of each SARS-CoV-2 variant was performed as follows:

10-fold serial dilutions of virus stock for each variant were prepared in a round bottom plate using MEM-based as infection medium. Each virus samples were titrated per plate in 8 replicates starting from 1:10 as first dilution step from column 1 to column 11, taking column 12 as cell control. After completing the dilutions, the samples were transferred to the culture plates with Vero E6 cell monolayers and incubated for 60 min at RT. One hour later the inoculum was replaced with CMC 1%, 2% and 3% (three different plates were used for each variant) and incubated for 8, 24 and 32 hours in a humidified atmosphere at 37°C without external supplementation of CO2. The same procedure as in MN Virospot assay (Method II) was followed for the immunostaining (section 4.2.1). The plates were subsequently scanned with the CTL UV Analyzer to detect the spot count . Cell control wells were included as a virus-

negative control condition (IM only). For each dilution the spot size and the spot number were evaluated.

RUN	CONDITIONS	NUMBER OF SAMPLES	SARS-CoV-2 VARIANTS
I	serum samples VS plasma samples + CMC1%	11 serum and plasma samples	WT, Alpha, Beta, Gamma
II	DMEM + CO2 VS MEM -CO2 +CMC1%	11 serum and plasma samples	WT, Alpha, Beta, Gamma
III	pre-incubation 37°C VS RT and different time-points 30,60,120min +CMC1%	H-P serum/plasma M-P serum/plasma L-P serum/plasma	WT, Gamma
IV	(mix sample-virus/cells) different time points 30,60, 120 min +CMC1%	H-P- serum/plasma M-P serum/plasma L-P serum/plasma	WT, Gamma
V	CMC 1%,2%,3% Different time points (8,24,32 hours)	W/O samples	WT, Alpha, Beta, Gamma

Table 2. Conditions evaluated for the optimization of the Virospot MN assay performed by using a panel of serum samples and plasma samples from the same donor against SARS-CoV-2 Wild type, Alpha, Beta and Gamma variants.

4.2 Statistical analysis

In the Project I, Friedman test was used to compare viral titres obtained at different time points during viral growth in cell culture. A p value <0.5 was considered statistically significant. To verify the similarity between MN CPE and Colorimetric MN assay (Project II), and MN CPE and Virospot MN assay (Project II), different types of statistics have been considered. Log2-transformed MN titers were compared by simple non-linear regression curve fit, and the coefficient of correlation (r^2) was determined. Moreover, to investigate the relationship

between the errors in measurement and the true values, the Bland-Altmann analysis was performed. The differences between the pairs of measurements (expressed as log2 titers) were plotted against their means. The lower and upper limits of agreement were evaluated based on the (normal) distribution of the differences. Points outside the limits of agreements indicated statistically significant difference. The plot puts also in evidence a possible systematic bias between the two kinds of measurements.[73]

In the Project I, further analyses were performed; A single score intraclass correlation (ICC). The log2-transformed MN titers obtained with each platform (MN CPE and Colorimetric Mn assay) were analyzed through a two-way mixed ANOVA test using the R software, and the ICC was calculated according to the following formula:

$$ICC = \frac{\sigma_B^2}{\sigma_B^2 + \sigma_W^2}$$

where σ_B^2 is the variance between the *n* sample units ("between variance"), and σ_W^2 is the common variance within each sample unit ("within variance"). The total variance σ_T^2 of the measurements is given by the sum of these two components, i.e., $\sigma_T^2 = \sigma_B^2 + \sigma_W^2$.
According to the scale of Koo & Li [74] the results of the ICC analysis were interpreted as follows:

- Less than 0.50: Poor reliability
- Between 0.5 and 0.75: Moderate reliability
- Between 0.75 and 0.9: Good reliability
- Greater than 0.9: Excellent reliability

Furthermore, in the Project I, the equivalence test was used. This test compares the means of the two sets of data and provides a more informative results, whereby it is possible to compare the statistical significance with the analytical significance. The equivalence acceptability criterion, EAC, was set to EAC=1, since in terms of titers, a difference between pairs of results (log2-units) in the range of ±1 is to be considered acceptable. In the Project III, T-test analysis was performed to compare the use of DMEM with CO2 and MEM and the without CO2. The T-test analysis is an inferential statistical test that determines whether there is a statistically significant difference between the means in two independent groups. To apply this test, a continuous normally distributed variable (Test variable) and a categorical variable with two categories (Grouping variable) are used. Further mean, SD, and number of observations of the group 1 and group 2 are used to compute significance level. In this procedure, first significance level of Levene's test is computed and when it is insignificant ($P > 0.05$), equal variances otherwise ($P < 0.05$), unequal variances are assumed between the groups and according to *P* value is selected for independent samples *t* test.[75]

Project I data analysis was performed using GraphPad Prism Version 5, Microsoft® Excel® 2019, and the R software (for intra-class correlation); analyses of Project II and III were evaluated through GraphPad Prism Version 4 and Microsoft® Excel® 2019.

5. RESULTS

5.1 RESULTS I

5.1.1 High viral load for VERO and VERO E6, no propagation for Huh-7

In the first project, the SARS-CoV-2 Wild type propagation has been performed three times in three independent experiments using three different cell lines: VERO, VERO E6, and Huh-7 cells. These specific cell lines were chosen to investigate the viral growth because, as reported in literature, they are the preferred lines for SARS-CoV-2 Wild type isolation and replication [77-78]. Infection curves for each cell line have been evaluated through different harvest time-points: 36, 48-52 and 72-76 hours post infection. For VERO and VERO E6 cells a high viral titer was observed. In both cell lines two different multiplicity of infection (MOI) (0.001 and 0.01) were used starting from a viral stock containing $10^{7.25}$ TCID50/mL (only the results obtained with MOI = 0.001 are reported in this study). Neither CPE nor infection plaques in the cell monolayer were observed in any of the three cell lines after 24 hours post infection. After 36 hours, VERO E6 and VERO showed 30%-40% of CPE ($10^{3.63}$ TCID50/mL ± 0.14 SD) and 15%-20% ($10^{3.78}$ TCID50/mL ± 0.2 SD), respectively. Both cell lines (VERO, VEROE6) reached the 80% of CPE (**Fig. 9**), after 48-52 hours post infection, recording a significant increase of the viral titre according to Friedman test with a mean equal to $10^{7,63}$ TCID50/mL ± 0.38 SD for VERO E6 cells, and $10^{7.17}$ TCID50/mL ± 0.1 SD for VERO cells.

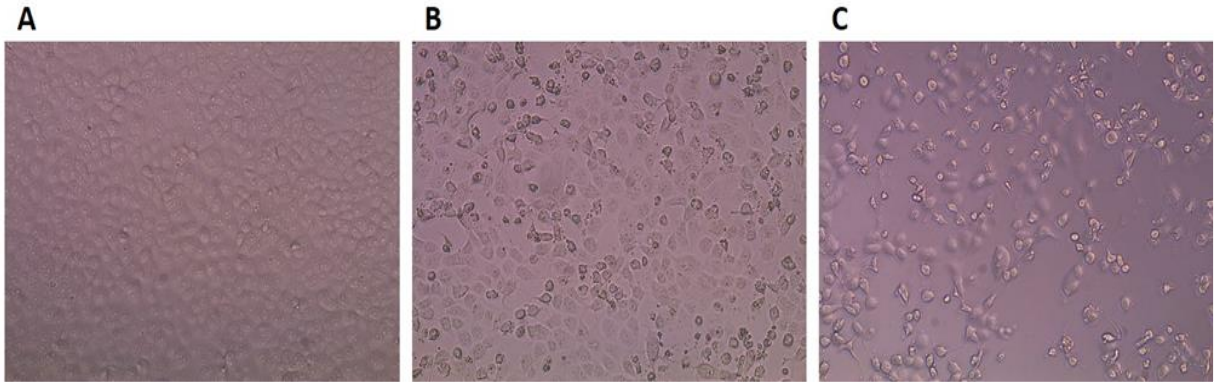

Figure 9. **Vero E6 cells at different stage of infection.** A, Not infected VERO E6 cell monolayer after 72 hours, complete absence of CPE. B, SARS-CoV-2 infected VERO E6 cell monolayer after 36 hours postinfection, 20%-30% of CPE recovered. C, SARS-CoV-2 infected VERO E6 after 52 hours postinfection, 80% of CPE recovered. CPE, cytopathic effect; SARS-CoV-2, Severe Acute Respiratory Syndrome-Coronavirus-2

After 72 -76 hours post infection, a decrease in the viral titers were registered in VERO ($10^{6.5}$ TCID50/mL ± 0.2 SD) and VERO E6 ($10^{6.4}$ TCID50/mL ± 0.13 SD) flasks, with cell monolayer showing 100% of CPE (**Figure 10**). No detectable CPE was observed for Huh-7 cells up to the

7th day after infection. To further check the viral production in Huh-7 cells, the supernatant was passed on VERO E6 cells but 0% of CPE was detected in this cell line. This confirms that Huh-7 cells are not able to support the viral replication of this Coronavirus strain, as already showed by Harcourt et al.[76]

The supernatants derived from VERO, VERO E6 and Huh-7 were titrated in 96-well plates, which were read after 72 hours; Titres reached ranged from $10^{6.2}$ to $10^{7.8}$ TCID50/mL either for VERO and VERO E6-derived virus; no titre has been detected for Huh-7-derived virus (data not shown).

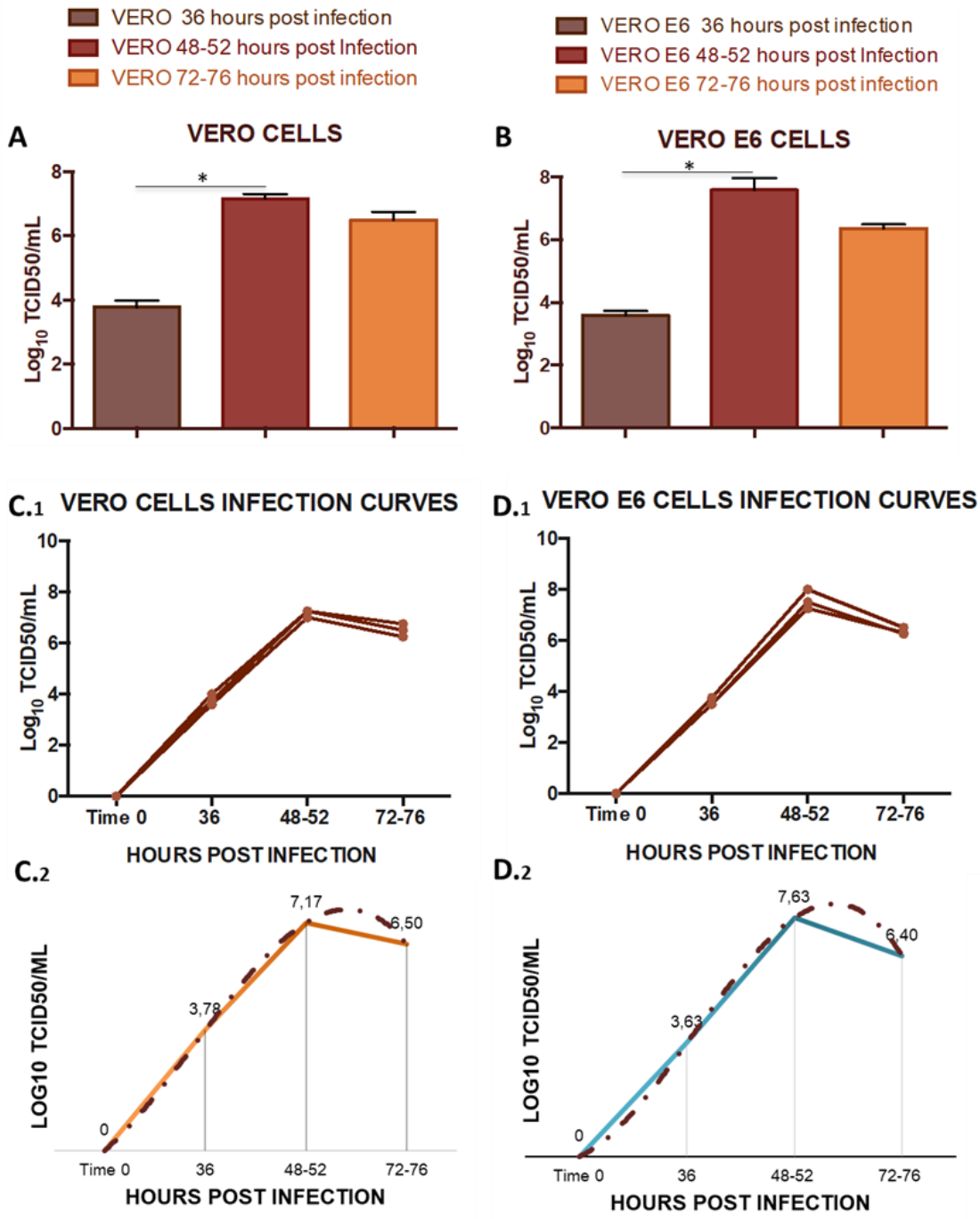

Figure 10. Viral titres reached for VERO and VERO E6 in three different viral infection experiments in T-175 flasks. A, Titres registered in triplicate (n = 3) for VERO cells after 36, 48 to 52 and 72 to 76 hours post infection. A significant increase in the viral titre has been registered after 48 to 52 hours according to Friedman test ($P < .05$), error bars indicate the standard deviation among the three independent measures. B, Titres registered (n = 3) for VERO E6 cells after 36, 48 to 52 and 72 to 76 hours post infection. A significant increase in the viral titre has been registered after 48 to 52 hours according to Friedman test ($P < .05$), error bars indicate the standard deviation among the three independent measures. C.1, Infection curves for VERO cells for three independent experiments of viral growth. C.2, Polynomial infection curve derived from the average of the three experimental curves for VERO cells. D.1, Infection curves for VERO E6 for three independent experiments of viral growth. D.2, Polynomial infection curve derived from the average of the three experimental curves for VERO E6 cells.

5.1.2 Comparison between ELISA and MN assays

The ELISA assay was used as pre-screening for 83 serum samples for evaluating the presence of neutralising antibodies against SARS-CoV-2 Wild type strain. Results showed 42 samples positive, 20 borderline and the remaining 21 negative. The same panel was tested using the MN assay and, to evaluate the specificity of the MN assay for the SARS-CoV-2 Wild type, several animal sera, that were high responders to different viruses, such as Influenza virus (seasonal and pandemic) and Adenovirus type 4, were tested. All animal samples tested against Influenza and Adenovirus type 4 proved completely negative, confirming the specificity of the MN assay in the detection of anti-SARS-CoV-2 nAbs (data not shown).
Neutralization test results of the human serum samples confirmed the complete absence (100%) of nAbs in samples already negative in ELISA. 22 out of 42 samples positive in ELISA (52.3%) confirmed the presence of CPE-inhibiting nAbs in the cell monolayer, showing high MN titers. 3 out of 20 borderline ELISA samples (15%) confirmed the neutralizing activity against the SARS-CoV-2 Wild type in MN assay (**Table 3**). To confirm and validate the results obtained, each sample was tested in duplicate by two different operators (analyst 1 and 2). Finally, each sample was evaluated through a colorimetric read- out and the MN titers were compared to those obtained with the MN CPE method.

5.1.3 MN CPE Viral dose: 100 TCID50/well VS 25 TCID50/well

Based on the assumption that there are not defined indications of the viral dose required for functional assays such as MN or plaque reduction, along with the fact that 100 TCID50 is the viral load used for other respiratory viruses such as Influenza, to assess the MN CPE assay sensitivity in detecting neutralizing antibody against SARS-CoV-2 Wild Type, two different viral infective doses were used: a standard dose of 100 TCID50/well and a lower dose of 25 TCID50/well.

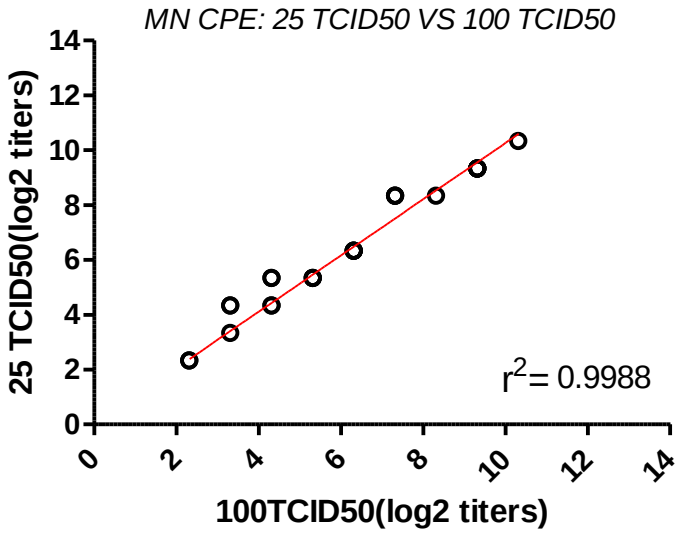

Figure 11. MN positive CPE titers (converted in log2) tested against 100TCID50 and 25TCID50 SARS-CoV-2. Mn titers were analysed by GraphPad using Linear regression analysis.

The MN titers converted in log2 yielded by MN CPE using the lower infective dose (25 TCID50) were in line with those obtained with the standard infective dose (**Figure 11**), showing a good concordance of results (correlation coefficient r^2= 0.9988); Only 7 samples (samples 22,43,45,49,52,56,58) showed a MN titre that was one dilution step higher using 25TCID50 compared to titers obtained with 100TCID50 (**Table 3**). Nevertheless, the 88,8 % of samples resulted to have the same titer using both 25TCID50 and 100TCID50 confirming the sensitivity of the SARS-CoV-2 MN CPE using a lower infective dose.

5.1.4 Absence of neutralizing activity for human IgG1 monoclonal antibody CR3022

The CR3022 monoclonal antibody (mAb) has high capability of neutralizing the SARS-CoV strain [79], and we included this mAb (IgG1) within the human serum samples in our MN assay. The CR3022 antibody targets a highly conserved epitope on the RBD of SARS-CoV. The concentrations tested in MN ranged from 10 µg down to 0.009 µg. A 60 minutes pre-incubation was performed between the monoclonal antibody and 100TCID50 of live SARS-CoV-2 Wild type and then the mixture was passed on the VERO E6 monolayer. After 72 hours of incubation, no neutralizing activity was obtained at any of the concentrations tested. By contrast, very high ELISA titers were detected (data not shown). CR3022, unlike other SARS-CoV monoclonal antibodies, recognizes a different epitope from that one recognized on the RBD by the ACE2 receptor. Moreover, the C-terminal RBD residue of SARS-CoV-2 virus has been found to be quite different from that of SARS-CoV, which may have a critical impact on the cross-reactivity of neutralizing antibodies:[80] Moreover, as already reported by Tian et al [80] some antibodies with a high capability of neutralizing SARS-CoV, were found to be unable to bind the S protein of the SARS-CoV-2 virus. Currently, 3 anti-SARS-CoV-2 monoclonal antibody products have received Emergency Use Authorizations (EUAs) from the Food and

Drug Administration (FDA) for the treatment of mild to moderate COVID-19 in non hospitalized patients with laboratory-confirmed SARS-CoV-2 infection who are at high risk for progressing to severe disease and/or hospitalization.[81]

Sample ID	ELISA ASSAY	MN CPE titer(log2) Analyst1 100TCID50	MN CPE titer(log2) Analyst2 100TCID50	Colorimetric MN titer(log2) 100TCID50	MN CPE titer(log2) 25TCID50	Difference MN CPE titers(log2) 100TCID50/25TCID50	Difference MN CPE titers(log2)/Colorimetric MN titers(log2)
From 1 to 21	Negative	2,32	2,32	2,32	2,32	0,00	0,00
22	Borderline	2,32	2,32	2,32	2,32	0,00	0,00
23	Borderline	2,32	2,32	2,32	2,32	0,00	0,00
24	Borderline	2,32	2,32	2,32	2,32	0,00	0,00
25	Borderline	2,32	2,32	2,32	2,32	0,00	0,00
26	Borderline	2,32	2,32	2,32	2,32	0,00	0,00
27	Borderline	2,32	2,32	2,32	2,32	0,00	0,00
28	Borderline	2,32	2,32	2,32	2,32	0,00	0,00
29	Borderline	2,32	2,32	2,32	2,32	0,00	0,00
30	Borderline	2,32	2,32	2,32	2,32	0,00	0,00
31	Borderline	2,32	2,32	2,32	2,32	0,00	0,00
32	Borderline	2,32	2,32	2,32	2,32	0,00	0,00
33	Borderline	2,32	2,32	2,32	2,32	0,00	0,00
34	Borderline	2,32	2,32	2,32	2,32	0,00	0,00
35	Borderline	2,32	2,32	2,32	2,32	0,00	0,00
36	Borderline	2,32	2,32	2,32	2,32	0,00	0,00
37	Borderline	2,32	2,32	2,32	2,32	0,00	0,00
38	Borderline	2,32	2,32	2,32	2,32	0,00	0,00
22	Borderline	4,32	4,32	4,32	5,32	-1,00	0,00
23	Borderline	6,32	5,32	6,32	6,32	0,00	-1,00
24	Borderline	4,32	4,32	4,32	4,32	0,00	0,00
42	Positive	9,32	9,32	9,32	9,32	0,00	0,00
43	Positive	4,32	4,32	4,32	5,32	-1,00	0,00
44	Positive	8,32	8,32	8,32	8,32	0,00	0,00
45	Positive	9,32	8,32	8,32	9,32	-1,00	0,00
46	Positive	5,32	5,32	5,32	5,32	0,00	0,00
47	Positive	9,32	9,32	9,32	9,32	0,00	0,00
48	Positive	4,32	4,32	4,32	4,32	0,00	0,00
49	Positive	3,32	4,32	3,32	4,32	-1,00	1,00
50	Positive	7,32	8,32	8,32	8,32	0,00	0,00
51	Positive	5,32	5,32	5,32	5,32	0,00	0,00
52	Positive	7,32	7,32	7,32	8,32	-1,00	0,00
53	Positive	9,32	9,32	9,32	9,32	0,00	0,00
54	Positive	6,32	6,32	6,32	6,32	0,00	0,00
55	Positive	10,32	11,32	10,32	10,32	0,00	1,00
56	Positive	7,32	7,32	7,32	8,32	-1,00	0,00
57	Positive	6,32	6,32	6,32	6,32	0,00	0,00
58	Positive	3,32	3,32	3,32	4,32	-1,00	0,00
59	Positive	6,32	6,32	6,32	6,32	0,00	0,00
60	Positive	9,32	9,32	9,32	9,32	0,00	0,00
61	Positive	3,32	3,32	3,32	3,32	0,00	0,00
62	Positive	5,32	5,32	5,32	5,32	0,00	0,00
63	Positive	5,32	5,32	5,32	5,32	0,00	0,00
64	Positive	2,32	2,32	2,32	2,32	0,00	0,00
65	Positive	2,32	2,32	2,32	2,32	0,00	0,00
66	Positive	2,32	2,32	2,32	2,32	0,00	0,00
67	Positive	2,32	2,32	2,32	2,32	0,00	0,00
68	Positive	2,32	2,32	2,32	2,32	0,00	0,00
69	Positive	2,32	2,32	2,32	2,32	0,00	0,00
70	Positive	2,32	2,32	2,32	2,32	0,00	0,00
71	Positive	2,32	2,32	2,32	2,32	0,00	0,00
72	Positive	2,32	2,32	2,32	2,32	0,00	0,00
73	Positive	2,32	2,32	2,32	2,32	0,00	0,00
74	Positive	2,32	2,32	2,32	2,32	0,00	0,00
75	Positive	2,32	2,32	2,32	2,32	0,00	0,00
76	Positive	2,32	2,32	2,32	2,32	0,00	0,00
77	Positive	2,32	2,32	2,32	2,32	0,00	0,00
78	Positive	2,32	2,32	2,32	2,32	0,00	0,00
79	Positive	2,32	2,32	2,32	2,32	0,00	0,00
80	Positive	2,32	2,32	2,32	2,32	0,00	0,00
81	Positive	2,32	2,32	2,32	2,32	0,00	0,00
82	Positive	2,32	2,32	2,32	2,32	0,00	0,00
83	Positive	2,32	2,32	2,32	2,32	0,00	0,00

Table 3. ELISA and neutralization titer results converted in log2 for 83 human serum samples tested against SARS-CoV-2 Wild type strain. Differences between MN titers using 100TCID50 were compared with titers obtained with 25TCID50 testing

the same serum sample panel. Moreover, differences between MNCPE and Colorimetric MN CPE are reported. Differences of 1log2 are highlighted in red. *Note: Negative samples are indicated in the first row of the table. Neutralizing titres, obtained with CPE (100 and 25TCID50 infective dose) and colorimetric read-out methods, are indicated for each sample.*

5.1.5 MN assay read-out: Subjective vs Objective method

The results obtained in the MN assay in all serum samples were evaluated through two methods of read-out: By inspecting the inhibition of the CPE at each serum dilution (subjective method) with an inverted optical microscope, and by applying a colorimetric method in which the healthy cell monolayer is stained with a neutral red solution (vital dye). As shown in **Figure 12**, colums 11th and 12th of each plate were set up as Cell Control (CC) and Viral Control (CV), respectively. Serum samples were progressively diluted 2-fold from column 1 up to column 10. The cut-off value has been calculated as the average of the CC ODs divided by two. Wells that showed OD values lower than the cut-off were considered virus-positive, and hence infected.

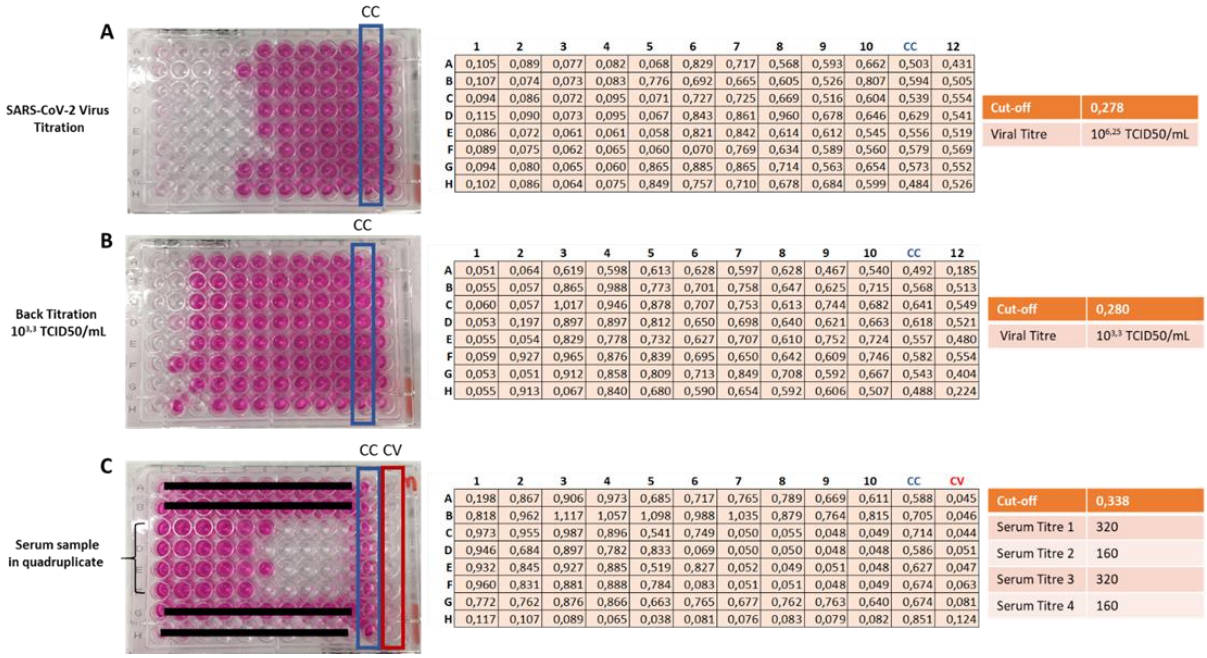

	1	2	3	4	5	6	7	8	9	10	CC	12
A	0,105	0,089	0,077	0,082	0,068	0,829	0,717	0,568	0,593	0,662	0,503	0,431
B	0,107	0,074	0,073	0,083	0,776	0,692	0,665	0,605	0,526	0,807	0,594	0,505
C	0,094	0,086	0,072	0,095	0,071	0,727	0,725	0,669	0,516	0,604	0,539	0,554
D	0,115	0,090	0,073	0,095	0,067	0,843	0,861	0,960	0,678	0,646	0,629	0,541
E	0,086	0,072	0,061	0,061	0,058	0,821	0,842	0,614	0,612	0,545	0,556	0,519
F	0,089	0,075	0,062	0,065	0,060	0,070	0,769	0,634	0,589	0,560	0,579	0,569
G	0,094	0,080	0,065	0,060	0,865	0,885	0,865	0,714	0,563	0,654	0,573	0,552
H	0,102	0,086	0,064	0,075	0,849	0,757	0,710	0,678	0,684	0,599	0,484	0,526

Cut-off	0,278
Viral Titre	$10^{6,25}$ TCID50/mL

	1	2	3	4	5	6	7	8	9	10	CC	12
A	0,051	0,064	0,619	0,598	0,613	0,628	0,597	0,628	0,467	0,540	0,492	0,185
B	0,055	0,057	0,865	0,988	0,773	0,701	0,758	0,647	0,625	0,715	0,568	0,513
C	0,060	0,057	1,017	0,946	0,878	0,707	0,753	0,613	0,744	0,682	0,641	0,549
D	0,053	0,197	0,897	0,897	0,812	0,650	0,698	0,640	0,621	0,663	0,618	0,521
E	0,055	0,054	0,829	0,778	0,732	0,627	0,707	0,610	0,752	0,724	0,557	0,480
F	0,059	0,927	0,965	0,876	0,839	0,695	0,650	0,642	0,609	0,746	0,582	0,554
G	0,053	0,051	0,912	0,858	0,809	0,713	0,849	0,708	0,592	0,667	0,543	0,404
H	0,055	0,913	0,067	0,840	0,680	0,590	0,654	0,592	0,606	0,507	0,488	0,224

Cut-off	0,280
Viral Titre	$10^{3,3}$ TCID50/mL

	1	2	3	4	5	6	7	8	9	10	CC	CV
A	0,198	0,867	0,906	0,973	0,685	0,717	0,765	0,789	0,669	0,611	0,588	0,045
B	0,818	0,962	1,117	1,057	1,098	0,988	1,035	0,879	0,764	0,815	0,705	0,046
C	0,973	0,955	0,987	0,896	0,541	0,749	0,050	0,055	0,048	0,049	0,714	0,044
D	0,946	0,684	0,897	0,782	0,833	0,069	0,050	0,050	0,048	0,048	0,586	0,051
E	0,932	0,845	0,927	0,885	0,519	0,827	0,052	0,049	0,051	0,048	0,627	0,047
F	0,960	0,831	0,881	0,888	0,784	0,083	0,051	0,051	0,048	0,049	0,674	0,063
G	0,772	0,762	0,876	0,866	0,663	0,765	0,677	0,762	0,763	0,640	0,674	0,081
H	0,117	0,107	0,089	0,065	0,038	0,081	0,076	0,083	0,079	0,082	0,851	0,124

Cut-off	0,338
Serum Titre 1	320
Serum Titre 2	160
Serum Titre 3	320
Serum Titre 4	160

Figure 12. Schematic overview of the colorimetric MN read-out. A, SARS-CoV-2 virus titration. B, Titration of the working viral solution. C, Neutralization plate with a serum sample tested in quadruplicate. In each plate, the column highlighted in blue is the cell control (highest OD value), while the column highlighted in red is the virus control (no OD values). The viral titres in both the stock solution (A) and the working viral solution (B) are calculated by means of the Reed and Muench method. The titre of the serum sample (C) was calculated as the reciprocal of the highest dilution at which the OD value was higher than or equal to the cut-off value. OD, optical density; SARS-CoV-2, Severe Acute Respiratory Syndrome-Coronavirus-2.

Results of the comparison between ELISA and MN (**Table 3**) suggested that a well-trained operator is able to read the CPE, thereby providing the same results as the spectrophotometer in terms of titre without differences between the results provided by the two different operators and the spectrophotometric evaluation of the ODs.

5.1.5.1 MN CPE- Colorimetric MN agreement: Linear regression analysis

As presented in **Table 3**, MN CPE and Colorimetric MN demostrated high agreement. Only 3 out 83 samples (samples 23,49 and 55) differ each other only for 1 log2 step, which is considered acceptable. To further analyse the agreement between these two read-out methods, a comparison of log2-tranformed MN titers of each serum sample using the colorimetric MN and MN CPE results, was performed through a linear regression analysis (**Figure 13**).

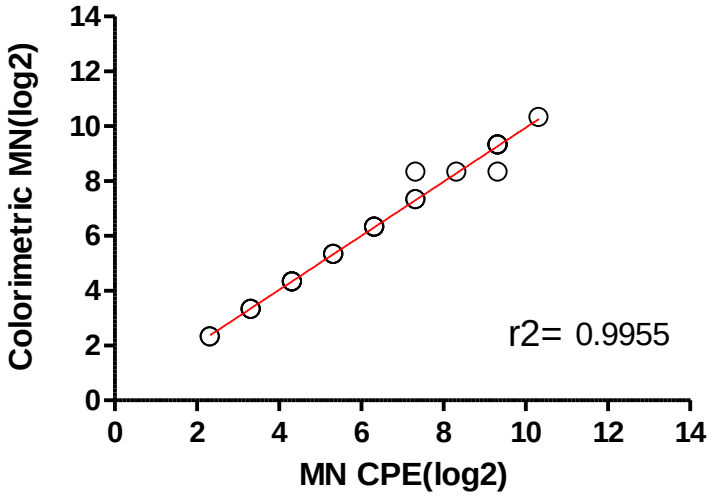

Figure 13. Comparison between MN titers obtained through the MN CPE and the colorimetric MN assay using SARS-CoV-2 Wild type strain. Results are represented as $\log_2$ of MN titers.

As shown in the correlation graph, the MN CPE and the Colorimetric MN titers showed a strong correlation confirmed by the correlation coefficient (r^2), obtained from each paired comparison of MN titers, with a high value (r^2 =0.9955) and hence indicative of a strong positive correlation.

5.1.5.2 MN CPE- Colorimetric MN agreement: Bland-Altman analysis

It should be noted that a concordance measure constructed with the classic correlation coefficient does not theoretically represent the best choice when assessing the agreement between two variables. In fact, the r^2 quantifies the relationship between variables but not their difference. In the Bland-Altman plot, the differences between the pairs of measurements are plotted against their means. The lower and upper limits of agreement are evaluated based on the (normal) distribution of the differences. Points outside the limits of agreements indicate statistically significant difference. The plot puts also in evidence a possible systematic bias between the two kinds of measurements.

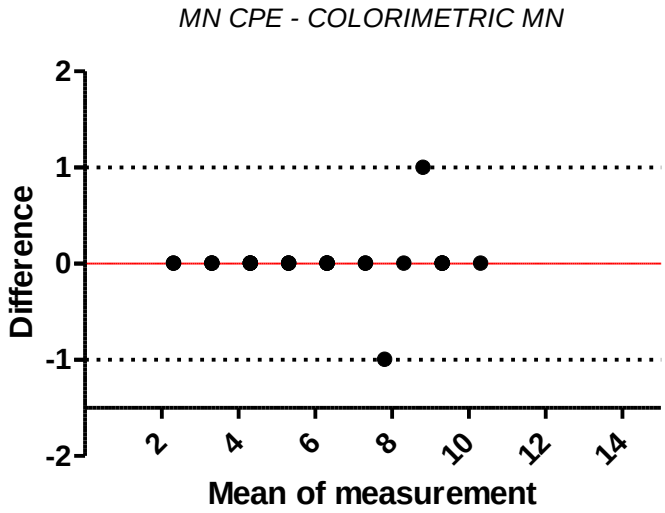

Figure 14. **Bland-Altman plot of the differences between MN CPE Log_2 titers and MN colorimetric Log_2 titers**. The limit of agreement (±1,0, stippled black line) and the overall mean of the differences (bias, red line) are shown.

This analysis confirmed that titers measured by using two different MN read out methods are comparable, showing no significant differences at high or low titers (Bias 0; 95%CI-0.11;0.11) (**Figure 14**). No values are outside the intervals defined as "limits of agreement" (Upper Limit of Agreement +1,0; Lower Limit of Agreement -1,0).

5.1.5.3 MN CPE and Colorimetric MN agreement: Single score intraclass correlation (ICC) analysis

ICC is a measure of reliability of measurements that allows two or more data vectors to be compared simultaneously. Reliability informs us on how much variability in measurements is an expression of the underlying phenomenon (similar to the concept of r^2). A two-way random effects approach was followed for calculating the ICC coefficient. According to the scale of Koo & Li [74], results of the ICC were interpreted as follows:

- Less than 0.50: Poor reliability
- Between 0.5 and 0.75: Moderate reliability
- Between 0.75 and 0.9: Good reliability
- Greater than 0.9: Excellent reliability

ICC	*F-stat*	*p*	*95%CI_lower Agreement*	*95%CI_upper Agreement*	*Agreement*
0.993	289	<0.0001	0.985	0.997	Excellent reliability

Table 4. Single Score intraclass correlation (ICC) analysis of MN CPE and MN Colorimetric log2 titers.

An ICC value 0.993 (95% C.I. 0.985-0.997; p = <0.0001) was obtained when comparing log2 MN titers obtained with the MN CPE and the colorimetric MN (**Table 4**). This value can be

interpreted as an excellent level of reliability (ICC ≥ 0.9) of the measures according to the Cicchetti scale. [82]

5.5.4 MN CPE and Colorimetric MN agreement: Equivalence test

The comparability between MN-CPE and MN Colorimetric readouts was also assessed by using the equivalence test. It allows to compare the means of the two sets of data and provides a more informative results, whereby we can compare the statistical significance with the analytical significance. The equivalence acceptability criterion (EAC) in this case is set to EAC=1, since in terms of titers, a difference between pairs of results (log2-units) in the range of ±1 is to be considered acceptable.

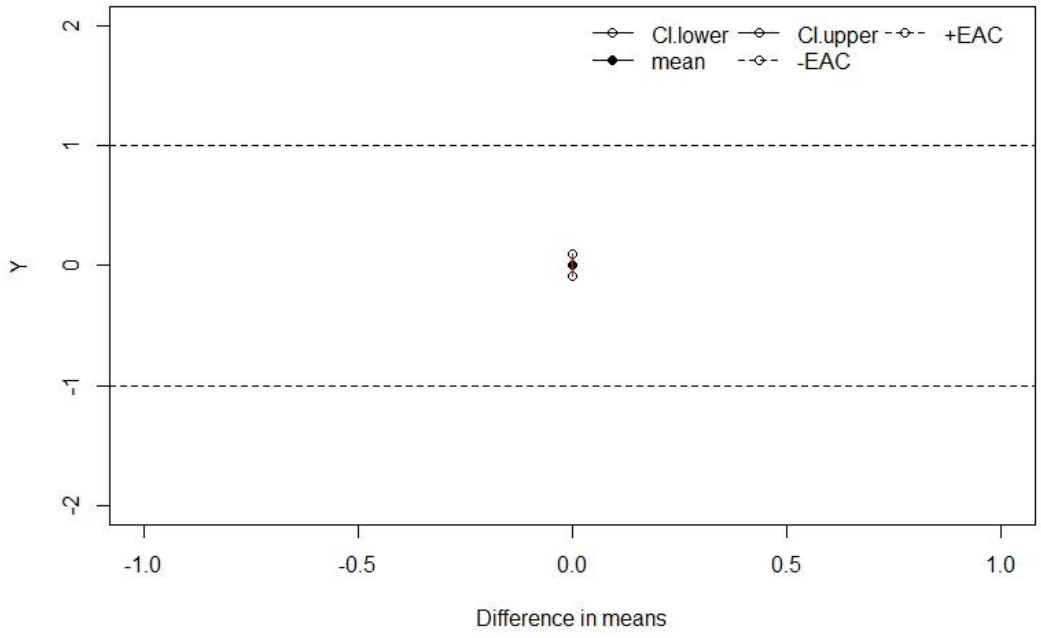

mean MN-CPE	*mean Colorimetric-MN*	*95%CI_difference _lower*	*95%CI_difference _upper*	Comment
6135	6135	-0.09	0.09	Equivalent results

Figure 15. Equivalence test analysis of MN CPE and MN Colorimetric log2 titers.

Mean differences (MN CPE= 6135; MN Colorimetric MN=6135) and 95% confidence intervals (0.09, 0.09) showed that these two MN assays have equivalent results (**Figure 15**).

In summary, Correlation, Bland-Altman, and ICC analysis confirmed that the MN CPE and the colorimetric MN showed comparable MN titers against SARS-CoV-2 Wild type strain, suggesting the suitability of performing the MN assay using an 'objective' read out methods.

One of the advantages of the colorimetric read-out is that being a completely automated method, it offers a higher throughput, while inspection of each dilution well by means of the optical microscope slows down the process.

5.2 RESULTS II

5.2.1 Comparison between MN CPE and Virospot MN assay

The second project aimed at evaluating how MN antibody titers correlate with each other when comparing the classical MN CPE with a new MN platform immunostaining read-out-based (Virospot MN). For this study, the same panel of 47 human serum samples previously used in Project I was used against either SARS-CoV-2 Wild type (WT) or Alpha variant.

5.2.1.1 MN CPE vs Virospot MN assay: SARS-CoV-2 Wild type

In the MN CPE assay, the neutralization titer of each sample was determined as the highest serum dilution that protects more than 50% of VERO E6 cells from the cytopathic effect. Serum samples previously diluted (2-fold serial dilution) were mixed with an equal volume of viral solution containing 100 TCID50 of SARS-CoV-2 Wild type strain or Alpha variant. After the incubation period, virus/samples mixture was added in duplicate to a cell plate containing a 80-90% confluent VERO E6 monolayer. The plates were incubated for 3 (WT strain) or 4 (Alpha variant) days at 37°C in a humidified atmosphere with 5% CO2.

For the Virospot MN assay, a standard number of infectious units (30-350 spots/well) of SARS-CoV-2 Wild type strain was incubated with 2-fold serial dilutions of serum samples, starting from 1:8 as first serum dilution. The mixture was added to 80%-90% confluent monolayer of VERO E6 cells. Afterwards, the plates were washed once with 120µl of infection medium, then 100 µl of new infection medium was added. The plates were then incubated for 24 hours at 37°C in a humidified atmosphere with 5% CO2. After this incubation, the immunostaining was performed and the plates were read by a CTL ImmunoSpot analyzer to quantify the Nucleoprotein (NP)-positive cells (= virus signal). The 80% and 90% neutralization titers of each sample were calculated according to the method described by Zielinska et al. [61] This titer calculation is based on the serum dilutions above and below the two reduction points 80% and 90% of neutralization.

MN CPE results were compared to MN Virospot results expressed as the 80% and 90% of reduction point (MN80, MN90, respectively). A difference in titers of 1.0 log2 dilution step (corresponding to a maximum titer difference of 2-fold) has been defined as acceptable.

Results of this comparison are plotted in **Figure 16.A** (MN CPE vs Virospot MN80 titers) and **Figure 16. B** (MN CPE vs Virospot MN90 titers). In the test performed with the SARS-COV-2 WT, the very low difference between mean values observed with MN CPE (4.42; 95% C.I. 3.89-4.95) Virospot MN80 (4.72; 95% C.I.4.09-5.35) and Virospot MN90 (4.30; 95% C.I. 3,75-4,85) suggests that there is a strong agreement between the CPE-based and the immunostaining-

based MN assays when the original virus is used. The MN CPE and the Virospot MN assay show a comparable trend either when the MN CPE is compared to the Virospot MN titers expressed in MN80 (**Figure 16.A**) or MN90 values (**Figure 16.B**).

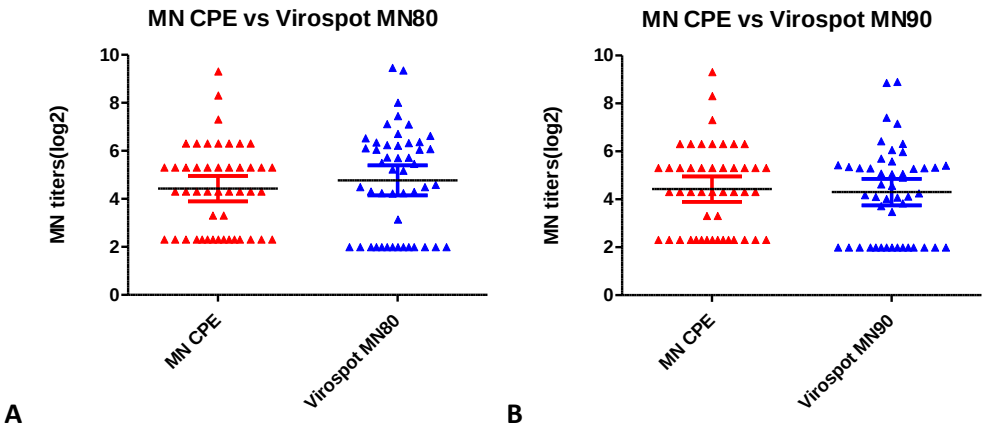

Figure 16. MN titers obtained by testing serum samples with MN CPE and Virospot MN. MN titers are converted in log2. MN CPE results were compared with both MN Virospot reduction point results, 80% (MN80, Fig. A) and 90% (MN90, Fig. B), using SARS-CoV-2 Wild type strain. The Mean of the samples tested with the two MN methods and the 95% Confidence intervals (C.I) of the Mean are shown.

In conclusion, an overall agreement between the two different MN methods to detect neutralizing antibody against the WT strain was observed. Additionally, pre-pandemics samples do not show any protection from the WT virus in either of the two assays, indicating that the methods show identical ability to detect negative titers.

5.2.1.2 MN CPE vs Virospot MN assay: SARS-CoV-2 Alpha variant

The same panel of 47 human serum samples previously tested in the 1st run against SARS-CoV-2 Wild type strain was tested against SARS-CoV-2 Alpha variant.

A standard number of infectious units (30-350 spots/well) of SARS-CoV-2 Alpha variant was incubated with serial dilutions of serum samples, starting from 1:8 as first dilution. The same procedure used in the 1st run was then followed. The log2-trasformed neutralization titers of all the 47 samples obtained through the MN CPE were compared to those obtained calculating the Virospot MN80 and MN90.

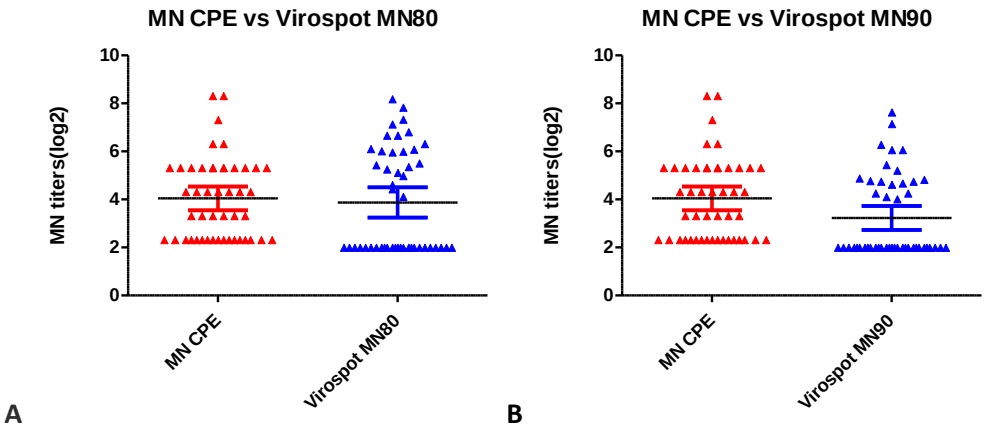

Figure 17. MN titers obtained by testing serum samples with MN CPE and Virospot MN. MN titers are converted in log2. MN CPE results were compared with both MN Virospot reduction point results, 80% (MN80, Fig. A) and 90% (MN90, Fig. B), using SARS-CoV-2 Alpha variant. The Mean of the samples tested with the two MN methods and the 95% C.I of the Mean are shown.

As shown in **Figure 17**, the MN assays performed with SARS-CoV-2 Alpha variant showed similar ability to detect virus-specific neutralizing antibodies. When the MN CPE titers were compared to the Virospot MN80 titers (**Figure 17.A**), the Mean values are very close to each other (4.04; 95% C.I. 3.54-4.54; and 3.87; 95% C.I. 3.24-4.50, respectively). A slightly higher difference in mean titers was observed when comparing MN CPE and Virospot MN90 results (**Figure 17.B**), with lower titers obtained by using the MN Virospot with the 90% reduction point readout (Mean titer: 3.23; 95% C.I. 2.73-3.73). However, the means differ by less than 1log2, hence they are still regarded as similar.

SAMPLE ID	SARS-CoV-2 Wild type					SARS-CoV-2 Alpha variant				
	MN CPE titers(log2)	Virospot MN80 titers (log2)	Virospot MN90 titers (log2)	Diff MN CPE titers(log2)/Virospot MN80 titers (log2)	Diff MN CPE titers(log2)/Virospot MN90 titers (log2)	MN CPE titers(log2)	Virospot MN80 titers (log2)	Virospot MN90 titers (log2)	Diff MN CPE titers(log2)/Virospot MN80 titers (log2)	Diff MN CPE titers(log2)/Virospot MN90 titers (log2)
1	6,32	7,13	5,71	-0,81	0,62	6,32	6,81	6,07	-0,49	0,26
2	6,32	6,64	6,07	-0,32	0,25	4,32	5,44	4,89	-1,11	-0,57
3	4,32	4,50	4,09	-0,18	0,23	2,32	2,00	2,00	0,32	0,32
4	5,32	6,06	5,31	-0,74	0,01	5,32	6,32	5,45	-1,00	-0,13
5	8,32	9,47	8,91	-1,15	-0,59	8,32	8,19	7,64	0,14	0,69
6	6,32	6,34	5,42	-0,01	0,90	5,32	5,51	4,63	-0,19	0,69
7	6,32	5,71	5,30	0,61	1,02	5,32	5,97	4,68	-0,64	0,64
8	6,32	6,72	6,33	-0,40	0,00	5,32	6,02	4,83	-0,69	0,49
9	4,32	5,51	5,06	-1,19	-0,74	4,32	5,26	2,00	-0,94	2,32
10	4,32	4,32	3,85	0,00	0,47	3,32	2,00	2,00	1,32	1,32
11	9,32	9,36	8,87	-0,03	0,45	8,32	7,84	7,15	0,48	1,17
12	5,32	6,23	5,34	-0,91	-0,02	5,32	6,09	4,26	-0,77	1,06
13	5,32	6,38	5,07	-1,06	0,25	4,32	4,61	4,02	-0,29	0,30
14	4,32	5,73	5,36	-1,41	-1,04	3,32	4,44	2,00	-1,12	1,32
15	5,32	6,06	5,29	-0,74	0,03	5,32	6,67	5,21	-1,34	0,12
16	3,32	4,30	4,13	-0,98	-0,81	3,32	4,12	2,00	-0,80	1,32
17	3,32	4,25	3,49	-0,93	-0,16	2,32	2,00	2,00	0,32	0,32
18	7,32	8,02	7,42	-0,70	-0,09	6,32	7,14	6,29	-0,82	0,03
19	5,32	6,54	5,99	-1,22	-0,67	4,32	6,00	4,78	-1,68	-0,45
20	4,32	5,47	4,92	-1,15	-0,60	3,32	2,00	2,00	1,32	1,32
21	5,32	6,25	5,44	-0,92	-0,11	5,32	2,00	2,00	3,32	3,32
22	6,32	6,36	5,60	-0,04	0,72	5,32	6,11	4,75	-0,79	0,57
23	5,32	5,24	5,09	0,09	0,23	5,32	2,00	2,00	3,32	3,32
24	4,32	4,60	4,11	-0,28	0,21	4,32	2,00	2,00	2,32	2,32
25	4,32	4,24	4,03	0,08	0,30	4,32	2,00	2,00	2,32	2,32
26	5,32	4,50	4,26	0,82	1,07	5,32	4,99	4,11	0,34	1,21
27	4,32	5,19	4,64	-0,87	-0,32	3,32	2,00	2,00	1,32	1,32
28	5,32	5,74	4,58	-0,42	0,74	4,32	6,67	6,07	-2,35	-1,75
29	4,32	3,15	2,00	1,17	2,32	3,32	2,00	2,00	1,32	1,32
30	5,32	6,09	4,19	-0,77	1,13	5,32	5,12	4,26	0,21	1,06
31	2,32	2,00	2,00	0,32	0,32	2,32	2,00	2,00	0,32	0,32
32	2,32	2,00	2,00	0,32	0,32	2,32	2,00	2,00	0,32	0,32
33	2,32	2,00	2,00	0,32	0,32	2,32	2,00	2,00	0,32	0,32
34	2,32	2,00	2,00	0,32	0,32	2,32	2,00	2,00	0,32	0,32
35	2,32	2,00	2,00	0,32	0,32	2,32	2,00	2,00	0,32	0,32
36	2,32	2,00	2,00	0,32	0,32	2,32	2,00	2,00	0,32	0,32
37	2,32	2,00	2,00	0,32	0,32	2,32	2,00	2,00	0,32	0,32
38	2,32	2,00	2,00	0,32	0,32	2,32	2,00	2,00	0,32	0,32
39	2,32	2,00	2,00	0,32	0,32	2,32	2,00	2,00	0,32	0,32
40	2,32	2,00	2,00	0,32	0,32	2,32	2,00	2,00	0,32	0,32
41	2,32	2,00	2,00	0,32	0,32	2,32	2,00	2,00	0,32	0,32
42	2,32	2,00	2,00	0,32	0,32	2,32	2,00	2,00	0,32	0,32
43	2,32	2,00	2,00	0,32	0,32	2,32	2,00	2,00	0,32	0,32
44	2,32	2,00	2,00	0,32	0,32	2,32	2,00	2,00	0,32	0,32
45	2,32	2,00	2,00	0,32	0,32	2,32	2,00	2,00	0,32	0,32
46	6,32	7,46	7,17	-1,14	-0,85	7,32	7,34	4,75	-0,02	2,57
47	5,32	6,12	5,31	-0,80	0,01	5,32	5,36	2,00	-0,04	3,32

Table 4. Comparison of Individual MN titer values obtained from the MN CPE and Virospot MN (expressed in MN80 and MN90 results). Titers are converted in log2. For each sample, difference ("Diff") in log2-titers of samples tested with the use of MN CPE and Virospot MN80 ("Diff MN CPE titers(log2)/Virospot MN80 titers(log2)") or MN CPE and Viropot MN90 ("Diff MN CPE titers(log2)/Virospot MN90 titers (log2)"), are shown for both SARS-CoV-2 WT and Alpha variant. Differences greater than 1log2 are highlighted in red.

Table 4 shows that results obtained by using these two different MN methods are highly reproducible, with MN titer of each sample being within 1log2 difference for many samples.
When the SARS-CoV-2 Wild type strain was used, MN CPE titers were similar to titers obtained using Virospot MN80 (column "Diff MN CPE titers(log2)/Virospot MN80 titers(log2) of **Table 4**) in 83% of the cases (39 out of 47). Similarly, 81% of Virospot MN90 titers are in agreement with MN CPE titers, with only 5 samples showing greater than 1log2 difference in titers obtained with the two different methods (column "Diff MN CPE titers(log2)/Virospot MN90 titers(log2) of **Table 4**).
When Alpha variant was used, a 72% agreement (34 ot of 47 samples) was observed when comparing MN CPE titers and Virospot MN titers expressed in MN80 values; and 64% of titers were instead similar (30 out of 47) when MN CPE results were compared with Virospot MN90 results.
In conclusion, the greatest differences were found when the CPE-based and the immunostaining-based methods were performed using the Alpha variant, showing a lower agreement (72% for the comparison MN CPE vs MN80; and 64%, for MN CPE vs MN90) than

that showed in the run where the Wild type strain was used (83% for MN CPE vs MN80; 81% for MN CPE vs MN90).

5.2.2 MN CPE and Virospot MN agreement: Linear regression analysis

A comparison of log2-tranformed MN titers using the two different coronavirus variants (Wild type and Alpha) was performed through the use of linear regression analysis (**Figure 18**).

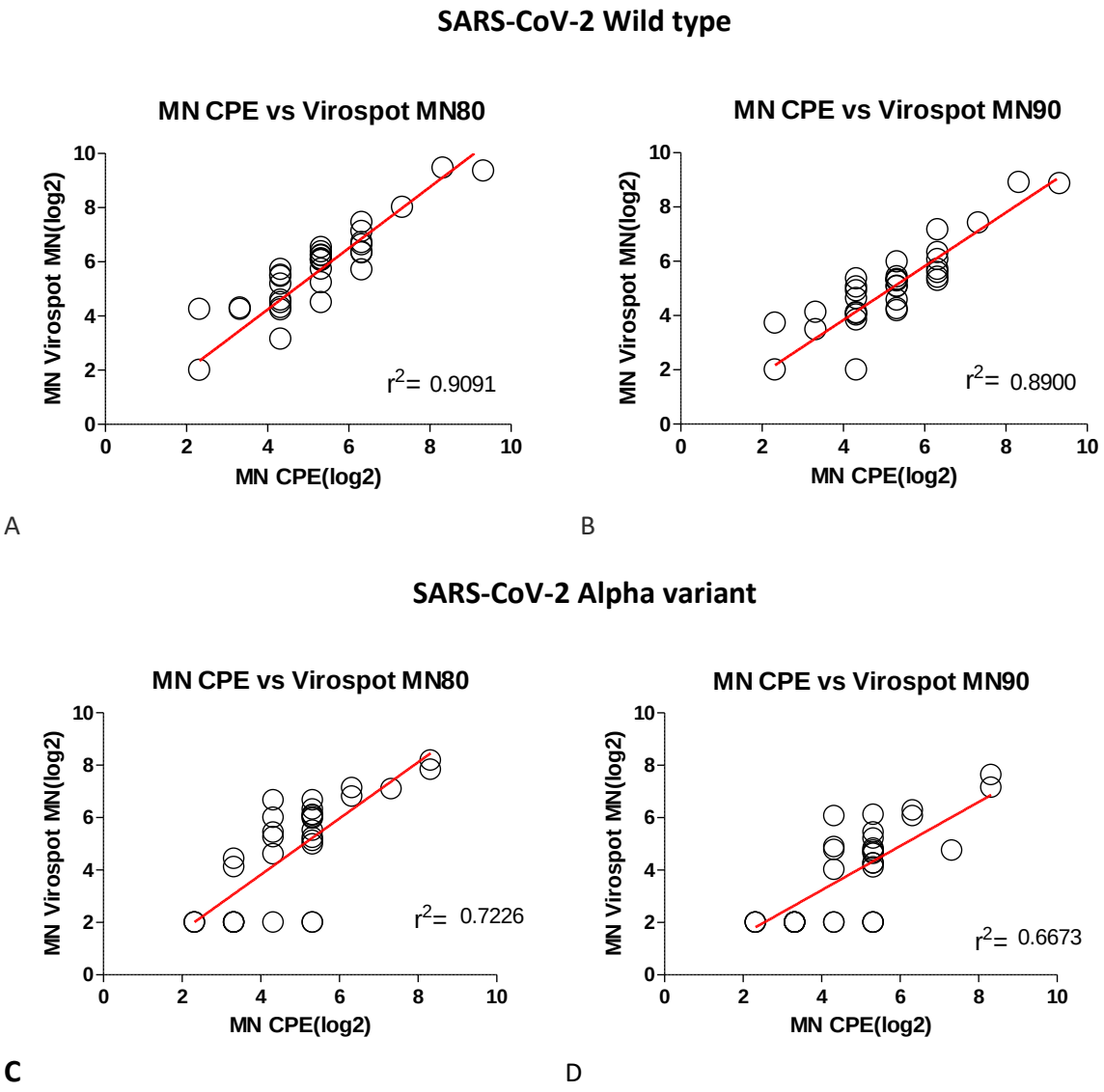

Figure 18. Correlation between MN titers obtained through the MN CPE and the Virospot MN assay, for both MN80 and MN90 results, using SARS-CoV-2 WT (A and B) and Alpha variant (C and D). Results are represented as $\log_2$ of MN titers.

The correlation of the two assays was assessed using Pearson's correlation. When the SARS-COV-2 WT was used (**Figure 18 A, B**) the MN CPE assay demonstrated an excellent correlation with either the Virospot MN 80% reduction point (r^2 = 0.9091*)*, or the Virospot MN 90% reduction points) (r^2 = 0.8900*)*. A decrease in the correlation values was observed when the

Alpha variant was used, showing r^2=0.7226 (MN CPE/Virospot MN80) (**Figure 18 C**) and r^2= 0.6673 (MN CPE/Virospot MN90) (**Figure 18 D**).

5.2.3 MN CPE- Virospot MN agreement: Bland-Altman analysis

To further analyse the concordance between the MN CPE and the Virospot MN results, the Bland-Altman analysis has been performed. Differences between the pairs of measurements were plotted against their means for each assay, and for each strain (Wild type; **Figure 19, A,B**); and Alpha; **Figure 19 C,D**). As shown in **Figure 19**, the Bland-Altman analysis shows only small differences in MN titers measured using MN CPE and MN Virospot (MN80 or MN90) regardless of the viral strain used (Wild type or Alpha variant).

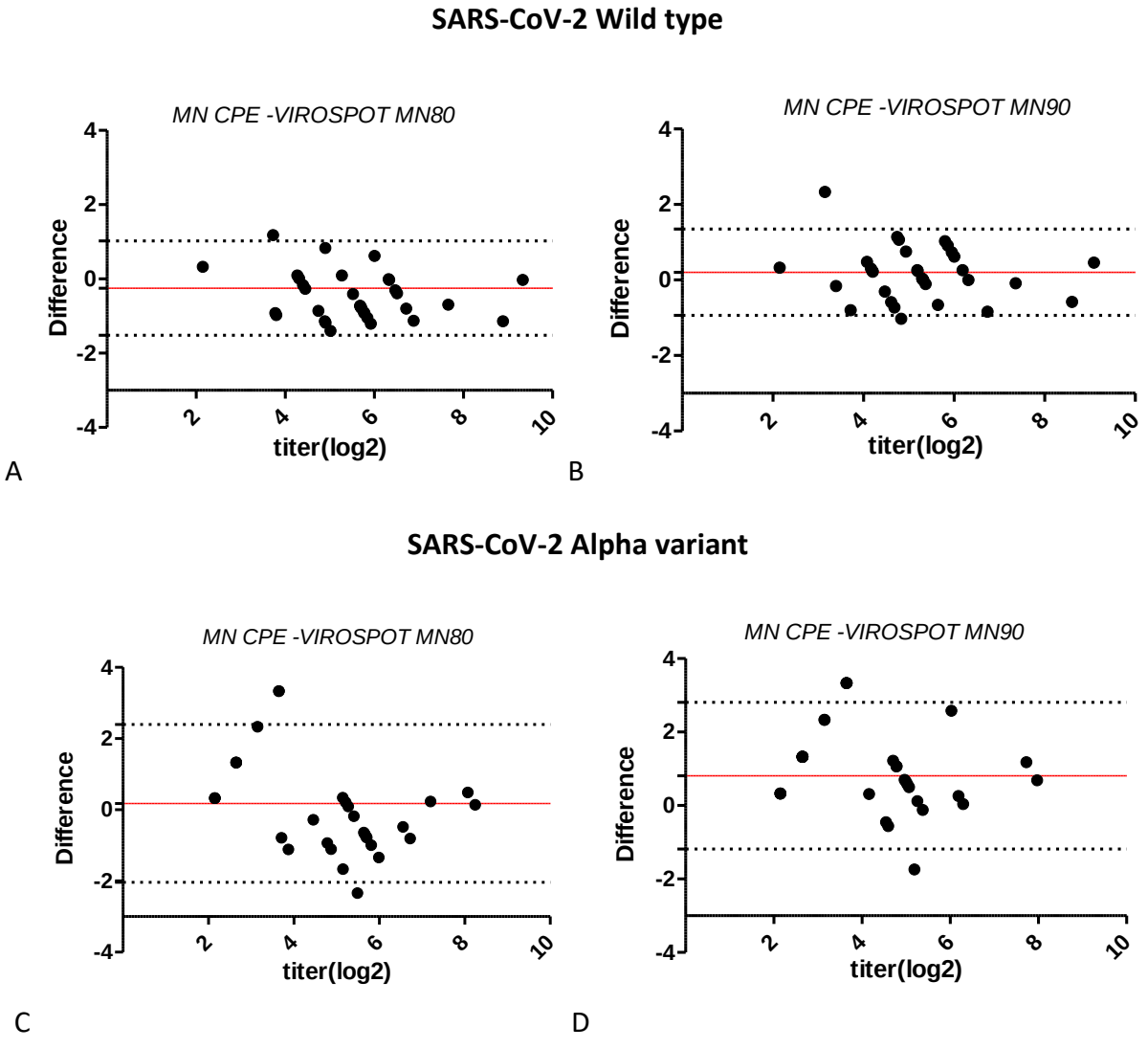

Figure 19: Bland-Altman plot of differences between MN CPE and Virospot MN80(A), or MN CPEand MN90(B) log2-converted titers converted, using the WT strain. Differences between MN CPE and Virospot MN80, or MN CPE and MN90 log2-converted titers using the Alpha strain are shown in Fig.C and D, respectively.

In **Figure 19**, the mean difference of each value (black bullets) between the two methods is plotted. The limits of agreement (stippled black lines) and the overall mean of differences (bias, red line) are shown.

In the assay run with the use of the Wild type strain (**Figure 19 A, B**) only one serum (sample n.29) showed a greater value than the higher limit of agreement when MN CPE titers were compared to the Virospot MN80 titers.

Instead, in the comparison between MN CPE and Virospot MN90 using the SARS-CoV-2 Alpha variant, a significant systematic bias (-0.812; 95% Limits of Agreement -1.18, 2.81) was found. O 4 out of 47 serum samples (sample n.21, 23, 24 and 25) showed a greater value than the higher limit of agreement (**Figure.19, C, D**) and one sample (sample n.28) exceeded the lower limit of agreement when comparing MN titers with either Virospot MN80 or MN90 titers. Samples 9, 46 and 47 showed a difference higher than the higher limit of agreement only in the comparison between MN CPE and Virospot MN90.

Overall, a higher concordance was found when comparing the MN CPE titers with Virospot MN80 (rather than MN90) titers for both SARS-COV-2 strains. However, while the use of WT strain yielded very similar results with either MN CPE, Virospot MN80 and Virospot MN90, greater differences were observed in the tests performed by using the Alpha variant, especially in the comparison MN CPE/Virospot MN90.

5.3 RESULTS III

5.3.1 SARS-CoV-2 Virospot MN assay: Optimization and robustness assessment

The Virospot MN assay performed in Project II has been validated for SARS-CoV-2 WT, variant BavPat1/2020, isolated in the beginning of the COVID-19 pandemic. However, since new viral variants have emerged, several new conditions (such as the choice of infection medium or the concentration of CMC to be used for plates overlay) needs to be adapted to optimize the method and make it more sensitive for the analysis of samples against the new variants. Moreover, to assess the assay robustness, different temperatures and incubation time points should be tested.

The optimization study carried out in this project (Project III) has been performed using four different SARS-CoV-2 variants (Wild Type, Alpha, Beta, and Gamma). To compare MN titer results of these different variants, the virus input should be similar and since they have different replication kinetics and spot morphologies, the use of CMC is necessary. After the initial infection and application of CMC, individual spot will begin to develop as viral infection and replication are constrained to the surrounding monolayer. Infected cells will continue the replication-lysis-infection cycle, further propagating the infection, resulting in increasingly

distinct and discrete spots. A CMC concentration of 1% was used in most of the optimization assays based on previous setup experiments (**Figure 20**). Different sample matrices (Optimization I), culture media (Optimization II), and incubation time/temperature (Optimization III and IV) were then assessed to evaluate test performance and robustness. Finally, a thorough assessment of CMC concentration was performed (Optimization V) on the optimized assay, so that to improve the spot count under the chosen conditions.

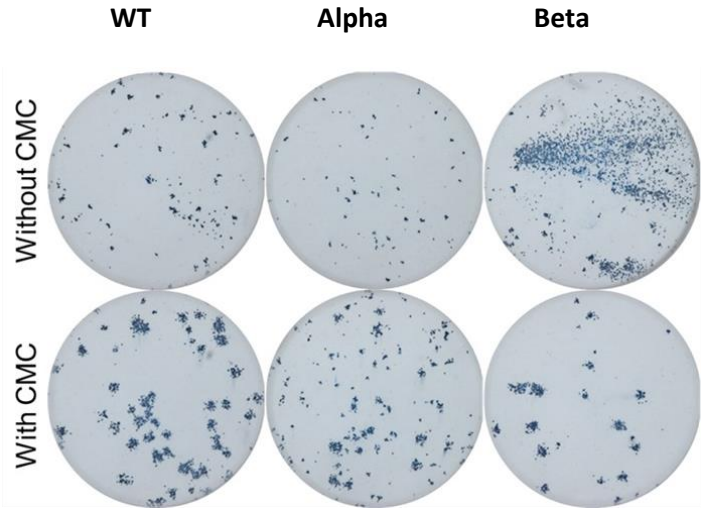

Figure 20. Overview of spots morphology without and with CMC 1% for SARS-CoV-2 Wild type, Alpha and Beta variant.

5.3.1.1 Optimization I – Sample matrix evaluation: Serum *vs* Plasma

In the first Optimization performed, DMEM was used as culture medium and CMC 1% was added as overlay after the incubation and removal of the mixture sample/virus on the VERO E6 cells. The SARS-CoV-2 neutralizing titer of 11 matched serum and EDTA plasma samples (from identical donations) were determined, in order to assess the effect of the sample matrix on the results. Incubations were carried out at 37°C, 5% CO2. Samples were tested against the four different SARS-CoV-2 viruses above mentioned (WT, Alpha, Beta and Gamma).

Both serum and plasma samples showed substantial neutralization against the WT variant, with a mean titer of 7.01 (95%C.I. 5.98-8.05) 4.92 (95%C.I. 4.11-5.76) and 2.78 (95%C.I. 2.37-3.18) in MN50, MN80 and MN90, respectively (**Figure.21 A,B,C**), The mean values for the other variants tested was lower than the mean obtained for the WT strain, independently of the matrix used (**Figure 22**) .

For each virus and reduction point evaluated (MN50, MN80 and MN90), T-test analysis was performed in order to assess whether the means of the two matrices (serum and plasma) were statistically different from each other. This analysis confirmed the similarity in titers between results obtained with serum and plasma samples ($p > 0.05$) (**Figure 21**).

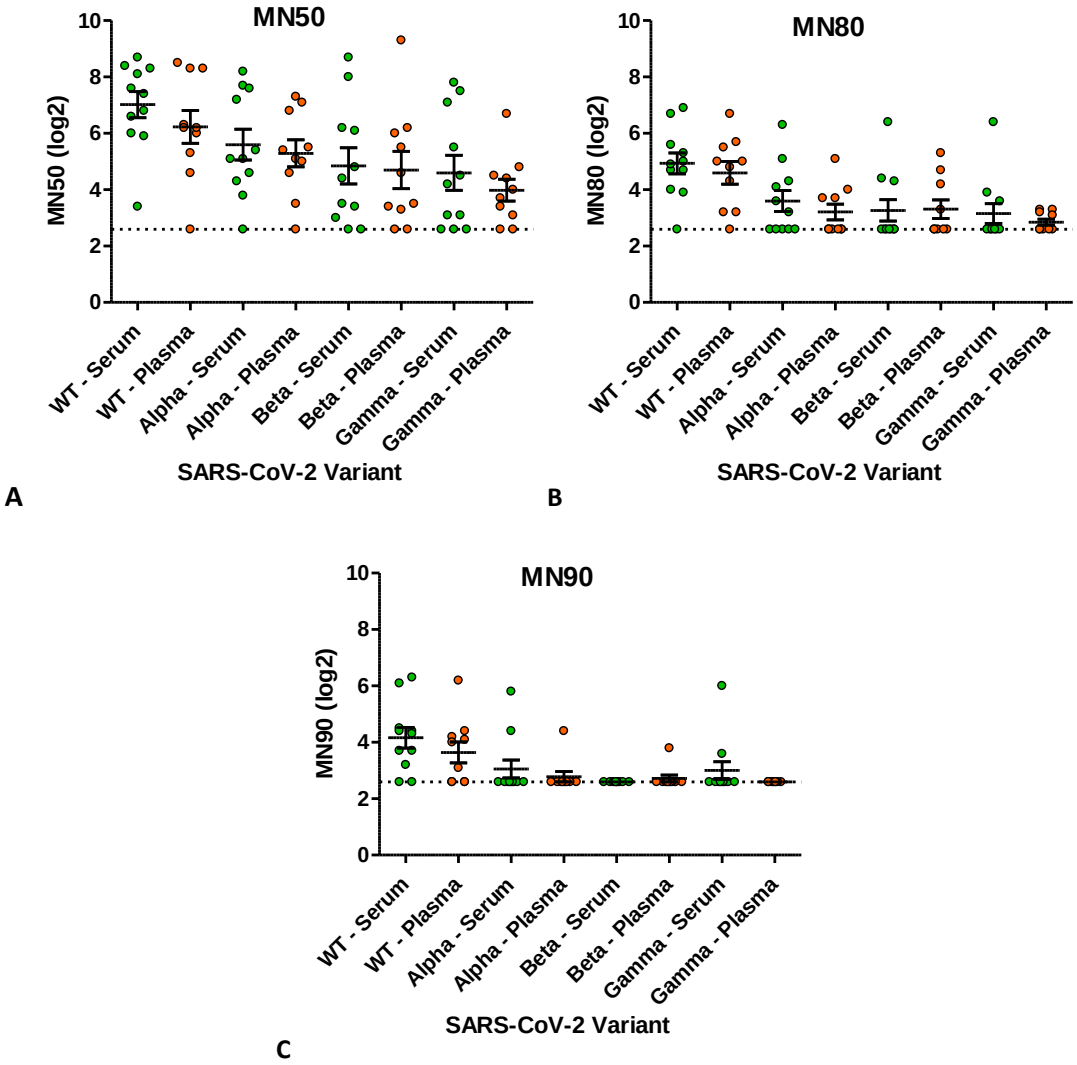

Figure 21, Mean of the converted log2 MN titers obtained by testing serum and plasma samples against four different SARS-CoV-2 variants (Wild Type, Alpha, Beta, Gamma) through Virospot MN. Results are reported for each reduction point, i.e. MN50, MN80 and MN90 titers (A, B, C, respectively). Horizontal dotted line indicates the lowest sample dilution tested. ($p>0.05$; paired t-test).

Comparison of mean titers obtained by using MN50, MN80 and MN90 showed that slightly different results can be obtained depending on the reduction point used. The highest means were reported when results were expressed as MN50 while the lowest when the MN90 was used as readout (**Figure 21**). Based on the virus variant tested, which might be more or less susceptible to neutralization compared to another variant, and the chosen reduction point, a sample can have a high or low MN titer result or can even be negative. As such it is expected and accepted that the number of MN titer results is not equal for all virus variants and reduction points.

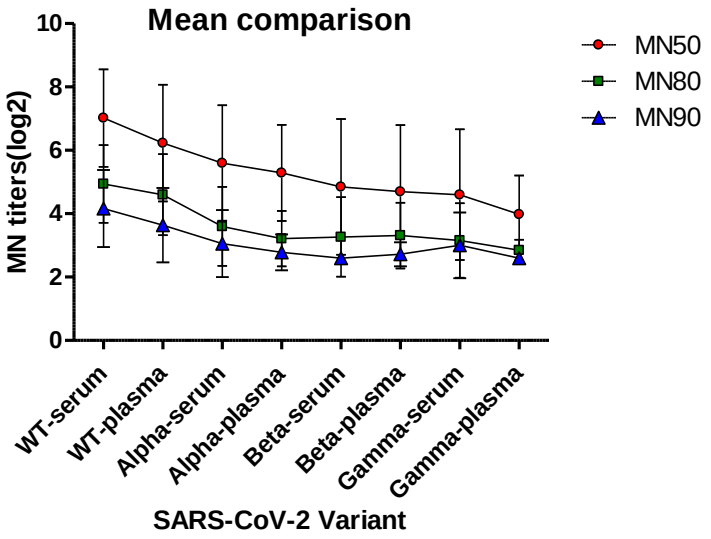

Figure22. Comparison analysis of Mean values for each reduction point (MN50, MN80, MN90) obtained by testing serum and plasma samples against four different SARS-CoV-2 variants (Wild Type, Alpha, Beta, Gamma).

Although still highly similar, as also confirmed with the t-test, the major differences between serum and plasma assessments were observed when using the WT strain (Difference in log2 mean titers between matrices - $Dmean_{matrix}$ – MN50: 0,79; MN80: 0,34; MN90: 0,52). Smaller differences were reported with Alpha ($Dmean_{matrix}$ MN50: 0,31; MN80: 0,39; MN90: 0,28) Beta ($Dmean_{matrix}$ MN50: 0,15; MN80: 0,05; MN90: 0,12) and Gamma variant ($Dmean_{matrix}$ MN50: 0,62; MN80: 0,31; MN90: 0,4). In comparison to the WT variant, the mean titer obtained by using the Alpha, Beta or Gamma variant as viral input was lower, showing differences in mean values between WT and Alpha, Beta, Gamma ranging between 0.86 (WT /Alpha mean) and 2.42 (WT/Gamma mean values) (**Table 5**).

SERUM VS PLASMA mean 50%			SERUM VS PLASMA mean 80%			SERUM VS PLASMA mean 90%		
WT	7.02	Serum	WT	4.94	Serum	WT	4.16	Serum
	6.23	Plasma		4.60	Plasma		3.64	Plasma
Alpha	5.60	Serum	Alpha	3.60	Serum	Alpha	3.06	Serum
	5.29	Plasma		3.21	Plasma		2.78	Plasma
Beta	4.85	Serum	Beta	3.26	Serum	Beta	2.60	Serum
	4.70	Plasma		3.31	Plasma		2.72	Plasma
Gamma	4.60	Serum	Gamma	3.16	Serum	Gamma	3.00	Serum
	3.98	Plasma		2.85	Plasma		2.60	Plasma
Mean values difference 50%			**Mean values difference 80%**			**Mean values difference 90%**		
WT/Alpha	Serum	1.00	WT/Alpha	Serum	1.34	WT/Alpha	Serum	1.11
	Plasma	0.94		Plasma	1.39		Plasma	0.86
WT/Beta	Serum	2.17	WT/Beta	Serum	1.67	WT/Beta	Serum	1.56
	Plasma	1.53		Plasma	1.29		Plasma	0.92
WT/Gamma	Serum	2.42	WT/Gamma	Serum	1.78	WT/Gamma	Serum	1.16
	Plasma	2.25		Plasma	1.75		Plasma	1.04

Table 5. Mean values for MN50, MN80 and MN80 of serum and plasma samples tested against SARS-CoV-2 Wild type, Alpha, Beta and Gamma variant. Difference between the mean value of each group of serum and plasma samples tested against WT and the mean value of samples tested with the other three variants (Alpha, Beta and Gamma) is shown.

In conclusion, these results demonstrate that serum and EDTA plasma are suitable and equivalent sample matrices to be tested in the SARS-CoV-2 Virospot MN assay, with a trend for larger (though acceptable) differences between the two matrices observed when *i)* the original SARS-CoV-2 virus is used, rather than its variants, and when *ii)* the MN50 is used as reduction point. The above evaluation also shows a general reduction in neutralization capacity of human serum/plasma samples towards SARS-CoV-2 variants (especially Beta and Gamma) as compared to activity showed against Wild Type SARS-CoV-2.

5.3.1.2 Optimization II - Effect of culture media on spot count and MN titer results

In this experiment the use of two different infection media, DMEM with CO2 and MEM without CO2 supplementation using the same cell line (VERO E6), was evaluated. Using the latter culture medium, it was previously demonstrated, performing a viral titration, that Vero E6 cells become more susceptible and permissive for SARS-CoV-2 (data not shown). Reducing the virus input may be regarded as an option in this case, but this might increase assay sensitivity and expenses of specificity. Therefore, the effect of the different culture media on neutralization titers was assessed testing a panel of 10 serum samples and 10 EDTA plasma samples against different infectious doses of SARS-CoV-2 Wild Type, Alpha, Beta and Gamma variants. A COVID-19 convalescent pooled serum, VC-Lot# VC-2120140051 used as positive control of the assay.

Variant	DMEM + CO_2		MEM - CO_2	
	Dilution factor stock	Mean spot count VC wells	Dilution factor stock	Mean spot count VC wells
WT	120	98	700	81
Alpha	5	111	100	22
Beta	75	67	200	119
Gamma	50	104	1,200	38

Table 6. Virus stock dilution factors and the mean of the Viral Control (VC) spot counts obtained using DMEM + CO2 and MEM-CO2 are showed for each variant (WT, Alpha, Beta and Gamma).

The SARS-CoV-2 neutralizing titers of eleven matched serum and EDTA plasma samples (from identical donations) were determined, using DMEM with CO2 (DMEM + CO2) and MEM without CO2 supplementation (MEM – CO2). SARS-CoV-2 WT, Alpha, Beta and Gamma variants that were used for this assessment were diluted as described in **Table 6**, and results were expressed as MN50, MN80 and MN90 (**Figure 23**).

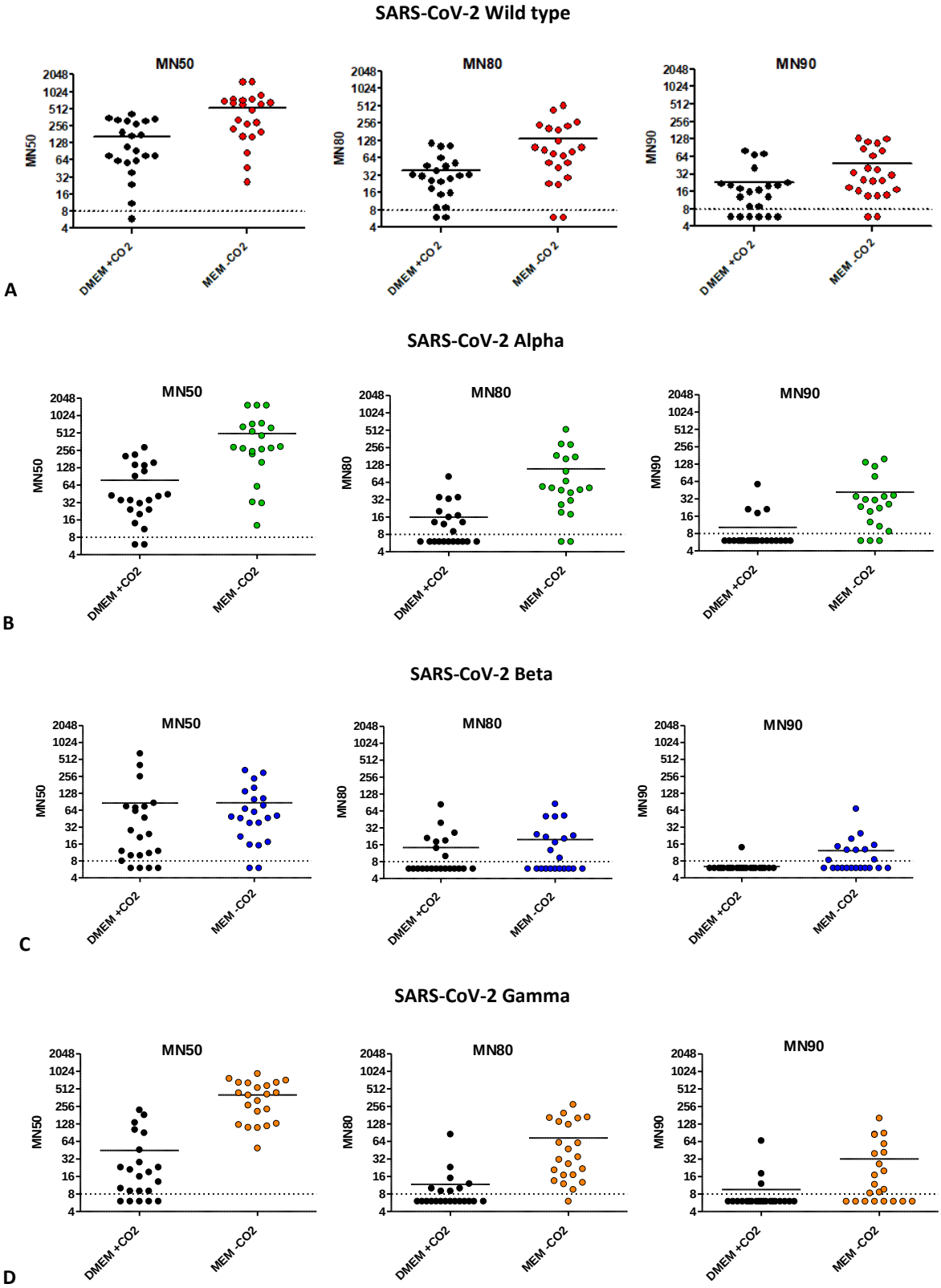

Figure 23. Comparison between MN50, MN80, MN90 titers for Wild type(A), Alpha(B), Beta(C), Gamma(D) variants obtained using two different media, DMEM + CO2 and MEM - CO2. MN50, MN80, MN90 titers are reported as the highest sample dilution where we have 50%,80%,90% of plaque reduction compared to the virus control.

Samples clearly showed higher MN titers when using MEM - CO2, compared to DMEM + CO2. The magnitude of the increase differed per variant virus used.

T-test analysis showed that means obtained with DMEM+CO2 and MEM-CO2 are significantly different, showing p values <0.05 (**Table 7**). Only in the case of the Beta variant MN50 and MN90 readout the p value is >0.05, so no difference between the two different media/incubation conditions is shown in MN titers when this SARS-CoV-2 variant was used.

	MN50 (*p value*)	**MN80 (*p value*)**	**MN90 (*p value*)**
WT	< 0.0001	0.0014	0.0002
Alpha	0.0003	0.0043	0.0027
Beta	0.9559	0.0240	0.0550
Gamma	< 0.0001	0.0009	0.0100

Table 7. T-test analysis. P values overview for MN50, MN80, MN90 titers obtained with SARS-CoV-2 Wild type, Alpha, Beta and Gamma variant using DMEM + CO2 and MEM - CO2 media. Not significant differences are highlighted in red.

Because of the increased sensitivity and the possibility of using a higher virus dilution, it was decided to perform all the following experiments using MEM without CO2 supplementation.

5.3.1.3 Optimization III - Sample/virus first incubation step: Different temperatures and time points

To investigate the robustness of the first incubation step between diluted samples and virus, the effect of three different incubation timepoints (30 min, 70min, 150 min) and two different incubation temperatures (37°C/room temperature) have been evaluated on MN titer results. MEM W/O CO2 was used as infection medium and CMC 1% as overlay post infection. A panel of 3 serum samples with High(H), Medium (M) and Low (L) titer and 3 EDTA plasma samples showing H, M, and L titer (Sample ID "I100557139001", "I100557150001", "I100557077001";"I100557160001", "I100557101001" "I100557078001", respectively) were selected from the Optimization II experiments and their MN titers were determined. Based on Optimization I and Optimization II experiments, it was chosen to express results as MN80. This reduction point seemed a good compromise as *i)* it results in low differences in mean titers when testing different human specimens (plasma or serum) from the same donor as compared to MN50 results (Optimization I; **Figure 21**); *ii)* when MEM w/o CO2 is used, there is a lower risk towards diminished sensitivity of the assay with the MN80 readout as compared to the MN90 readout (which instead might not spot low positive results); and *iii)* when MEM without CO2 is used, results expressed as MN80 show a lower tendency towards decreased specificity compared to the use of the MN50 reduction point (Optimization II; **Figure 23**). According to the Optimization I experiments, the major differences in mean titers of the same panel of samples were observed between Wild Type strain and Gamma variants results (Optimization I; **Table 5**). The two viruses also show significant differences in samples mean titer results when using different infection media to perform the Virospot MN. Hence, in order

to have an idea of the maximum variability possible when changing critical conditions (such as serum-virus incubation time, and incubation temperature), it was decided to prioritize the analysis of these two viruses over the other SARS-COV-2 variants. As reported in **Figure 24 A**, incubation of serum samples with the Wild type SARS-CoV-2 virus at 37°C results in an increase in MN titers which is time-dependent. While no major differences are observed between the minimum (30 minutes) and standard (60 minutes) incubation timepoints. A >1log2 increase in mean titers was reported when comparing results of the standard condition and the maximum incubation time (120 minutes), with a tendency for larger increase in neutralization when evaluating high-titer samples (Maximum difference observed: 2,93 log2). At RT, the effect of incubation time on WT MN titer is limited (**Figure 24 B**) regardless of the neutralization capacity of the sample of interest. Titers measured at 37°C and RT are very similar when the virus-sample mixture is incubated under the standard condition. Thus, we can conclude that using RT as incubation temperature makes the assay performed with the WT strain under the tested conditions (matrix: serum samples; infection medium: MEM; CO2 supplementation: none) more robust.

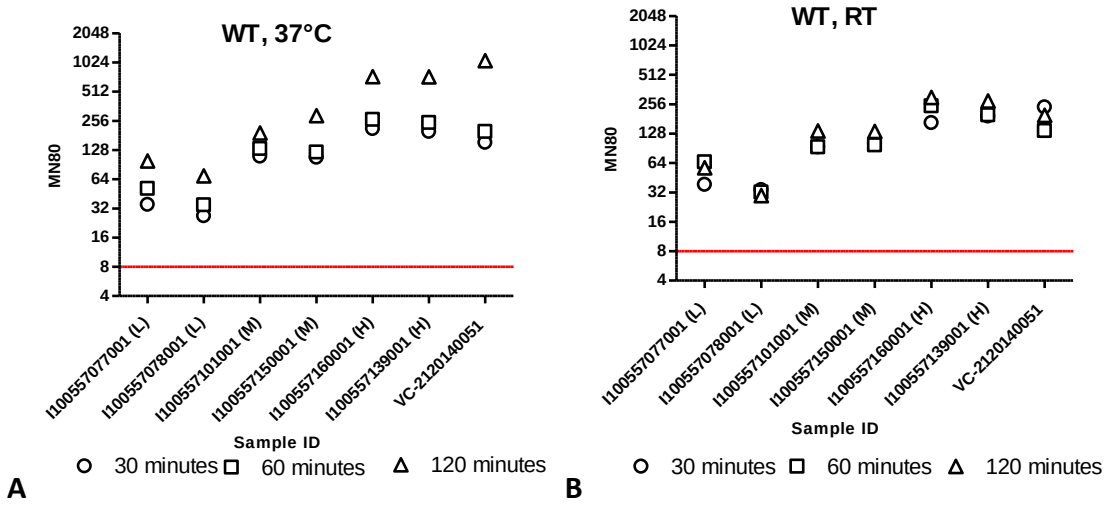

Figure 24. MN80 titers of samples I100557139001", "I100557150001", "I100557077001";"I100557160001", "I100557101001" "I100557078001" along with the positive control VC-2120140051 are showed using SARS-CoV-2 Wild type. Two temperatures (37°C and RT) and different time points (30min,60min,120min) were evaluated for the first incubation between samples and virus. Titers are reported as the highest sample dilution where we have 80% of plaque reduction compared to the virus control. The red line shows the lowest sample dilution step.

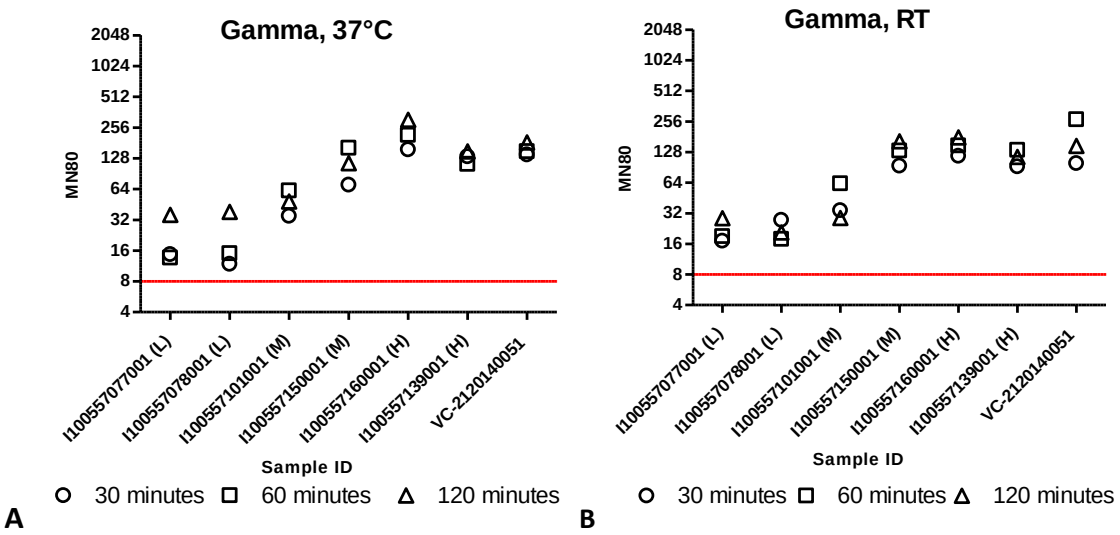

Figure 25. MN80 titers of samples I100557139001", "I100557150001", "I100557077001";"I100557160001", "I100557101001" "I100557078001" along with the positive control VC-2120140051 are showed using SARS-CoV-2 Gamma variant. Two temperatures (37°C and RT) and different time points (30min,60min,120min) were evaluated for the first incubation between samples and virus. Titers are reported as the highest sample dilution where we have 80% of plaque reduction compared to the virus control. The red line shows the lowest sample dilution step.

The effect of a different incubation temperature was less pronounced using the Gamma variant (**Figure 25**). No consistent increase in MN titers was generally observed in medium and high titers serum samples either at 37°C or RT, in any of the timepoint evaluated. Neverthless, a higher than 1log2 difference between the standard condition and the maximum incubation time was observed when testing low positive samples at 37°C (Maximum difference observed: 1,26 log2), showed in **Figure 25, A**, whereas no major differences were reported when evaluating the same timepoints at RT. This suggests once again that RT may be a suitable incubation temperature, able to provide an advantage in terms of assay robustness (**Figure 25,B**).

Mean titers reported in **Table 8** confirm the variation between different incubation conditions after 60 up to 120 minutes at 37°C using WT strain, with an increase of 2,02% . When performing the assay with the Gamma variant, Mean values did not show a significant variation in any of the different incubation conditions. A steady increase in Mean values has been observed at 37°C (0,3%-0,2% after 30 and 60 min, respectively) and a decrease at RT after 60 minutes of incubation (decrease of -0,12% compared to Mean after 60 minutes of incubation).

Serum/virus incubation: Mean values of MN titers						
Variant	37°C			Room Temperature		
	30min	60min	120min	30min	60min	120min
WT	120.2	149.6	452.7	123.4	123.8	161.3
Gamma	79.9	104.2	124.9	68.67	111.5	97.36

Table 8. Mean values overview for samples tested with WT and Gamma variant. During the first incubation period (sample/virus) different temperatures (37°C and RT) and different time points (30min,60min,120min) were evaluated.

Taken together these results indicate that the assay might be more robust when incubation is performed at RT, instead of 37°C. Therefore it was decided to perform the following experiments mantaining the sample/virus incubation step at room temperature with a limit to 60 minutes.

5.3.1.4 Optimization IV: Sample/virus mix on VEROE6 cells incubation step: Different time points

In the second incubation the mixture samples/virus is added on the VEROE6 cells. In the validated Virospot MN, after 60 min of incubation at 37°C, the mixture is removed, and fresh infection medium is added and incubated for 24 hours (final incubation).

To assess the robustness of the second incubation period, three time points were tested: 30, 60 and 120 minutes. The same panel of 6 samples previously used in the Optimization III experiments were tested against SARS-CoV-2 WT and Gamma variant. MN titers are reported as MN80 and are expressed as the highest sample dilution where there is a 80% plaque reduction compared to the virus control.

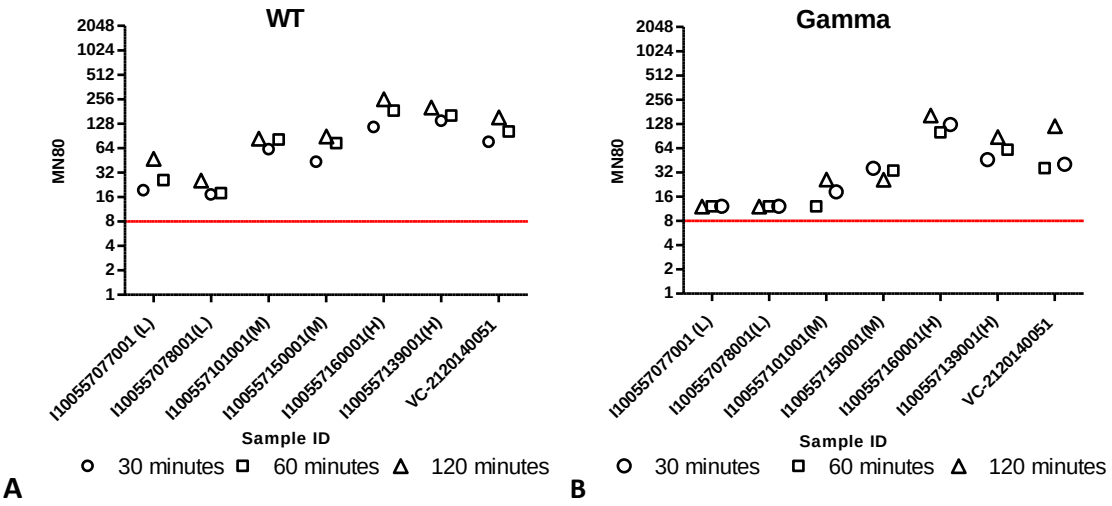

Figure 26. MN80 titers of samples I100557139001", "I100557150001", "I100557077001";"I100557160001", "I100557101001" "I100557078001" along with the positive control VC-2120140051 are showed using SARS-CoV-2 WT and Gamma variant. Different time points (30min,60min,120min) were evaluated for the second incubation of the mixture samples/virus on VEROE6 cells. Titers are reported as the highest sample dilution where we have 80% of plaque reduction compared to the virus control. The red line shows the lowest sample dilution step.

In **Table 9**, mean titer values are shown for WT and Gamma variant after 30,60 and 120 min of incubation. Using SARS-CoV-2 WT the MN titers were found to be higher with increasing incubation times (**Figure 26, A**). Analysis of the mean titer yielded at each timepoint confirmed a steady increase in mean values with the use of the WT variant (**Table 9**). A 26,8% Mean increase has been observed after 30 min of incubation and 25% increase after 60 min of incubation.

Second incubation time points	SARS-CoV-2 variant	
	WT(Mean titer)	Gamma(Mean titer)
30 min	67.14	41.19
60 min	91.71	37.99
120 min	122.2	63.81

Table 9. **Mean values overview for the second incubation step where serum/virus mixture was added on VEROE6 cells.** Different time points (30min,60min,120min) were evaluated.

More variable results were observed for the Gamma variant showing a slight decrease (-0,08%) after 30 min of incubation. Taken together the MN titers at 120 minutes were generally the highest. To avoid variation in titers and hence to have more stable MN titers, a period of 60 minutes has been chosen as the best timepoint to carry on for the second incubation between samples/virus mixture and VEROE6 cells.

5.3.1.5 Optimization V: Effect of different CMC concentration and incubation time on spot size and count

CMC overlay can be used as immobilizing overlay following the initial infection on VEROE6 cells to prevent SARS-CoV-2 infection from spreading indiscriminately in the well. Using this overlay, the virus input can be accurately estimated, depending on the concentration of CMC used (higher concentration causes smaller spots) and the total incubation time (longer incubation period causes bigger spots, which increase with the incubation time (8, 24, or 32 hours).

To investigate the optimal combination of the CMC percentage and optimal incubation time on the spot count, 1, 2 and 3% CMC were tested and different incubation time points (8, 24 and 32 hours) were evaluated on SARS-CoV-2 WT, Alpha, Beta and Gamma variant titrated in 8 replicates. Based on the performance of the experiment, CMC 3% plates were removed from this analysis because of the high viscosity that did not permit to dispense the solution in a proper way on the plates, hence that concentration was considered not practical enough. No samples were used in this experiment. SARS-CoV-2 WT, Alpha, Beta and Gamma variant were titrated as follows: 10-fold serial dilution, starting from virus stock sample. Each viral sample was titrated in 8 replicates starting from column 1 up to column 11. Column 12 was taken as cell control. To compare the variation in spot size and spot count, two columns of the 96 well plates were taken as representatives for each viral variant. Each column represents one single viral dilution in 8 replicates. In the following graphs the mean value of each column has been reported to analyze how the spot count and spot size differ after 8, 24 and 32 hours of incubation.

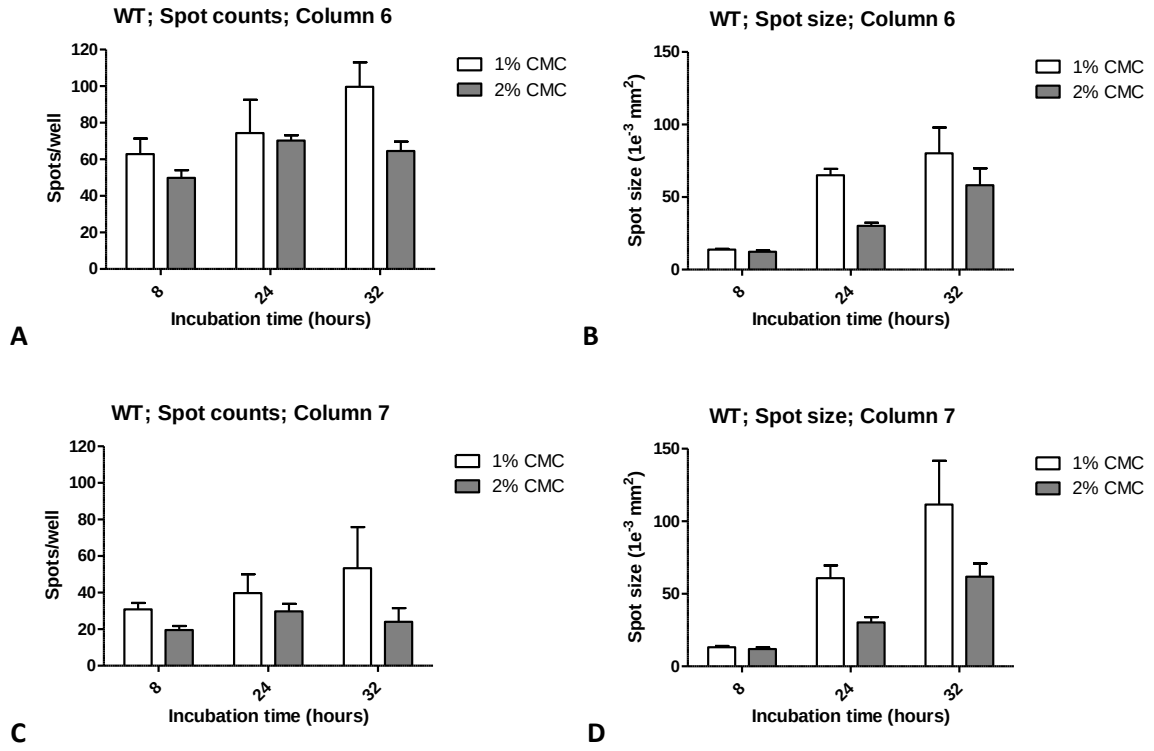

Figure 27. Effect of CMC 1% and 2% and different incubation time (8,24,32 hours) on WT spot count and spot size. Two columns (6,7) of 96 well plate are shown. Spot count (A, C) and spot size (B, D) are reported as the mean value of each column +/-SEM.

As reported in graphs of **Figure 27 A, C** up to 24 hours spot counts are relatively consistent when using 1% or 2% CMC and these counts do not increase with incubation time. At 32 hours the spot counts increase when 1% CMC is used compared to 2% CMC; This is due to overlapping spots, complicating the accurate counting of spots. Moreover, smaller plaques were formed under 2% CMC as compared to 1% CMC (**Figure 27 B,D**). A significant increase in spot size was observed after 24 hours of incubation when 1% CMC was used (51,3 mm^2; 47,61 mm^2 bigger than spot size after 8 hours) showed in **Figure 27**; **B** and **D**,respectively. When CMC 2% was used a lower and steady increase in the spot size has been observed increasing with the incubation time. After 48 hours an increase of 30mm^2, compared to results obtained after 24 hours of incubation, was detected.

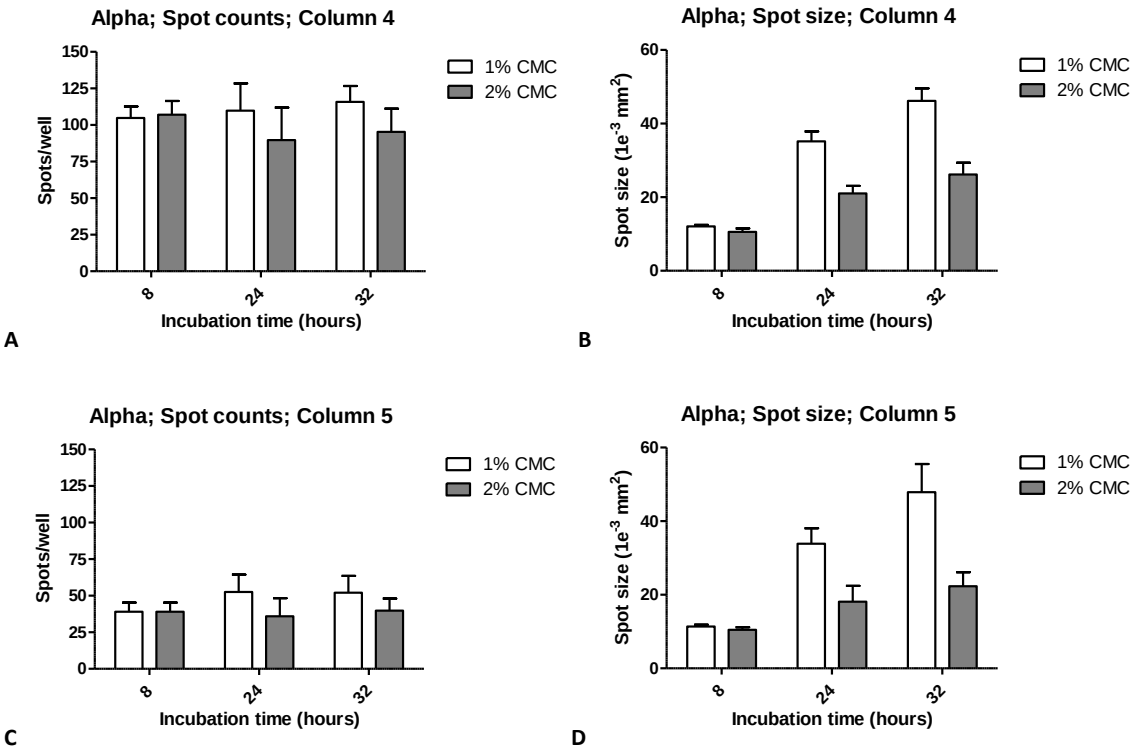

Figure 28. Effect of CMC 1% and 2% and different incubation time (8,24,32 hours) on Alpha variant spot count and spot size. Two columns (4,5) of 96 well plate are shown. Spot count (A, C) and spot size (B, D) are reported as the mean value of each column +/-SEM.

The same effect on the spot size was observed in Alpha variant using CMC 2%. Spots are smaller using 2% CMC compared to 1% CMC (**Figure 28 B,D**). A slight increase in the spot count with 1% CMC was noticed (**Figure 28 A,C**) after 24 hours, compared to 2% CMC; At 8 hours the spot counts is as high as 24 and 32 hours (104; 109; 115 number of spots in column 4 and 39; 52; 52 number of spots in column 5 after 8, 24 and 32 hours, respectively) when 1% CMC was used as overlay, indicating that the spot counts remain unaffected by time. This is due to overlapping spots, complicating the accurate counting.

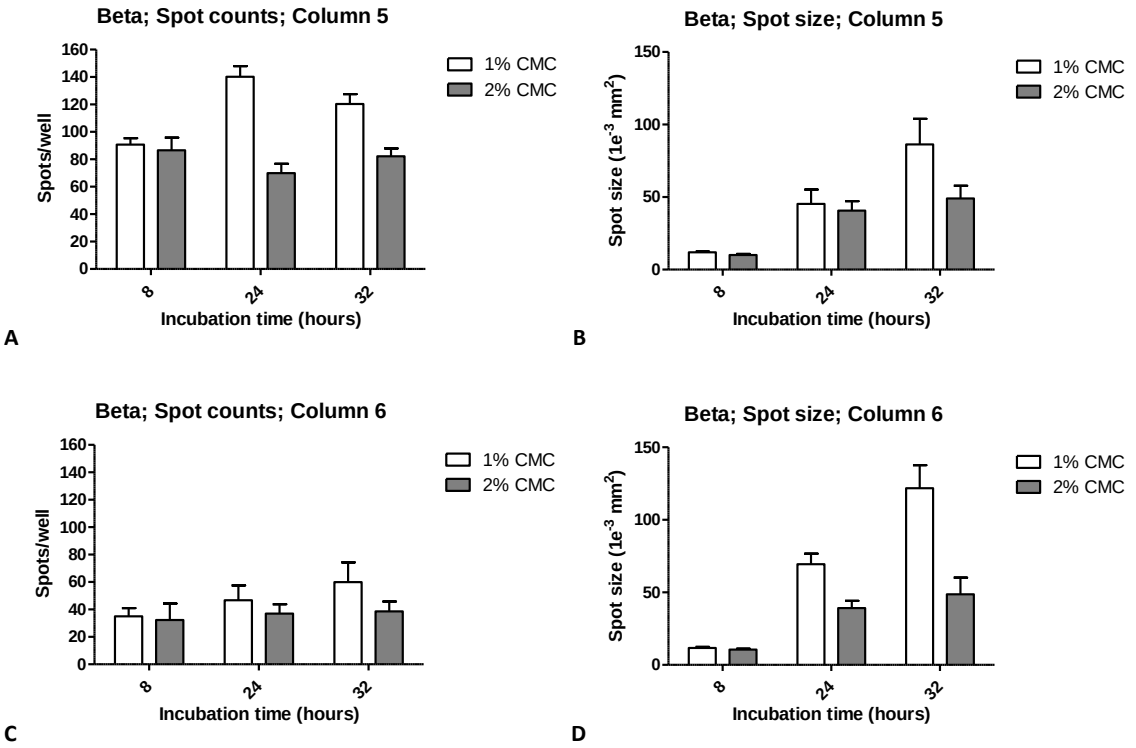

Figure 29. Effect of CMC 1% and 2% and different incubation time (8,24,32 hours) on Beta variant spot count and spot size. Two columns (5,6) of 96 well plate are shown. Spot count (A, C) and spot size (B, D) are reported as the mean value of each column +/-SEM.

Spots size steady increased with increasing the incubation time points when 1%CMC was used. Also when Beta variant was used, spots are smaller using 2% CMC compared to 1% CMC. After 8 hours no significant difference between the use of 1% CMC and 2% CMC has been detected in both columns neither in spot count nor in spot size (**Figure 29**). In column 5, a remarkable increase in spot count was observed in the 1% CMC plate after 24 hours (spot counts after 8 hours 90; spot count after 24 hours 140). A small decrease in spot counts after 24 hours was observed in column 5 with 2%CMC (**Figure 29, A**).

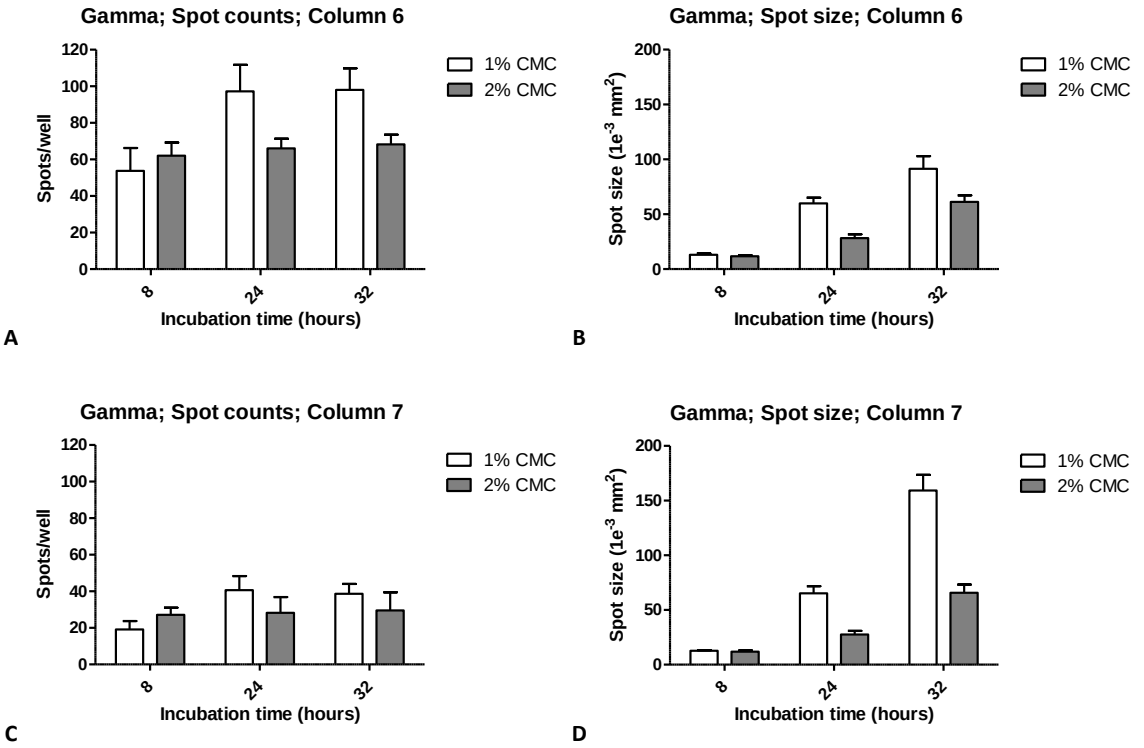

Figure 30. Effect of CMC 1% and 2% and different incubation time (8,24,32 hours) on Gamma variant spot count and spot size. Two columns (6,7) of 96 well plate are shown. Spot count (A, C) and spot size (B, D) are reported as the mean value of each column +/-SEM.

At 24 hours the spot counts increase when 1% CMC is used compared to 2% CMC also when Gamma variant was used (**Figure 30; A, C**). This again is due to overlapping spots, complicating the accurate counting of spots as in the Wild type strain.

In general, in all the SARS-CoV-2 variants a decrease in spot size has been observed in plates with 2%CMC , making a spot count more accurate. When CMC 1% was used, the spot count was found to have similar values in all three timepoints; this effect is due to the overlapping of spots and therefore to an incorrect count.
However, since 2% CMC gave better results specially for the Gamma and Beta variant compared to 1% CMC but it is not practical the use because of its viscosity, a concentration in between (1.6%) is suggested to perform next experiments. This specific concentration has been already used in a previous study. [43]

Taken toghether, the selected conditions to apply to the optimized SARS-CoV-2 Viropot MN assay are the following: MEM medium without CO2 will be used in place of DMEM with CO2; Pre-incubation of the serum dilutions mixed with virus will be performed at room temperature instead of 37°C. The incubation time will be 60 minutes; The incubation time of the serum/virus mixtures on the cells will be 60 minutes. Before the last incubation period, the inoculum is removed from the plate and replaced by infection medium containing 1.6% CMC and the plates will be incubated for a total duration of 24 hours.

6. DISCUSSION

In all epidemiological studies, the availability of a specific serological assay capable of providing the most reliable and accurate antibody response in a given sample, is an essential factor. This is mainly important during an emergency, such as epidemic or, even worse, a pandemic. Indeed, knowing which percentage of the population has already come in contact with the virus, and consequently developed a specific immune response, can drive the type and timing of prevention and containment measures. Virus nAbs can be induced by natural infection or vaccination, and they have a crucial role in controlling and limiting viral infection and transmission among people.

In the first project of this thesis work (Project I) different microneutralization methods are presented which can be used to evaluate anti-SARS-CoV-2 neutralizing antibodies (nAbs) in human samples. The aim of Project I was to compare a microneutralization assay (MN) with a read out based on evaluation of the cytophatic effect (CPE) via an optical microscope (subjective method) and a MN based on a colorimetric read out (objective method) for the detection of nAbs against SARS-CoV-2 Wild type strain. The performance of the MN assays was evaluated on a subset of samples that were previously tested by ELISA in the context of a seroepidemiological study at the University of Siena. A thorough setup of the MN assay performed with optical CPE readout was conducted before comparing it with the same assay performed with a colorimetric readout. First, to assess the MN CPE assay sensitivity in detecting neutralizing antibody against SARS-CoV-2 Wild Type, two different viral infective doses were used: a standard dose of 100 TCID50/well and a lower dose of 25 TCID50/well. Results of these experiments show that the 88,8 % of samples have the same titers using both 25TCID0 and 100 TCID50, confirming the sensitivity and robustness of the SARS-CoV-2 MN CPE using a lower infective dose.
Secondly, to evaluate the specificity of the MN CPE assay in detecting neutralizing antibodies against SARS-CoV-2 Wild type strain, four animal antisera against Influenza and Adenovirus and human CR3022 mAb were tested along with the other human serum samples. Since SARS-CoV-2 and SARS-CoV display a high sequence identity of the S protein, it is possible that SARS-CoV nAbs may elicit cross-neutralization activity against SARS-CoV-2. Results obtained confirmed the specificity of the MN CPE assay to evaluate antibodies against SARS-CoV-2 and no ability of the CR3022 mAb to prevent viral attachment and entry into cell monolayer, which developed CPE in less than 48 hours post infection. On the other hand, the high signal registered on ELISA confirmed the potential of the CR3022 mAb to bind with high affinity an epitope on the RBD of the SARS-CoV-2 S protein. For human serum samples, the MN CPE assay confirmed that at least 50% of the samples tested positive on ELISA assay presented antibodies with neutralizing ability. This finding is broadly in line with previous Influenza studies, in which that assay was able to detect all binding antibodies without a prediction of their functionality. The fact that fairly low neutralizing titres were detected in samples and

that only half of those resulted to be positive on ELISA may be due to different factors: (a) at this stage the human population is completely *naïve* about this CoV strain, and several waves of exposure to the pathogen may be necessary to stimulate a strong neutralizing response; (b) as it has already proved for other viruses, such as Lassa [83] neutralizing antibodies are not always elicited after vaccination or natural infection; in fact, other mechanisms of the immune system may be involved in the protection, such as the complement-fixation reaction mediated by IgG1 and IgG3, antigen-dependent cellular cytotoxicity and T-cell responses. Samples that are not able to show a high signal on ELISA (borderline samples) may, instead, have neutralizing capabilities, as it was confirmed by three of our samples.

Once assessed the main critical conditions of the MN-CPE, an objective method of read-out of the same assay was developed by using spectrophotometry and a solution containing 0.02% of neutral red (able to stain lysosomes and other cell organelles) in lieu of the assessment with the optical microscope. The CPE MN and the colorimetric MN CPE showed comparable MN titers of neutralizing antibody against SARS-CoV-2 Wild type strain, as also confirmed by Correlation, Bland-Altman, and ICC analysis. This suggests the suitability of performing the MN assay using an 'objective' read out method. One of the advantages of the colorimetric read-out is that being a completely automated method, it offers a higher throughput, while inspection of each dilution well by means of the optical microscope slows down the process.

However, the present study has limitations. At the time when the study was conducted, the major difficulty lied in the lack of a standardized positive control (now available) that would enable the proper standardization of the assays. Furthermore, the number of samples analysed in this preliminary assessment was small and to ensure that the colorimetric MN assay can provide clinically meaningful results, the method would require a validation. Moreover, since many others SARS-CoV-2 variants have emerged, the next step would be to include the analysis of neutralizing antibody in human serum samples against the new variants.

To further investigate if the classical MN CPE correlate with other MN assays, the MN CPE was compared to a new MN platform: the Virospot MN assay (Project II). The Viropot MN combines classic virus culture techniques with automated sensitive detection of immunostained virus infected cells. In this method, a virus specific immunostaining was used as readout and then the images of all wells were acquired by a CTL ImmunoSpot analyzer. The MN CPE and Virospot MN were compared using a panel of human serum samples against SARS-CoV-2 Wild type and Alpha variant. Thsee two methods were performed in two different laboratories (located in different companies) and at a distance of 4 months each other. The neutralization titer (Mnt) of each sample yielded with the MN CPE reflected the highest sample dilution capable of protecting at least 50% of the cells from CPE, whereas the Mnt in the MN Virospot was expressed as the 80% and 90% of reduction point (MN80 and MN90, respectively), hence the 80% and 90% of the plaques reduction compared to the viral control.Log2-transformed titers obtained with the two assays were then compared. A difference in titers of 1.0 log2 dilution step (corresponding to a maximum titer difference of

2-fold) was defined as acceptable. The two assays were quite well in agreement when the tests were executed using the Wild Type strain. Greater differences were found when the CPE-based and the immunostaining-based methods were performed using the Alpha variant, which shows a lower agreement (72% for the comparison MN CPE vs MN80; and 64%, for MN CPE vs MN90) compared to the run where the Wild type strain was used (83% for MN CPE vs MN80; 81% for MN CPE vs MN90). The lower concordance observed between the two methods in the Alpha variant assays was particularly evident when comparing MN CPE titer values and MN90 Virospot results. This slight disagreement might have been caused by the presence of lower MN titers against the Alpha variant, compared to those yielded against the Wild Type strain. It is in fact well accepted that titers are less likely to correlate when they tend to be lower. Additionally, using the 90% of reduction points to express titer results can increase the sensitivity of the Virospot MN assay, which might as well explain the differences observed between MN CPE and MN90.

Moreover, differences between the two MN assays may be explained by differences in readout: Virospot MN assay has a completely automated read-out, wells images are acquired by an immunospot analyzer equipped with software to quantitate the nucleocapsid-positive cells, then the serum samples titers are calculated according to the method described in previous reports. [61] On the other hand, the MN CPE read out is performed by the inspection of each well by an inverted optical microscope and can be affected by the subjective interpretation of the operator, although skilled and trained staff is unlikely to provide different results of the same evaluation.

Furthermore, the two MN assays were performed in different laboratories, hence the inherent variability of the two methods such as cell culture conditions and incubation times (24 hours for Virospot MN assay and 72 hours for MN CPE assay) influenced the results.

However, to ensure that the correlation can provide meaningful results, further analysis with a bigger number of samples and with other SARS-CoV-2 variants would be an added value. Moreover, to make the data more comparable it would be necessary convert all the results to international standard unit (IU/mL). The use of an International Standard (IS) with defined IU allows the accurate calibration of assays to an arbitrary unit, thereby reducing inter-laboratory variation and creating a common language for reporting data. This would facilitate standardization of serological methods and comparability of datasets across different laboratories. The currently available IS and International Reference Panels for anti-SARS-COV-2 immunoglobulins (provided by the National Institute for Biological Standards and Control, NIBSC) are pool of plasma samples obtained from COVID-19 convalescents people during the first semester of 2020, hence before SARS-COV2 VOC appearance. As such, these standards are only suitable to calibrate serological assays in which the Wild type SARS-COV-2 strain is used, and conversion to IU should be applied only to methods which utilize this virus. NIBSC is currently looking for sources of serum/plasma from vaccinated and/or recovered individuals for the development of working standards for each SARS-CoV-2 VOC. This material is supposed to be assessed in a WHO Collaborative study[84] as done for the previous IS[85].

Although beyond the scope of this thesis, the work performed in Project II also confirmed a trend for lower titers against the Alpha variant compared to those against the Wild type strain. As reported in literature in fact (Variants of concern), several mutations found in the Alpha variant can reduce the neutralizing activity of antibodies. The Alpha variant includes 17 mutations and among these, eight mutations (Δ69–70 deletion, Δ144 deletion, N501Y, A570D, P681H, T716I, S982A, and D1118H) are in the S protein. Of those mutations, N501Y within the RBD enhances virus binding affinity to ACE2 receptor of host cells, and P681H is adjacent to the furin cleavage site in spike, which is a key determinant for transmission. [65] These mutations affect the capabilities of the variant to infect cells and react with antibody-containing serum samples in in vitro assays. Both MN CPE and MN Virospot methods were validated only for SARS-CoV-2 WT, strain BavPat1/2020, isolated in the beginning of the COVID-19 pandemic, but different test parameters might need to be optimized to make these assays more specific and sensitive for the analysis of samples against the new variants.

In the last project (Project III), several new conditions were adapted in the SARS-CoV-2 Virospot MN assay in order to assess its robustness and make this assay more sensitive for the detection of neutralizing antibodies against new SARS-CoV-2 variants.

The selected conditions to apply to the new optimazed SARS-CoV-2 Viropot MN assay include the use of MEM medium without CO2 supplementation (MEM - CO2) instead of DMEM with CO2 (DMEM + CO2). The MEM medium has been formulated with components that enhance cellular metabolism production and utilization of CO2 such that an exogenous source of CO2 is not required for the maintenance of CO2-dependent cellular functions. Results demostrate that samples generally yield higher MN titers when using MEM - CO2, compared to DMEM + CO2. The magnitude of the increase differed per variant virus used. Only one virus (Beta variant) among those evaluated showed nearly identical titer results with the two media. As the use of MEM – CO2 seems to increase the assay sensitivity with no evident effect on assay specificity, it is suggested to further investigate the use of this medium in further optimization/validation tests. The introduction of the carboxymethyl cellulose after the virus inoculation has been used as an immobilizing overlay medium to prevent viral infection from indiscriminately spreading through the mechanical flow of the liquid in order to have a well-defined spots count. The results taken from each SARS-CoV-2 variant (WT, Alpha, Beta and Gamma) demonstrate that the spot sizes increase over time and the greatest increase is observed when using 1% CMC as opposed to 2% CMC. Also, because of increasing spot size, the spots will overlap when using 1% CMC, and this generates inaccurately high spot counts. However, since 2% CMC gave more readable results (especially for the Gamma and Beta variant) compared to 1% CMC but it is not practical to use because of its viscosity, a concentration in-between such as 1.6% can be suggested to improve the assay readout. This intermediate CMC concentration was already standardized in the Virospot assay optimized to evaluate anti-Influenza antibody response [43]and should be evaluated in further optimization experiments. .

Results of Project III also show that serum and EDTA plasma are both suitable matrices to be tested in the SARS-CoV-2 Virospot MN assay. T-test analysis demonstrates the similarity in titers between results obtained with serum and plasma samples showing a p value < 0.05. Results about different time points for the first and second incubation show that the longer is the incubation, the higher are the MN titers. Spot count was also affected with the increase of incubation time, resulting in an increase of the spot counts. Moreover, in the first incubation between samples and virus, this effect was most pronounced when incubation was performed at 37°C and less so at RT. These results indicate that the assay will be more robust when incubation is performed at RT, instead of 37°C. Limiting the acceptable incubation period will also lead to more reproducible results. Therefore, it is suggested to perform future SARS-CoV-2 MN Virospot assays performing the first incubation at room temperature and limiting the duration for the first and second incubation steps at 60 minutes. As for the readout evaluation, the MN80 has been chosen as the reduction point. According to our analysis, results expressed as the 80% of reduction point compared to the Viral Control of each plate. Expressing the results as MN80 allows to improve detection of low positive titer values, as opposed to the use of MN90, which might make the test loose sensitivity, or of MN50, which may result in over-sensitivity of the assay (especially when using the MEM without CO2).

In summary, the present work shows high correlation between the MN CPE assay and two different MN methods, Colorimetric MN and Virospot MN assay, in detecting neutralizing antibodies against SARS-CoV-2 in human serum samples. These two MN methods demonstrate to have advantages compared to the Classical MN CPE method, both being completely automated methods, and hence offering a higher throughput, while inspection of each dilution well by means of the optical microscope slows down the process.
Nevertheless, the SARS-CoV-2 Virospot MN assay offers attractive advantages over the MN assay with a read out based on the cytophatic effect, including the relative insensitivity to variation in amount of infectious virus used in the test, independence from virus replication kinetic and suitability for high throughput analyses. The selected conditions from the optimization study made the SARS-CoV-2 Viropot MN assay more sensitive and robust despite data on the SARS-CoV-2 variants tested (Alpha, Beta and Gamma) show that these variants may be less susceptible to neutralization with a general decrease in MN titers compared to the Wild type strain.

7. CONCLUSIONS AND FUTURE PERSPECTIVES

The SARS-CoV-2 microneutralization assays presented in this study resulted suitable for the quantification of the neutralizing antibody titre in serum samples. Together with ELISA assay, the microneutralisation assay should always be included for the evaluation and eventual licensing of the next generation vaccines in which the contribution of neutralizing antibodies directed against the virus is often crucial in seroepidemiological and immunogenicity studies. Nevertheless, the necessity for a BSL3 laboratory could certainly be a limiting factor for neutralizing antibodies studies using live viruses, but it is currently the most reliable method in terms of results provided. A validation of these assay with the new SARS-CoV-2 variants and a panel of clinical sera should ensure stronger reproducibility data in support of the present results.

8. REFERENCES

1. Holmes EC, Rambaut A. Viral evolution and the emergence of SARS coronavirus. Philos Trans R Soc Lond B Biol Sci. 2004 Jul 29;359(1447):1059-65. doi: 10.1098/rstb.2004.1478. PMID: 15306390; PMCID: PMC1693395.

2. Longdon B, Brockhurst MA, Russell CA, Welch JJ, Jiggins FM. The evolution and genetics of virus host shifts. PLoS Pathog. 2014 Nov 6;10(11): e1004395. doi: 10.1371/journal.ppat.1004395. PMID: 25375777; PMCID: PMC4223060.

3. Kim CH. SARS-CoV-2 Evolutionary Adaptation toward Host Entry and Recognition of Receptor O-Acetyl Sialylation in Virus-Host Interaction. Int J Mol Sci. 2020 Jun 26;21(12):4549. doi: 10.3390/ijms21124549. PMID: 32604730; PMCID: PMC7352545.

4. Yu P, Hu B, Shi ZL, Cui J. Geographical structure of bat SARS-related coronaviruses. Infect Genet Evol. 2019 Apr; 69:224-229. doi: 10.1016/j.meegid.2019.02.001. Epub 2019 Feb 6. PMID: 30735813; PMCID: PMC7106260.

5. Wang MY, Zhao R, Gao LJ, Gao XF, Wang DP, Cao JM. SARS-CoV-2: Structure, Biology, and Structure-Based Therapeutics Development. Front Cell Infect Microbiol. 2020 Nov 25;10:587269. doi: 10.3389/fcimb.2020.587269. PMID: 33324574; PMCID: PMC7723891.

6. Walls AC, Park YJ, Tortorici MA, Wall A, McGuire AT, Veesler D. Structure, Function, and Antigenicity of the SARS-CoV-2 Spike Glycoprotein. Cell. 2020 Apr 16;181(2):281-292.e6. doi: 10.1016/j.cell.2020.02.058. Epub 2020 Mar 9. Erratum in: Cell. 2020 Dec 10;183(6):1735. PMID: 32155444; PMCID: PMC7102599.

7. Kadam SB, Sukhramani GS, Bishnoi P, Pable AA, Barvkar VT. SARS-CoV-2, the pandemic coronavirus: Molecular and structural insights. J Basic Microbiol. 2021 Mar;61(3):180-202. doi: 10.1002/jobm.202000537. Epub 2021 Jan 18. PMID: 33460172; PMCID: PMC8013332.

8. Rando HM, MacLean AL, Lee AJ, Ray S, Bansal V, Skelly AN, Sell E, Dziak JJ, Shinholster L, McGowan LD, Guebila MB, Wellhausen N, Knyazev S, Boca SM, Capone S, Qi Y, Park Y, Sun Y, Mai D, Brueffer C, Byrd JB, Wang J, Lordan R, Velazquez R, Szeto GL, Barton JP, Goel RR, Mangul S, Lubiana T, Consortium CR, Gitter A, Greene CS. Pathogenesis, Symptomatology, and Transmission of SARS-CoV-2 through analysis of Viral Genomics and Structure. ArXiv [Preprint]. 2021 Feb 1:arXiv:2102.01521v2. PMID: 33594340; PMCID: PMC7885912.

9. Machhi J, Herskovitz J, Senan AM, Dutta D, Nath B, Oleynikov MD, Blomberg WR, Meigs DD, Hasan M, Patel M, Kline P, Chang RC, Chang L, Gendelman HE, Kevadiya BD. The Natural History, Pathobiology, and Clinical Manifestations of SARS-CoV-2 Infections. J Neuroimmune Pharmacol. 2020 Sep;15(3):359-386. doi: 10.1007/s11481-020-09944-5. Epub 2020 Jul 21. PMID: 32696264; PMCID: PMC7373339.

10. Manenti A, Maggetti M, Casa E, Martinuzzi D, Torelli A, Trombetta CM, Marchi S, Montomoli E. Evaluation of SARS-CoV-2 neutralizing antibodies using a CPE-based colorimetric live virus micro-neutralization assay in human serum samples. J Med Virol. 2020 Oct;92(10):2096-2104. doi: 10.1002/jmv.25986. Epub 2020 May 17. PMID: 32383254; PMCID: PMC7267461.

11. Forni D, Cagliani R, Clerici M, Sironi M. Molecular Evolution of Human Coronavirus Genomes. Trends Microbiol. 2017 Jan;25(1):35-48. doi: 10.1016/j.tim.2016.09.001. Epub 2016 Oct 19. PMID: 27743750; PMCID: PMC7111218.

12. Phan T. Serological Approaches for COVID-19: Epidemiologic Perspective on Surveillance and Control Infect Genet Evol. 2020 Jul;81:104260. doi: 10.1016/j.meegid.2020.104260. Epub 2020 Feb 21. PMID: 32092483; PMCID: PMC7106203.

13. Domingo E, Sheldon J, Perales C. Viral quasispecies evolution. Microbiol Mol Biol Rev. 2012 Jun;76(2):159-216. doi: 10.1128/MMBR.05023-11. PMID: 22688811; PMCID: PMC3372249.

14. Hoehl S, Rabenau H, Berger A, Kortenbusch M, Cinatl J, Bojkova D, Behrens P, Böddinghaus B, Götsch U, Naujoks F, Neumann P, Schork J, Tiarks-Jungk P, Walczok A, Eickmann M, Vehreschild MJGT, Kann G, Wolf T, Gottschalk R, Ciesek S. Evidence of SARS-CoV-2 Infection in Returning Travelers from Wuhan, China. N Engl J Med. 2020 Mar 26;382(13):1278-1280. doi: 10.1056/NEJMc2001899. Epub 2020 Feb 18. PMID: 32069388; PMCID: PMC7121749.

15. Shah VK, Firmal P, Alam A, Ganguly D, Chattopadhyay S. Overview of Immune Response During SARS-CoV-2 Infection: Lessons From the Past. Front Immunol. 2020 Aug 7;11:1949. doi: 10.3389/fimmu.2020.01949. PMID: 32849654; PMCID: PMC7426442.

16. Singhal T. A Review of Coronavirus Disease-2019 (COVID-19). Indian J Pediatr. 2020 Apr;87(4):281-286. doi: 10.1007/s12098-020-03263-6. Epub 2020 Mar 13. PMID: 32166607; PMCID: PMC7090728.

17. Ng Kee Kwong KC, Mehta PR, Shukla G, Mehta AR. COVID-19, SARS and MERS: A neurological perspective. J Clin Neurosci. 2020 Jul;77:13-16. doi: 10.1016/j.jocn.2020.04.124. Epub 2020 May 5. PMID: 32417124; PMCID: PMC7198407.

18. Jin Y, Yang H, Ji W, Wu W, Chen S, Zhang W, Duan G. Virology, Epidemiology, Pathogenesis, and Control of COVID-19. Viruses. 2020 Mar 27;12(4):372. doi: 10.3390/v12040372. PMID: 32230900; PMCID: PMC7232198.

19. Paces J, Strizova Z, Smrz D, Cerny J. COVID-19 and the immune system. Physiol Res. 2020 Jul 16;69(3):379-388. doi: 10.33549/physiolres.934492. Epub 2020 May 29. PMID: 32469225.

20. Ni L, Ye F, Cheng ML, Feng Y, Deng YQ, Zhao H, Wei P, Ge J, Gou M, Li X, Sun L, Cao T, Wang P, Zhou C, Zhang R, Liang P, Guo H, Wang X, Qin CF, Chen F, Dong C. Detection of SARS-CoV-2-Specific Humoral and Cellular Immunity in COVID-19 Convalescent Individuals. Immunity. 2020 Jun 16;52(6):971-977.e3. doi: 10.1016/j.immuni.2020.04.023. Epub 2020 May 3. PMID: 32413330; PMCID: PMC7196424.

21. Vabret N, Britton GJ, Gruber C, Hegde S, Kim J, Kuksin M, Levantovsky R, Malle L, Moreira A, Park MD, Pia L, Risson E, Saffern M, Salomé B, Esai Selvan M, Spindler MP, Tan J, van der Heide V, Gregory JK, Alexandropoulos K, Bhardwaj N, Brown BD, Greenbaum B, Gümüş ZH, Homann D, Horowitz A, Kamphorst AO, Curotto de Lafaille MA, Mehandru S, Merad M, Samstein RM; Sinai Immunology Review Project. Immunology of COVID-19: Current State of the Science. Immunity. 2020 Jun 16;52(6):910-941. doi: 10.1016/j.immuni.2020.05.002. Epub 2020 May 6. PMID: 32505227; PMCID: PMC7200337.

22. Rydyznski Moderbacher C, Ramirez SI, Dan JM, Grifoni A, Hastie KM, Weiskopf D, Belanger S, Abbott RK, Kim C, Choi J, Kato Y, Crotty EG, Kim C, Rawlings SA, Mateus J, Tse LPV, Frazier A, Baric R, Peters B, Greenbaum J, Ollmann Saphire E, Smith DM, Sette A, Crotty S. Antigen-Specific Adaptive Immunity to SARS-CoV-2 in Acute COVID-19 and Associations with Age and Disease Severity. Cell. 2020 Nov 12;183(4):996-1012.e19. doi: 10.1016/j.cell.2020.09.038. Epub 2020 Sep 16. PMID: 33010815; PMCID: PMC7494270.

23. Grifoni A, Weiskopf D, Ramirez SI, Mateus J, Dan JM, Moderbacher CR, Rawlings SA, Sutherland A, Premkumar L, Jadi RS, Marrama D, de Silva AM, Frazier A, Carlin AF, Greenbaum JA, Peters B, Krammer F, Smith DM, Crotty S, Sette A. Targets of T Cell Responses to SARS-CoV-2 Coronavirus in Humans with COVID-19 Disease and Unexposed Individuals. Cell. 2020 Jun 25;181(7):1489-1501.e15. doi: 10.1016/j.cell.2020.05.015. Epub 2020 May 20. PMID: 32473127; PMCID: PMC7237901.

24. Hosseini A, Hashemi V, Shomali N, Asghari F, Gharibi T, Akbari M, Gholizadeh S, Jafari A. Innate and adaptive immune responses against coronavirus. Biomed Pharmacother. 2020 Dec;132:110859. doi: 10.1016/j.biopha.2020.110859. Epub 2020 Oct 22. PMID: 33120236; PMCID: PMC7580677.

25. Wajnberg A, Amanat F, Firpo A, Altman DR, Bailey MJ, Mansour M, McMahon M, Meade P, Mendu DR, Muellers K, Stadlbauer D, Stone K, Strohmeier S, Simon V, Aberg J, Reich DL, Krammer F, Cordon-Cardo C. Robust neutralizing antibodies to SARS-CoV-2 infection persist for months. Science. 2020 Dec 4;370(6521):1227-1230. doi: 10.1126/science.abd7728. Epub 2020 Oct 28. PMID: 33115920; PMCID: PMC7810037.

26. Dan JM, Mateus J, Kato Y, Hastie KM, Yu ED, Faliti CE, Grifoni A, Ramirez SI, Haupt S, Frazier A, Nakao C, Rayaprolu V, Rawlings SA, Peters B, Krammer F, Simon V, Saphire EO, Smith DM, Weiskopf D, Sette A, Crotty S. Immunological memory to SARS-CoV-2 assessed for up to 8 months after infection. Science. 2021 Feb 5;371(6529):eabf4063. doi: 10.1126/science.abf4063. Epub 2021 Jan 6. PMID: 33408181; PMCID: PMC7919858.

27. Williams TC, Burgers WA. SARS-CoV-2 evolution and vaccines: cause for concern? Lancet Respir Med. 2021 Apr;9(4):333-335. doi: 10.1016/S2213-2600(21)00075-8. Epub 2021 Jan 29. PMID: 33524316; PMCID: PMC8009632.

28. Krammer F. SARS-CoV-2 vaccines in development. Nature. 2020 Oct;586(7830):516-527. doi: 10.1038/s41586-020-2798-3. Epub 2020 Sep 23. PMID: 32967006.

29. Karpiński TM, Ożarowski M, Seremak-Mrozikiewicz A, Wolski H, Wlodkowic D. The 2020 race towards SARS-CoV-2 specific vaccines. Theranostics. 2021 Jan 1;11(4):1690-1702. doi: 10.7150/thno.53691. PMID: 33408775; PMCID: PMC7778607.

30. Amanat F, Krammer F. SARS-CoV-2 Vaccines: Status Report. Immunity. 2020 Apr 14;52(4):583-589. doi: 10.1016/j.immuni.2020.03.007. Epub 2020 Apr 6. PMID: 32259480; PMCID: PMC7136867.

31. Rawat K, Kumari P, Saha L. COVID-19 vaccine: A recent update in pipeline vaccines, their design and development strategies. Eur J Pharmacol. 2021 Feb 5;892:173751. doi: 10.1016/j.ejphar.2020.173751. Epub 2020 Nov 25. PMID: 33245898; PMCID: PMC7685956.

32. Deming ME, Michael NL, Robb M, Cohen MS, Neuzil KM. Accelerating Development of SARS-CoV-2 Vaccines - The Role for Controlled Human Infection Models. N Engl J Med. 2020 Sep 3;383(10):e63. doi: 10.1056/NEJMp2020076. Epub 2020 Jul 1. PMID: 32610006; PMCID: PMC7968616.

33. Baxter D. Active and passive immunity, vaccine types, excipients and licensing. Occup Med (Lond). 2007 Dec;57(8):552-6. doi: 10.1093/occmed/kqm110. PMID: 18045976.

34. Tumban E. Lead SARS-CoV-2 Candidate Vaccines: Expectations from Phase III Trials and Recommendations Post-Vaccine Approval. Viruses. 2020 Dec 31;13(1):54. doi: 10.3390/v13010054. PMID: 33396343; PMCID: PMC7824305.

35. Robert-Guroff M. Replicating and non-replicating viral vectors for vaccine development. Curr Opin Biotechnol. 2007 Dec;18(6):546-56. doi: 10.1016/j.copbio.2007.10.010. Epub 2007 Dec 11. PMID: 18063357; PMCID: PMC2245896.

36. Kubina R, Dziedzic A. Molecular and Serological Tests for COVID-19 a Comparative Review of SARS-CoV-2 Coronavirus Laboratory and Point-of-Care Diagnostics. Diagnostics (Basel). 2020 Jun 26;10(6):434. doi: 10.3390/diagnostics10060434. PMID: 32604919; PMCID: PMC7345211.

37. Zhu N, Zhang D, Wang W, Li X, Yang B, Song J, Zhao X, Huang B, Shi W, Lu R, Niu P, Zhan F, Ma X, Wang D, Xu W, Wu G, Gao GF, Tan W; China Novel Coronavirus Investigating and Research Team. A Novel Coronavirus from Patients with Pneumonia in China, 2019. N Engl J Med. 2020 Feb 20;382(8):727-733. doi: 10.1056/NEJMoa2001017. Epub 2020 Jan 24. PMID: 31978945; PMCID: PMC7092803.

38. Mazzini L, Martinuzzi D, Hyseni I, Benincasa L, Molesti E, Casa E, Lapini G, Piu P, Trombetta CM, Marchi S, Razzano I, Manenti A, Montomoli E. Comparative analyses of SARS-CoV-2 binding (IgG, IgM, IgA) and neutralizing antibodies from human serum samples. J Immunol Methods. 2021 Feb;489:112937. doi: 10.1016/j.jim.2020.112937. Epub 2020 Nov 28. PMID: 33253698; PMCID: PMC7695554.

39. Trombetta CM, Remarque EJ, Mortier D, Montomoli E. Comparison of hemagglutination inhibition, single radial hemolysis, virus neutralization assays, and ELISA to detect antibody levels against seasonal influenza viruses. Influenza Other Respir Viruses. 2018 Nov;12(6):675-686. doi: 10.1111/irv.12591. Epub 2018 Aug 11. PMID: 30019448; PMCID: PMC6185893.

40. Weisblum Y, Schmidt F, Zhang F, DaSilva J, Poston D, Lorenzi JC, Muecksch F, Rutkowska M, Hoffmann HH, Michailidis E, Gaebler C, Agudelo M, Cho A, Wang Z, Gazumyan A, Cipolla M, Luchsinger L, Hillyer CD, Caskey M, Robbiani DF, Rice CM, Nussenzweig MC, Hatziioannou T, Bieniasz PD. Escape from neutralizing antibodies by SARS-CoV-2 spike protein variants. Elife. 2020 Oct 28;9:e61312. doi: 10.7554/eLife.61312. PMID: 33112236; PMCID: PMC7723407.

41. Walker GJ, Naing Z, Ospina Stella A, Yeang M, Caguicla J, Ramachandran V, Isaacs SR, Agapiou D, Bull RA, Stelzer-Braid S, Daly J, Gosbell IB, Hoad VC, Irving DO, Pink JM, Turville S, Kelleher AD, Rawlinson WD. SARS Coronavirus-2 Microneutralisation and Commercial Serological Assays Correlated Closely for Some but Not All Enzyme Immunoassays. Viruses. 2021 Feb 4;13(2):247. doi: 10.3390/v13020247. PMID: 33557418; PMCID: PMC7915197.

42. Smither SJ, Lear-Rooney C, Biggins J, Pettitt J, Lever MS, Olinger GG Jr. Comparison of the plaque assay and 50% tissue culture infectious dose assay as methods for measuring filovirus infectivity. J Virol Methods. 2013 Nov;193(2):565-71. doi: 10.1016/j.jviromet.2013.05.015. Epub 2013 Jun 5. PMID: 23748121.

43. Van Baalen CA, Jeeninga RE, Penders GH, van Gent B, van Beek R, Koopmans MP, Rimmelzwaan GF. ViroSpot microneutralization assay for antigenic characterization of human influenza viruses. Vaccine. 2017 Jan 3;35(1):46-52. doi: 10.1016/j.vaccine.2016.11.060. Epub 2016 Nov 26. PMID: 27899226.

44. Picarazzi F, Vicenti I, Saladini F, Zazzi M, Mori M. Targeting the RdRp of Emerging RNA Viruses: The Structure-Based Drug Design Challenge. Molecules. 2020 Dec 3;25(23):5695. doi: 10.3390/molecules25235695. PMID: 33287144; PMCID: PMC7730706.

45. Denison MR, Graham RL, Donaldson EF, Eckerle LD, Baric RS. Coronaviruses: an RNA proofreading machine regulates replication fidelity and diversity. RNA Biol. 2011 Mar-Apr;8(2):270-9. doi: 10.4161/rna.8.2.15013. Epub 2011 Mar 1. PMID: 21593585; PMCID: PMC3127101.

46. Domingo E. Quasispecies Theory in Virology. J Virol. 2002 Jan 1;76(1):463-465. doi: 10.1128/JVI.76.1.463-465.2002. PMID: 33739796; PMCID: PMC135734.

47. Duarte EA, Novella IS, Weaver SC, Domingo E, Wain-Hobson S, Clarke DK, Moya A, Elena SF, de la Torre JC, Holland JJ. RNA virus quasispecies: significance for viral disease and epidemiology. Infect Agents Dis. 1994 Aug;3(4):201-14. PMID: 7827789.

48. Chaplin DD. Overview of the immune response. J Allergy Clin Immunol. 2010 Feb;125(2 Suppl 2): S3-23. doi: 10.1016/j.jaci.2009.12.980. PMID: 20176265; PMCID: PMC2923430.

49. Zhu J, Paul WE. Peripheral CD4+ T-cell differentiation regulated by networks of cytokines and transcription factors. Immunol Rev. 2010 Nov;238(1):247-62. doi: 10.1111/j.1600-065X.2010.00951.x. Erratum in: Immunol Rev. 2011 Mar;240(1):317. PMID: 20969597; PMCID: PMC2975272.

50. Luo H, Jia T, Chen J, Zeng S, Qiu Z, Wu S, Li X, Lei Y, Wang X, Wu W, Zhang R, Zou X, Feng T, Ding R, Zhang Y, Chen YQ, Sun C, Wang T, Fang S, Shu Y. The Characterization of Disease Severity Associated IgG Subclasses Response in COVID-19 Patients. Front Immunol. 2021 Mar 4;12:632814. doi: 10.3389/fimmu.2021.632814. PMID: 33763078; PMCID: PMC7982848.

51. Stern PL. Key steps in vaccine development. Ann Allergy Asthma Immunol. 2020 Jul;125(1):17-27. doi: 10.1016/j.anai.2020.01.025. Epub 2020 Feb 7. PMID: 32044451.

52. Krammer F, Simon V. Serology assays to manage COVID-19. Science. 2020 Jun 5;368(6495):1060-1061. doi: 10.1126/science.abc1227. Epub 2020 May 15. PMID: 32414781.

53. Krammer F. A correlate of protection for SARS-CoV-2 vaccines is urgently needed. Nat Med. 2021 Jul;27(7):1147-1148. doi: 10.1038/s41591-021-01432-4. PMID: 34239135.

54. Khoury DS, Cromer D, Reynaldi A, Schlub TE, Wheatley AK, Juno JA, Subbarao K, Kent SJ, Triccas JA, Davenport MP. Neutralizing antibody levels are highly predictive of immune protection from symptomatic SARS-CoV-2 infection. Nat Med. 2021 Jul;27(7):1205-1211. doi: 10.1038/s41591-021-01377-8. Epub 2021 May 17. PMID: 34002089.

55. Manenti A, Molesti E, Maggetti M, Torelli A, Lapini G, Montomoli E. The theory and practice of the viral dose in neutralization assay: Insights on SARS-CoV-2 "doublethink" effect. J Virol Methods. 2021 Nov;297:114261. doi: 10.1016/j.jviromet.2021.114261. Epub 2021 Aug 14. PMID: 34403775; PMCID: PMC8364219.

56. Klimov A, Balish A, Veguilla V, Sun H, Schiffer J, Lu X, Katz JM, Hancock K. Influenza virus titration, antigenic characterization, and serological methods for antibody detection. Methods Mol Biol. 2012;865:25-51. doi: 10.1007/978-1-61779-621-0_3. PMID: 22528152.

57. Okuno Y, Tanaka K, Baba K, Maeda A, Kunita N, Ueda S. Rapid focus reduction neutralization test of influenza A and B viruses in microtiter system. J Clin Microbiol. 1990 Jun;28(6):1308-13. doi: 10.1128/jcm.28.6.1308-1313.1990. PMID: 2380359; PMCID: PMC267925.

58. Bachmann MF, Ecabert B, Kopf M. Influenza virus: a novel method to assess viral and neutralizing antibody titers in vitro. J Immunol Methods. 1999 May 27;225(1-2):105-11. doi: 10.1016/s0022-1759(99)00034-4. PMID: 10365787.

59. World Health Organization; Manual for the Laboratory Diagnosis and Virological Surveillance of Influenza, WHO Press (2011), pp. 63-77

60. Sicca F, Martinuzzi D, Montomoli E, Huckriede A. Comparison of influenza-specific neutralizing antibody titers determined using different assay readouts and hemagglutination inhibition titers: good correlation but poor agreement. Vaccine. 2020 Mar 4;38(11):2527-2541. doi: 10.1016/j.vaccine.2020.01.088. Epub 2020 Feb 7. PMID: 32044163.

61. Zielinska E, Liu D, Wu HY, Quiroz J, Rappaport R, Yang DP. Development of an improved microneutralization assay for respiratory syncytial virus by automated plaque counting using imaging analysis. Virol J. 2005 Nov 9;2:84. doi: 10.1186/1743-422X-2-84. PMID: 16281972; PMCID: PMC1308871.

62. Sanyaolu A, Okorie C, Marinkovic A, Haider N, Abbasi AF, Jaferi U, Prakash S, Balendra V. The emerging SARS-CoV-2 variants of concern. Ther Adv Infect Dis. 2021 Jun 18;8:20499361211024372. doi: 10.1177/20499361211024372. PMID: 34211709; PMCID: PMC8216402.

63. Galloway SE, Paul P, MacCannell DR, Johansson MA, Brooks JT, MacNeil A, Slayton RB, Tong S, Silk BJ, Armstrong GL, Biggerstaff M, Dugan VG. Emergence of SARS-CoV-2 B.1.1.7 Lineage - United States, December 29, 2020-January 12, 2021. MMWR Morb Mortal Wkly Rep. 2021 Jan 22;70(3):95-99. doi: 10.15585/mmwr.mm7003e2. PMID: 33476315; PMCID: PMC7821772.

64. Cosar B, Karagulleoglu ZY, Unal S, Ince AT, Uncuoglu DB, Tuncer G, Kilinc BR, Ozkan YE, Ozkoc HC, Demir IN, Eker A, Karagoz F, Simsek SY, Yasar B, Pala M, Demir A, Atak IN, Mendi AH, Bengi VU, Cengiz Seval G, Gunes Altuntas E, Kilic P, Demir-Dora D. SARS-CoV-2 Mutations and their Viral Variants. Cytokine Growth Factor Rev. 2021 Jul 2:S1359-6101(21)00053-8. doi: 10.1016/j.cytogfr.2021.06.001. Epub ahead of print. PMID: 34580015; PMCID: PMC8252702.

65. Choi JY, Smith DM. SARS-CoV-2 Variants of Concern. Yonsei Med J. 2021 Nov;62(11):961-968. doi: 10.3349/ymj.2021.62.11.961. PMID: 34672129; PMCID: PMC8542474.

66. Shiehzadegan S, Alaghemand N, Fox M, Venketaraman V. Analysis of the Delta Variant B.1.617.2 COVID-19. Clin Pract. 2021 Oct 21;11(4):778-784. doi: 10.3390/clinpract11040093. PMID: 34698149; PMCID: PMC8544471.

67. COVID-19 WeeklyEpidemiologicalUpdate(WHO) Edition 63, published 26October 2021

68. Aleem A, Akbar Samad AB, Slenker AK. Emerging Variants of SARS-CoV-2 And Novel Therapeutics Against Coronavirus (COVID-19). 2021 Jul 18. In: StatPearls [Internet]. Treasure Island (FL): StatPearls Publishing; 2021 Jan–. PMID: 34033342.

69. Garcia-Beltran WF, Lam EC, St Denis K, Nitido AD, Garcia ZH, Hauser BM, Feldman J, Pavlovic MN, Gregory DJ, Poznansky MC, Sigal A, Schmidt AG, Iafrate AJ, Naranbhai V, Balazs AB. Multiple SARS-CoV-2 variants escape neutralization by vaccine-induced humoral immunity. Cell. 2021 Apr 29;184(9):2372-2383.e9. doi: 10.1016/j.cell.2021.03.013. Epub 2021 Mar 12. Erratum in: Cell. 2021 Apr 29;184(9):2523. PMID: 33743213; PMCID: PMC7953441.

70. Li DD, Li QH. SARS-CoV-2: vaccines in the pandemic era. Mil Med Res. 2021 Jan 6;8(1):1. doi: 10.1186/s40779-020-00296-y. PMID: 33402220; PMCID: PMC7785400.

71. Lin Y, Gu Y, Wharton SA, Whittaker L, Gregory V, Li X, Metin S, Cattle N, Daniels RS, Hay AJ, McCauley JW. Optimisation of a micro-neutralisation assay and its application in antigenic characterisation of influenza viruses. Influenza Other Respir Viruses. 2015 Nov;9(6):331-340. doi: 10.1111/irv.12333. PMID: 26073976; PMCID: PMC4605415.

72. Reed, L.J. and Muench, H. (1938) A Simple Method of Estimating Fifty Percent Endpoints. American Journal of Hygiene, 27, 493-497.

73. Bland JM, Altman DG. Statistical methods for assessing agreement between two methods of clinical measurement. Lancet. 1986 Feb 8;1(8476):307-10. PMID: 2868172.

74. Koo TK, Li MY. A Guideline of Selecting and Reporting Intraclass Correlation Coefficients for Reliability Research. J Chiropr Med. 2016 Jun;15(2):155-63. doi: 10.1016/j.jcm.2016.02.012. Epub 2016 Mar 31. Erratum in: J Chiropr Med. 2017 Dec;16(4):346. PMID: 27330520; PMCID: PMC4913118.

75. Mishra P, Singh U, Pandey CM, Mishra P, Pandey G. Application of student's *t*-test, analysis of variance, and covariance. Ann Card Anaesth. 2019 Oct-Dec;22(4):407-411. doi: 10.4103/aca.ACA_94_19. PMID: 31621677; PMCID: PMC6813708.

76. Harcourt J, Tamin A, Lu X, Kamili S, Sakthivel SK, Murray J, Queen K, Tao Y, Paden CR, Zhang J, Li Y, Uehara A, Wang H, Goldsmith C, Bullock HA, Wang L, Whitaker B, Lynch B, Gautam R, Schindewolf C, Lokugamage KG, Scharton D, Plante JA, Mirchandani D, Widen SG, Narayanan K, Makino S, Ksiazek TG, Plante KS, Weaver SC, Lindstrom S, Tong S, Menachery VD, Thornburg NJ. Severe Acute Respiratory Syndrome Coronavirus 2 from Patient with Coronavirus Disease, United States. Emerg Infect Dis. 2020 Jun;26(6):1266-1273. doi: 10.3201/eid2606.200516. Epub 2020 Jun 17. PMID: 32160149; PMCID: PMC7258473.

77. Kaye M. SARS-associated coronavirus replication in cell lines. Emerg Infect Dis. 2006 Jan;12(1):128-33. doi: 10.3201/eid1201.050496. PMID: 16494729; PMCID: PMC3291385.

78. Lu Y, Liu DX, Tam JP. Lipid rafts are involved in SARS-CoV entry into Vero E6 cells. Biochem Biophys Res Commun. 2008 May 2;369(2):344-9. doi: 10.1016/j.bbrc.2008.02.023. Epub 2008 Feb 13. PMID: 18279660; PMCID: PMC7092920.

79. ter Meulen J, van den Brink EN, Poon LL, Marissen WE, Leung CS, Cox F, Cheung CY, Bakker AQ, Bogaards JA, van Deventer E, Preiser W, Doerr HW, Chow VT, de Kruif J, Peiris JS, Goudsmit J. Human monoclonal antibody combination against SARS coronavirus: synergy and coverage of escape mutants. PLoS Med. 2006 Jul;3(7):e237. doi: 10.1371/journal.pmed.0030237. PMID: 16796401; PMCID: PMC1483912.

80. Tian X, Li C, Huang A, Xia S, Lu S, Shi Z, Lu L, Jiang S, Yang Z, Wu Y, Ying T. Potent binding of 2019 novel coronavirus spike protein by a SARS coronavirus-specific human monoclonal antibody. Emerg Microbes Infect. 2020 Feb 17;9(1):382-385. doi: 10.1080/22221751.2020.1729069. PMID: 32065055; PMCID: PMC7048180.

81. COVID-19 Treatment Guidelines Panel. Coronavirus Disease 2019 (COVID-19) Treatment Guidelines. National Institutes of Health. Available at https://www.covid19treatmentguidelines.nih.gov//

82. Guidelines, Criteria, and Rules of Thumb for Evaluating Normed and Standardized Assessment Instrument in Psychology, December 1994Psychological Assessment 6(4):284-290. DOI:10.1037/1040-3590.6.4.284

83. Abreu-Mota T, Hagen KR, Cooper K, Jahrling PB, Tan G, Wirblich C, Johnson RF, Schnell MJ. Non-neutralizing antibodies elicited by recombinant Lassa-Rabies vaccine are critical for protection against Lassa fever. Nat Commun. 2018 Oct 11;9(1):4223. doi: 10.1038/s41467-018-06741-w. PMID: 30310067; PMCID: PMC6181965.la

84. https://www.nibsc.org/about_us/latest_news/collaboration.aspx

85. Mattiuzzo et al. Establishment of the WHO International Standard and Reference Panel for anti-SARS-CoV-2 antibody. 2020, WHO Expert Committee on Biological Standardization. WHO/BS/2020.2403

86. Cantoni D, Mayora-Neto M, Temperton N. The role of pseudotype neutralization assays in understanding SARS CoV-2. Oxf Open Immunol. 2021 Mar 13;2(1):iqab005. doi: 10.1093/oxfimm/iqab005. PMID: 33738456; PMCID: PMC7928640.

87. Hyseni I, Molesti E, Benincasa L, Piu P, Casa E, Temperton NJ, Manenti A, Montomoli E. Characterisation of SARS-CoV-2 Lentiviral Pseudotypes and Correlation between Pseudotype-Based Neutralisation Assays and Live Virus-Based Micro Neutralisation Assays. Viruses. 2020 Sep 10;12(9):1011. doi: 10.3390/v12091011. PMID: 32927639; PMCID: PMC7551040.

88. Carnell GW, Ferrara F, Grehan K, Thompson CP, Temperton NJ. Pseudotype-based neutralization assays for influenza: a systematic analysis. Front Immunol. 2015 Apr 29;6:161. doi: 10.3389/fimmu.2015.00161. PMID: 25972865; PMCID: PMC4413832.

89. Garbutt M, Liebscher R, Wahl-Jensen V, Jones S, Möller P, Wagner R, Volchkov V, Klenk HD, Feldmann H, Ströher U. Properties of replication-competent vesicular stomatitis virus vectors expressing glycoproteins of filoviruses and arenaviruses. J Virol. 2004 May;78(10):5458-65. doi: 10.1128/jvi.78.10.5458-5465.2004. PMID: 15113924; PMCID: PMC400370.

90. Fukushi S, Watanabe R, Taguchi F. Pseudotyped vesicular stomatitis virus for analysis of virus entry mediated by SARS coronavirus spike proteins. Methods Mol Biol. 2008;454:331-8. doi: 10.1007/978-1-59745-181-9_23. PMID: 19057867; PMCID: PMC7120752.

APPENDIX 1. SAMPLE LIST AND CLINICAL INFORMATION

Number of sample	Sample ID	Type of sample	Symptoms	Date of swab collection for COVID-19 PC	Result of COVID-19 PCR
1	I100557073001	Serum	fever, shortness of breath, diarrhea	18.03.2020	positive
2	I100557074001	Plasma	fever, shortness of breath, diarrhea	18.03.2021	positive
3	I100557077001	Serum	shortness of breath, sore throat, headache, nasal congestion, diarrhea, lost sense of taste and sense of smell	18.03.2021	positive
4	I100557078001	Plasma	shortness of breath, sore throat, headache, nasal congestion, diarrhea, lost sense of taste and sense of smell	18.03.2020	positive
5	I100557085001	Serum	perature, cough, shortness of breath, muscle & joint pain, headache, diarrhea, lost sense of taste and sense of smell	not specified	not specified
6	I100557086001	Plasma	perature, cough, shortness of breath, muscle & joint pain, headache, diarrhea, lost sense of taste and sense of sme	not specified	not specified
7	I100557096001	Serum	fever, cough, shortness of breath, muscle & joint pain, sore throat, headache,	not specified	not specified
8	I100557097001	Plasma	fever, cough, shortness of breath, muscle & joint pain, sore throat, headache	not specified	not specified
9	I100557101001	Serum	shortness of breath, muscle & joint pain, sore throat, headache, diarrhea, lost sense of taste and sense of smell	not specified	not specified
10	I100557102001	Plasma	shortness of breath, muscle & joint pain, sore throat, headache, diarrhea, lost sense of taste and sense of smel	not specified	not specified
11	I100557106001	Serum	fever, headache	not specified	not specified
12	I100557107001	Plasma	fever, headache	not specified	not specified
13	I100557119001	Serum	shortness of breath, muscle & joint pain, sore throat, headache, nasal congestion, diarrhea	24.03.2020	positive
14	I100557120001	Plasma	shortness of breath, muscle & joint pain, sore throat, headache, nasal congestion, diarrhea	24.03.2020	positive
15	I100557129001	Serum	fever, cough, muscle & joint pain, headache, lost sense of taste and sense of smell	not specified	not specified
16	I100557130001	Plasma	fever, cough, muscle & joint pain, headache, lost sense of taste and sense of smell	not specified	not specified
17	I100557138001	Serum	cough, muscle & joint pain, sore throat, diarrhea, lost sense of taste and sense of smell	not specified	not specified
18	I100557139001	Plasma	cough, muscle & joint pain, sore throat, diarrhea, lost sense of taste and sense of smell	not specified	not specified
19	I100557149001	Serum	fever, cough, shortness of breath, headache, diarrhea, lost sense of taste and sense of smell	not specified	not specified
20	I100557150001	Plasma	fever, cough, shortness of breath, headache, diarrhea, lost sense of taste and sense of smell	not specified	not specified
21	I100557160001	Serum	fever, cough, shortness of breath, muscle & joint pain, diarrhea, lost sense of taste and sense of smell	20.03.2020	positive

9. ACKNOWLEDGMENTS

First, I would like to thank Professor Emanuele Montomoli for giving me the opportunity to undertake this precious path thanks to which I have had the chance to make many experiences that made me grow both professionally and personally. Thanks also to my company tutor Silvia Grappi that followed me in this work and to Pietro Piu for helping me with part of the statistical analysis.

A special thanks to my colleagues and Vismederi's friends who made me live unforgettable moments. Moreover, I would like to dedicate a special thanks to my colleague and friend Giulia Piccini who helped and supported me throughout this work.

In addition, I would like to acknowledge my colleagues from my internship at Viroclinics Biosciences for the opportunity I was given to further my research in their laboratories. It has been the most intense and challenging period so far but at the same time a rewarding experience.

Finally, I reserve a big thank to my best friends Flavia, Besjan, Brusca, Elena e Giulia and to my special family that always guide and support me with their wise counsels. I am blessed to have all of you in my life.